STRUCTURAL AND FUNCTIONAL STUDIES OF PORINS FROM PATHOGENIC BACTERIA

Luana G. M. Ferrara

A Thesis Submitted for the Degree of PhD
at the
University of St Andrews

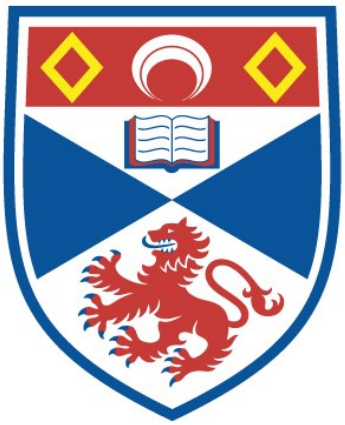

2018

Structural and functional studies of porins from pathogenic bacteria

Luana G.M. Ferrara

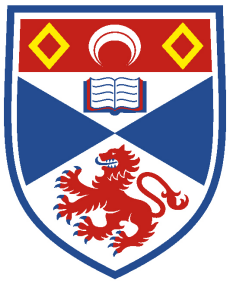

University of
St Andrews

This thesis is submitted in fulfillment for the degree of
Doctor of Philosophy

October 2017

Supervisor: Prof. James H. Naismith

I. Declarations

I, Luana G.M. Ferrara, hereby certify that this thesis, which is approximately 24,000 words in length, has been written by me, and that it is the record of work carried out by me, or principally by myself in collaboration with others as acknowledged, and that it has not been submitted in any previous application for a higher degree.

I was admitted as a research student in October 2013 and as a candidate for the degree of Doctor of Philosophy in October 2017; the higher study for which this is a record was carried out in the University of St Andrews between 2013 and 2017.

Date 05/03/2018 Signature of candidate 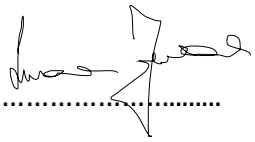

I hereby certify that the candidate has fulfilled the conditions of the Resolution and Regulations appropriate for the degree of Doctor of Philosophy in the University of St Andrews and that the candidate is qualified to submit this thesis in application for that degree.

Date 05/03/2018 Signature of supervisor 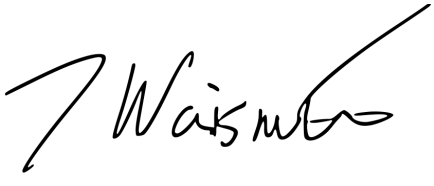

In submitting this thesis to the University of St Andrews I understand that I am giving permission for it to be made available for use in accordance with the regulations of the University Library for the time being in force, subject to any copyright vested in the work not being affected thereby. I also understand that the title and the abstract will be published, and that a copy of the work may be made and supplied to any bona fide library or research worker, that my thesis will be electronically accessible for personal or research use unless exempt by award of an embargo as requested below, and that the library has the right to migrate my thesis into new electronic forms as required to ensure continued access to the thesis. I have obtained any third-party copyright permissions that may be required in order to allow such access and migration, or have requested the appropriate embargo below.

The following is an agreed request by candidate and supervisor regarding the publication of this thesis:

Access to printed copy and electronic publication of the thesis through the University of St Andrews.

Date…05/03/2018…… Signature of candidate 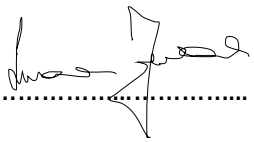 ……..

Date…05/03/2018…….. Signature of supervisor 

II. Abstract

Multi-drug resistant bacteria have become a real threat to public health worldwide. Gram-negative bacteria, in particular, have shown high level of antibiotic resistance due to the presence of an additional membrane, known as outer-membrane (OM), that acts as an extra barrier. Most antibiotics enter the cells via a particular class of outer-membrane proteins (OMPs) known as porins. Porins are β-barrel channels that allow the passive diffusion of hydrophobic compounds. The porins are known to select against molecules on the basis of size and charge. When exposed to antibiotics, bacteria can modify the OM permeability by altering their porins profile. Mutations affecting the size and conductivity of the pore channel, and modification of the level of porins expression are just few examples of how the bacteria can decrease the influx of antibiotics.

In order to better understand their interaction with antibiotics, this thesis presents structural and functional studies on porins from pathogenic bacteria. The structure of the natively expressed major outer-membrane protein (MOMP) from *Campylobacter jejuni* was determined, reveling the presence of a calcium-binding site inside the channel. Electrophysiology and *in silico* modeling analysis have shown to be important for the stability and the function of the protein. Omp50 from *C. jejuni* was expressed in *E. coli* and its tyrosine kinase activity was analyzed *in vitro*. Finally, the structures of the two major porins from *Enterobacter aerogens* were determined and compared to their orthologs within the *Enterobacteriaceae* family. Further, a liposome-swelling assay (LSA) was used

to determine the rate of permeation of clinically relevant antibiotics through a series of porins. Combining these data allow a more detailed molecular understanding of translocation.

III. Acknowledgments

Firstly, I would like to express my sincere gratitude to my supervisor Prof. James H. Naismith for giving me the opportunity to join his team for the great journey that was my PhD, for his guidance and for his continuous support through all my research. A special thanks goes to Dr. Huanting Liu for his help and advice on gene cloning and gene mutation, but also for his wisdom and kind friendship. I would also like to thank Dr. Lucile Moynié for helping me with crystals fishing and data collection. I might not have been the perfect PhD student, but I am pretty sure I was her favorite. A big thanks goes also to Mr. Antoni Tortajada for his help and lovely chats. And surely, I can't not express my gratitude to all Prof Naismith's lab team for the useful and motivating discussions and for the inevitable (and very much appreciated) coffee breaks.

My PhD wouldn't have been the same without my girls, Laura W, Laura G, Emilia, Audrey and Miriam. Our Friday nights pub, shopping afternoons and home-made dinners made these past four years much easier, and for this I would like to thank them.

A very special thanks goes to Joe, for his endless support and care (especially in the last few months). I have the feeling that writing up my dissertation was as painful for me as it was for him.

None of this would have been possible without my parents, Angela and Giovanni, and my siblings. They are, without a doubt, my personal fan club and I couldn't

possibly thank them enough for being always there for me. Finally a “requested” thanks goes to my little sister, Francesca, for making me smile when I need it the most.

IV.Table of Contents

V. List of figure and tables

V.1 List of figures

V.2 List of tables

VI. Abbreviations

A

ADP	Adenosine diphosphate
AMP	Adenosine monophosphate
ATP	Adenosine triphosphate

B

BAM	β-barrel assembly machinery
BME	β-mercaptoethanol
β-OG	n-Octyl-β-D-glucoside

C

CAMPs	Cationic Antimicrobial Peptides
CCP4	Collaborative Computing Project Number 4
CD	Circular Dichroism
C_8E_4	Tetraethylene glycol monooctyl ether
CMC	Critical Micelle Concentration
C-terminus	Carboxyl terminus
CV	Column Volume

D

DDM	*n*-Dodecyl-β-maltopyranoside
DNA	Deoxyribonucleic acid

E

EDTA	Ethylenediaminetetracetic acid
EM	Electron microscopy
Ery	Erytromicin

F

FQ	Fluoroquinolones
FS	Fisher Syndrome

G

GBS	Guillian-Barré Syndrome
GF	Gel Filtration

H

Hep	Heptose
HR	High Resolution
HPS	Heat Shock Protein

I

IB	Inclusion Body
IBS	Irritable Bowel Syndrome
IM	Inner-Membrane
IPTG	Isopropyl β-D-thiogalactopyranoside

K

kDa	kilo Dalton
Kdo	3-deoxy-D-manno-octulosonic acid

L

LB	Luria Bertani
LDAO	N,N-Dimethyldodecylamine N-oxide
LOS	Lipooligosacharide
LPS	Lipopolysaccharide
LSA	Liposome Swelling Assay

M

MDR	Multi Drug Resistance
MIC	Minimal Inhibitory Concentration
MOMP	Major Outer-Membrane Protein
MR	Molecular Replacement
MS	Mass Spectrometry
MW	Molecular Weight

N

Ni-NTA	Nickel Nitrilotriacetic acid
N-terminus	amino terminus

O

Occ	Outer-membrane Carboxyl acid
OD	Optical Density
OM	Outer-membrane
OMP	Outer-membrane Protein
OPOE	n-Octyl-oligo-oxyethylene

P

PAGE	Polyacrylamide Gel Electrophoresis
PCR	Polymerase Chain Reaction
PDB	Protein Data Bank
PE	Periplasm
PEG	Polyethylene glycol
PEI	Polyethylenimine
POTRA	Polypeptide Associated Transport

PPi	Pirophosphate
pS	pico Siemens
PVDF	Polyvinylidene Difluoride
R	
RNA	Ribonucleic acid
RMSD	Root-Mean-Square-Deviation
RMSF	Root-Mean-Square-Flactuation
RPM	Revolution Per Minute
S	
SDS	Sodium Dodecyl Sulphate
SEC	Size Exclusion Chromatography
Skp	Seventeen Kilodalton Protein
T	
T3SS	Type 3 Secretory System
TAT	Twin-Arginine Translocation
TB	Terrific Broth
TCEP	Tris(2-Carboxyethyl)phosphine
TE	Tris-EDTA
TEV	Tobacco Etch Virus protease
TLC	Thin Liquid Chromatography
TLS	Translation, Libration and Screw-rotation
TPB	Tryptose Phosphate Broth

U

UV	Ultraviolet

Amino Acids

Alanine	Ala	A	Leucine	Leu	L
Arginine	Arg	R	Lysine	Lys	K
Asparagine	Asn	N	Methionine	Met	M
Aspartic Acid	Asp	D	Phenylalanine	Phe	F
Cysteine	Cys	C	Proline	Pro	P
Glutamic acid	Glu	E	Serine	Ser	S
Glutamine	Gln	Q	Threonine	Thr	T
Glycine	Gly	G	Tryptophan	Trp	W
Histidine	His	H	Tyrosine	Tyr	Y
Isoleucine	Ile	I	Valine	Val	V

Nucleic acids

A- Adenosine	C-Cytosine	G-Guanine	T-Thymidine

Chapter 1: Structure and function of outer-membrane proteins

1.1 Introduction

1.1.1 Gram-negative outer-membrane: an overview

Bacteria, like all living cells, possess an envelope that allows them to protect the cytoplasmic contents from the surrounding environment. In addition to this membrane, Gram-positive and Gram-negative bacteria [1] have a peptidoglycan layer. Gram-negative bacteria possess a further additional 'outer' membrane that has a distinctive composition. This introduction will focus on the membrane structure and composition of the Gram-negative bacteria, with a particular interest in the outer-membrane.

Gram-negative bacteria are composed of two chemically distinct membranes, the inner membrane (IM) (separates cytoplasm from periplasm), and the outer-membrane (OM) (separates periplasm from extra-cellular space). The periplasm, is an aqueous compartment containing a layer of peptidoglycan. While the IM is composed of a bilayer of phospholipids (with ethanolamine and phosphatidyl glycerol being the most abundant phospholipids), the composition of the OM is more complex. The inner leaflet of the OM (facing the periplasm) shows a similar composition to the IM, whereas the outer leaflet is mainly composed of glycolipids, which form the lipopolysaccharide (LPS) [2].

The LPS is essential for the Gram-negative survival and is therefore ubiquitously produced in all species. The structure of the LPS has been extensively studied in the last few decades, and it has now been well characterized. The LPS is organized

in three main regions (from the outer leaflet to the extra-cellular space): Lipid A, the core and the O-chain (Figure 1.1) [3]. Lipid A is the most hydrophobic part of the LPS and it is mainly formed by β-D-GlcN-(1-6)-α-D-GlcN disaccharide with two phosphoryl groups attached [4] and it is this molecule that functions as endotoxin. Endotoxin is responsible for the activation of an immune response in mammals, which, in severe cases can lead to septic shock and eventually death [5]. The core is composed of repeating units of sugar. The section of the core close to the Lipid A, also known as inner core, is primarily composed of 3-deoxy-D-manno-octulosonic acid (Kdo) and L-glycero-D-manno heptose (Hep), while the outer core, in proximity to the O-chain, is composed of hexoses and hexosamine. Finally, the O-chain is the most exposed and the most variable part of the LPS [6]. It is comprised of repeating units of polysaccharides, of which the lengths and composition vary from species to species. Some mutants do not express the O-antigen and, in this case the LPS is termed rough [7].

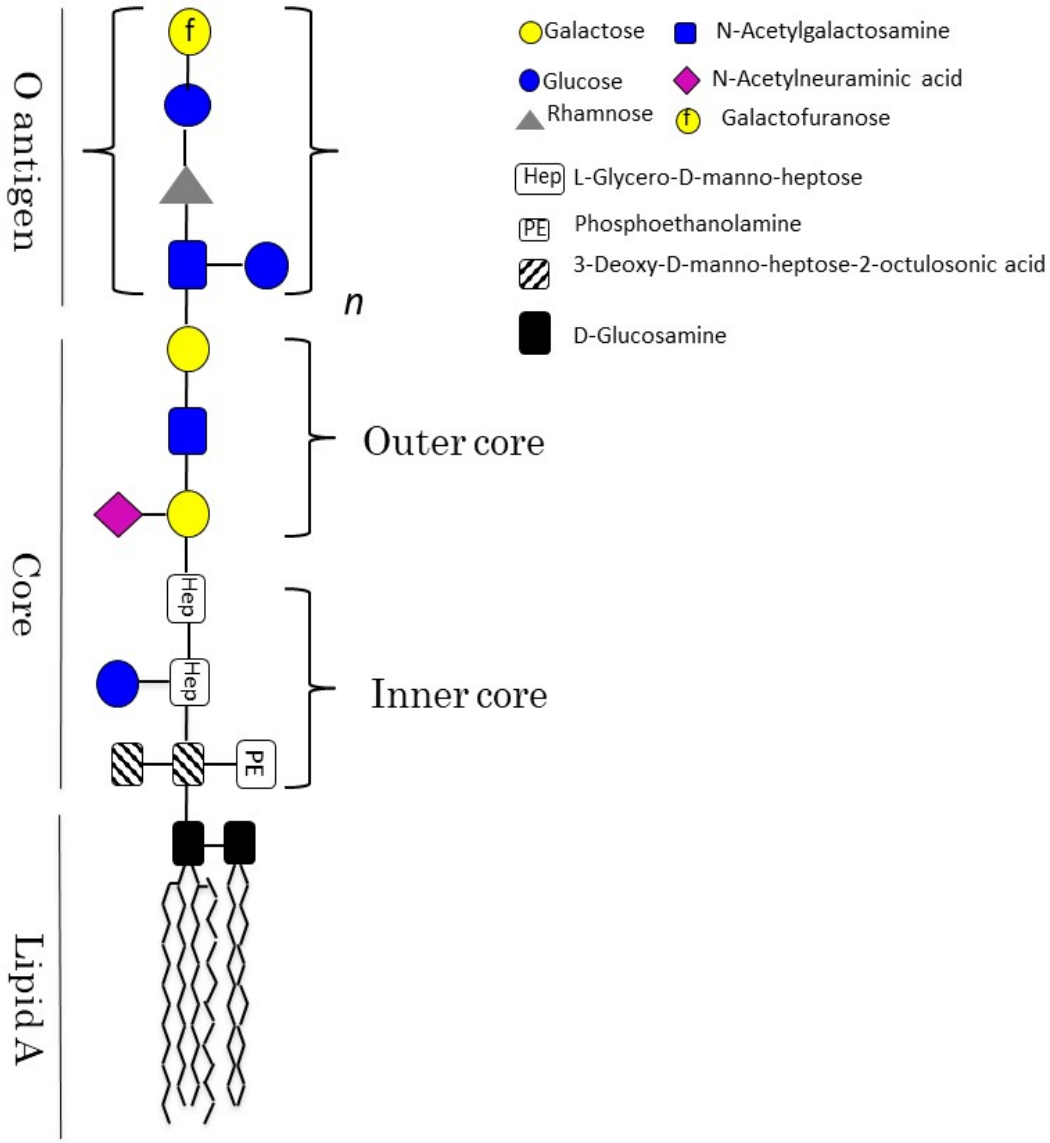

Figure 1.1: LPS schematic representation. The three main regions forming the LPS (Lipid A, Core and O-antigen) are highlighted in the figure. The O16 *E. coli* O antigen is used as an example. The lipid A is structurally composed of a β-(1-6)-linked D-GlcN disaccharide, to which are attached up to four (per monosaccharide) acyl acids chains (e.g. palmitic and myristic fatty acids) . The lipid A is directly connected to the inner core through a α2-6 bond between, the Kdo and the glucosamine. The outer core is composed of several 1-3 β bound hexoses (D-glucose, D-mannose, D-galactose), with the last hexose directly bound to the O-antigen. The O-antigen is a glycan polymer in the outermost part of the LPS. Figure adapted from [8].

1.1.2 Outer-membrane proteins

The outer-membrane is embedded with proteins that display a characteristic β-barrel arrangement. To date, many outer-membrane protein (OMP) structures have been solved by X-ray crystallography and almost all of these share common features that can be summarized as follows: i) they are made of antiparallel β-strands connected to each other (the number of the β-strands differs amongst the OMPs, ranging from a minimum of 8 to a maximum of 26), (Wza was the first exception to this rule [9]) ii) both the N- and the C-terminus face the periplasmic space, iii) the β-strands are connected by longs loops (L) facing the extra-cellular space and short turns (T) facing the periplasmic space, iv) the loops represent the most variable part of the barrel, vi) in most (but not in all) the OMPs the L3 folds back inside the channel to form the so-called constriction zone or eyelet, vii) when trimerized, a non-polar core is formed along the threefold axis, viii) the external surface of the barrel (embedded in the lipid bilayer) consists mainly of hydrophobic, uncharged amino-acids[10],[11].

The OMPs play multiple roles that are essential for the viability of bacteria, they form channels for the uptake of nutrients, maintain the bilayer asymmetry, are involved in cellular adhesion, and can also act as enzyme (e.g. protease) [12],[13].

1.1.3 Passive transport through the OM: Porins

Porin transporters exemplified by OmpC are water filled channels embedded in the OM, allowing the passive diffusion of polar molecules [14]. Like most other

OMP, porins show a β-barrel structure with several long external loops and short periplasmic turns (Figure 1.2). Porins can adopt either a monomeric or (homo)trimeric conformation [15],[16]. The latter is stabilized due to the interaction within the L2 of one monomer and the β-strands of the neighbor monomer. *In vitro*, this interaction can be disturbed using chaotropic agents or by heat, leading to the partial or complete dissociation of the trimer [17]. β-barrel proteins benefit from a high level of stability due to numerous hydrogen bonds formed among the β-sheets [18]. Several studies, however, have identified "weakly stable" regions within the transmembrane domain of trimeric porins [19],[20],[21]. Interestingly, those regions are stabilized by the formation of protein-protein interfaces (oligomerization). In OmpF, a trimeric porin of *E. coli*, the amino acids R100, G19, G135, and N141 have been identified as weakly stable residues [21]. Site-directed mutagenesis of these residues leads to both a stable dimer and monomer of OmpF [21].

L3 plays an important role in the diffusion of molecules through the pore. This loop folds back halfway through the channel, narrowing its diameter. Inside the barrel, negatively charged amino acids, lying in the L3, interact with positively charged amino acids (either Lys or Arg) located opposite the Loop [22],[23]. The distribution of the charges creates an internal electric field, which compensates for desolvation and permits the translocation of polar molecules [24]. The outside of the barrel, unlike the inside, is predominantly uncharged and hydrophobic, as it would be expected for proteins inserted in a lipidic membrane.

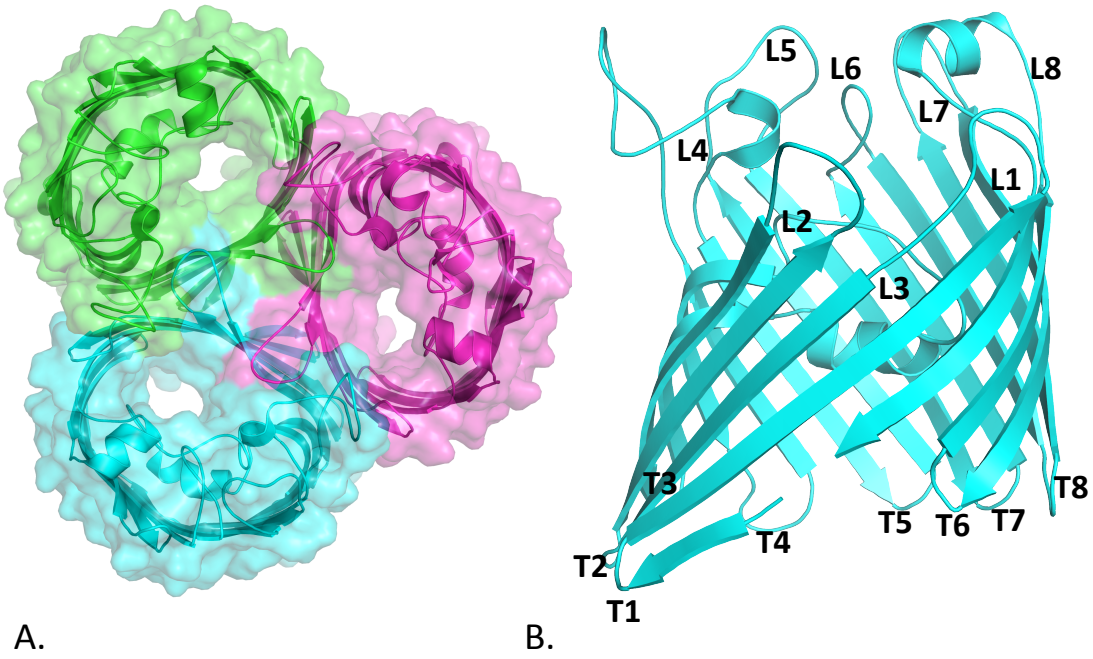

Figure 1.2: Cartoon representation of OmpC from *E. coli*. (A) Extracellular view of OmpC trimer (B) Side view of OmpC monomer. Extracellular loops are indicated with L and periplasmic turns with T. (PDB code: 2J1n)

Non-specific (also known as general) and specific porins are differentiated based on the level of specificity shown for their substrates. Normally 16-β-stranded, general porins allow permeation of substances with a MW lower than 600 Da with a slight selectivity for cations. Cation-selectivity in general porins – such as in OmpC [25] and OmpF [26] from *E. coli,* and in OmpK36 and OmpK35 from *Keisbiella pneumonia* [27] – has been largely demonstrated by single channel experiments. Selectivity is caused by an excess of negatively charged residues located inside the channel [28],[29],[30],[27]. The majority of Gram-negative bacteria possess at least one general porin, typically expressed in high copies number [31]. For instance, it has been estimated that OmpF from *E. coli* is normally present at 10^5 copies per cells [31].

The maltoporin LamB from *E. coli* [32] and the sucrose-specific porin SrcY from *Salmonella typhimurium* [33],[34] are well-characterized examples of specific (sugar) porins. A common feature of sugar transporting porins is an array of aromatic amino acids which run in lanes inside the inner wall of the channel, commonly known as "greasy slide" (Figure 1.3) [35]. Site-directed mutagenesis studies have shown the importance of the greasy slide on sugar translocation [36]. The aromatic residues help lining the sugars inside the channel by interacting with their hydroxide groups, lowering the energy barrier for permeation [37],[38]. Specific porins are expressed in low copy numbers and their expression depends upon certain limiting growth conditions.

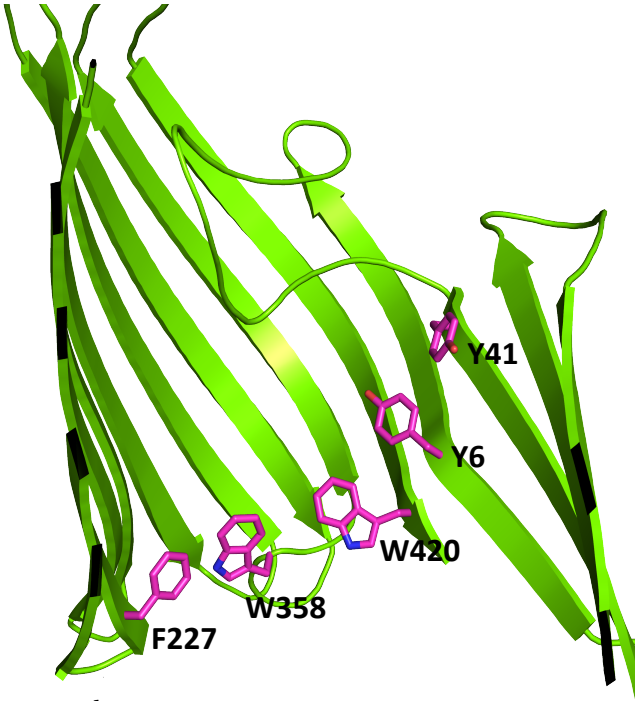

Figure 1.3: Greasy slide in LamB from *E. coli.* LamB monomer is colored in green. The amino acids forming the greasy slide are shown in sticks and colored in magenta (PDB code: 1MAL).

Pseudomonas aeruginosa possess another class of substrate-specific porins. This is called the "Outer membrane Carboxylic acid Channel" (Occ)[39]. Interestingly, no general porins have been identified in *P. aeruginosa*, perhaps correlating with this pathogens inherent resistance to permeation of antibiotics [40],[41]. The Occ porins can be divided in two sub families OccD (specific for amino acids) and OccK (specific for cyclic negatively charged molecules) [42],[43]. In the Occ porins the substrates are guided through the pore due to a so-called "basic ladder". This is a string of basic amino acids (Lys and Arg) that interact with the substrate's carboxyl group [44] (Figure 1.4). To date, several structures of the Occ members have been solved, showing that although trimeric in solution, these porins crystallize as monomers of 18-β-strands [45].

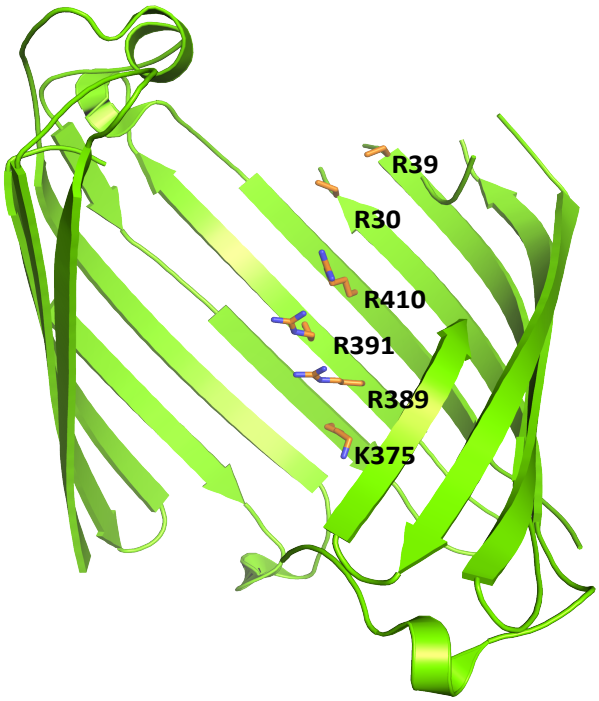

Figure 1.4: Basic ladder in OccD1 from *Pseudomonas aeruginosa*. OccD1 monomer is colored in green. Amino acids forming the so-called "basic ladder" are shown in sticks and colored in orange (PDB code: 4FOZ).

In the last decade, an increased number of porin structures have become available [10], uncovering the presence of porins with unusual characteristics [46]. For example, recently, the x-ray structure of the cyclodextrin metabolism A (CymA) porin from *Klebsiella oxytoca* has uncovered a diverse organization of the internal loops and thus a peculiar mechanism of uptake [47],[48]. CymA is a 14-β-sheets cyclodextrine-specific channel with shorts extracellular loops. Interestingly, none of them fold back to constrict the pore [48] (Figure 1.5 A-B). In CymA, in fact, the pore is kept closed due to an N-terminus inner plug that interacts with the wall of the channel. Such interaction is disturbed when the cyclodextrines approach, leading to the opening of the channel and subsequent translocation [48].

Another particularly unusual 14-β-strand porin is OmpG from *E. coli* K-12. Unlike any other porins described so far, OmpG channel is entirely open, due to the lack of the L3, or any inner plugs (Figure 1.5 C-D) [16]. The large diameter of the pore could allow the entry of highly toxic compounds that would compromise the OM permeability and hence, the bacterial viability. It is, probably for this reason that, OmpG is not constitutively expressed but expression occurs under specific conditions [16].

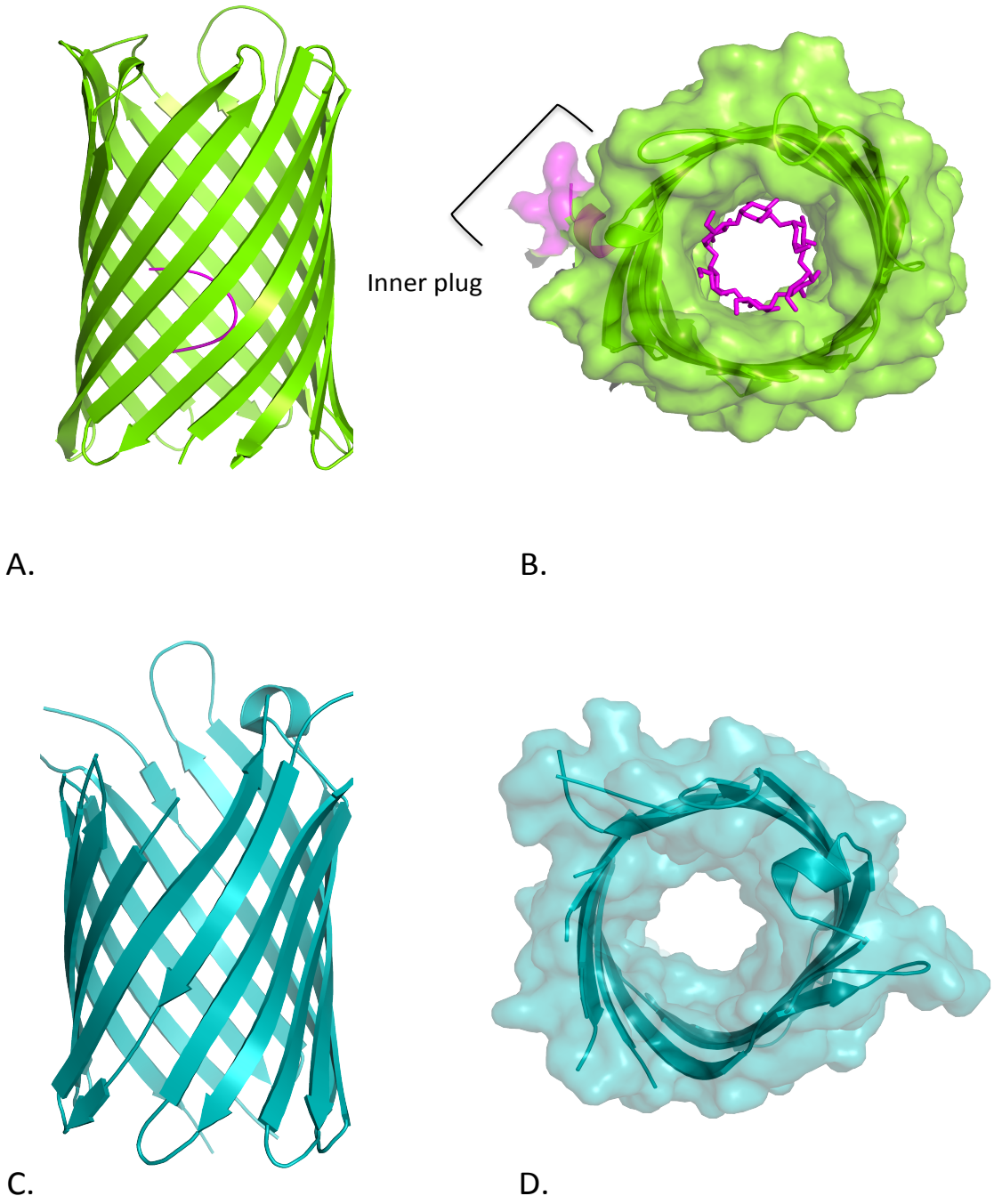

Figure 1.5: Cartoon representation of 14-β-stranded porins. (A) Side view of CymA. The barrel is colored in green and the inner plug in magenta. (B) Extracellular view of CymA. The substrate, cyclodextrine, is bound to the binding site. The molecule of cyclodestrine is displayed in stick and colored in magenta. (C) Side and (D) extracellular view of OmpG from E. coli (PDB code: 4D5B and 2F1C, respectively).

1.1.4 Active transport through OM: TonB-dependent transporters

TonB-dependent transporters (TBDTs) are a class of OMPs which allow active translocation of essential substances such as iron (chelates to specific molecules called siderophore), cobalt and nickel. It also allows the translocation of substances such as vitamin B12 and carbohydrates [49]. To date, several structures of TBDTs have been reported, including FhuA [50], FepA [51], PiuA, PirA [52] and BtuB [53]. Those structures revealed that the TBTDs are 22-β stranded barrel with an inner "plug domain", folded back inside the barrel (Figure 1.6).

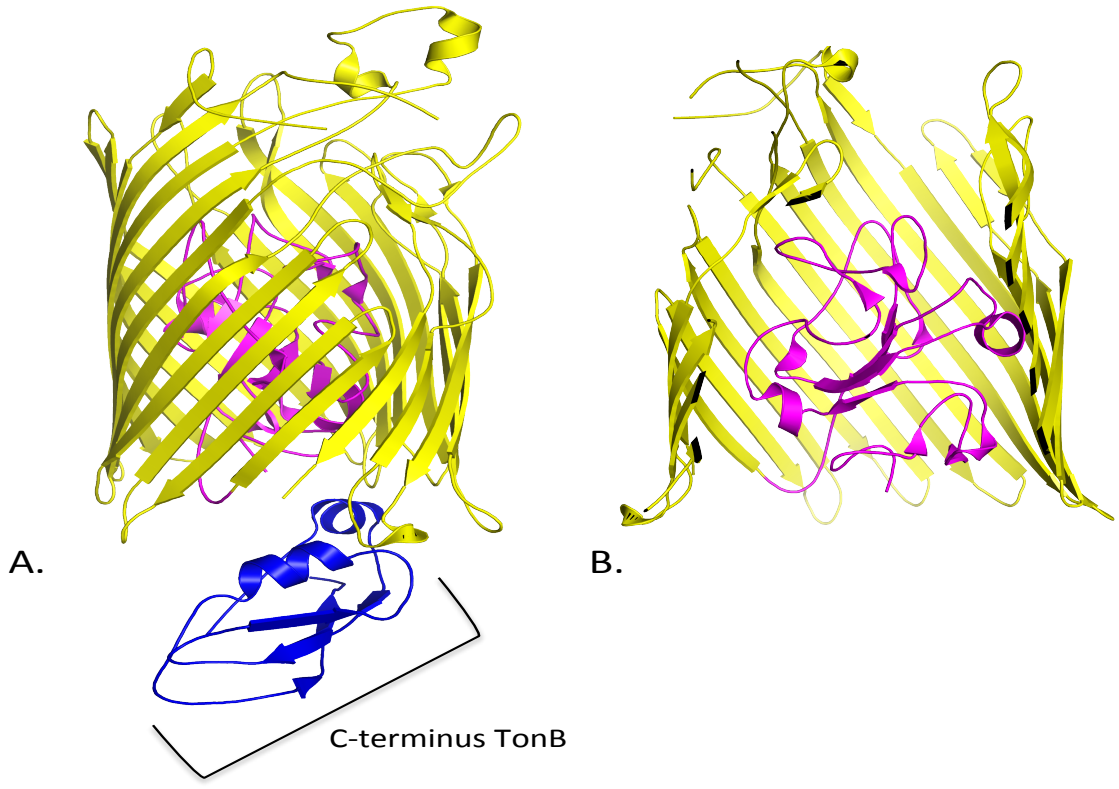

Figure 1.6: FhuA, TonB dependent transporter of E. coli. (A) FhuA in complex to TonB C-terminus. FhuA is colored in yellow, the inner plug in magenta and TonB in blue. (B) Shows the inner plug. Some β-sheets were removed to improve the view of the plug (PDB code: 2GRX).

As no source of energy is available at the level the OM, active translocation occurs by transducing the proton motive force (pmf) generated in the IM by a protein complex, namely TonB-ExbB-ExbD [49][54][55]. Specifically, as a result of the binding of the ligand, the TBDTs undertake conformational changes that lead the N-terminal of the plug domain, also known as TonB box, to reach and interact with the C-terminal domain of the TonB protein, at the level of the periplasmic space. Such interaction is necessary to transfer the energy for the ligand translocation (Figure 1.7) [56],[57]. Although the crystal structure of the TonB-ExbB-ExbD complex has been recently determined [58],[59], the transport mechanism has yet to be understood.

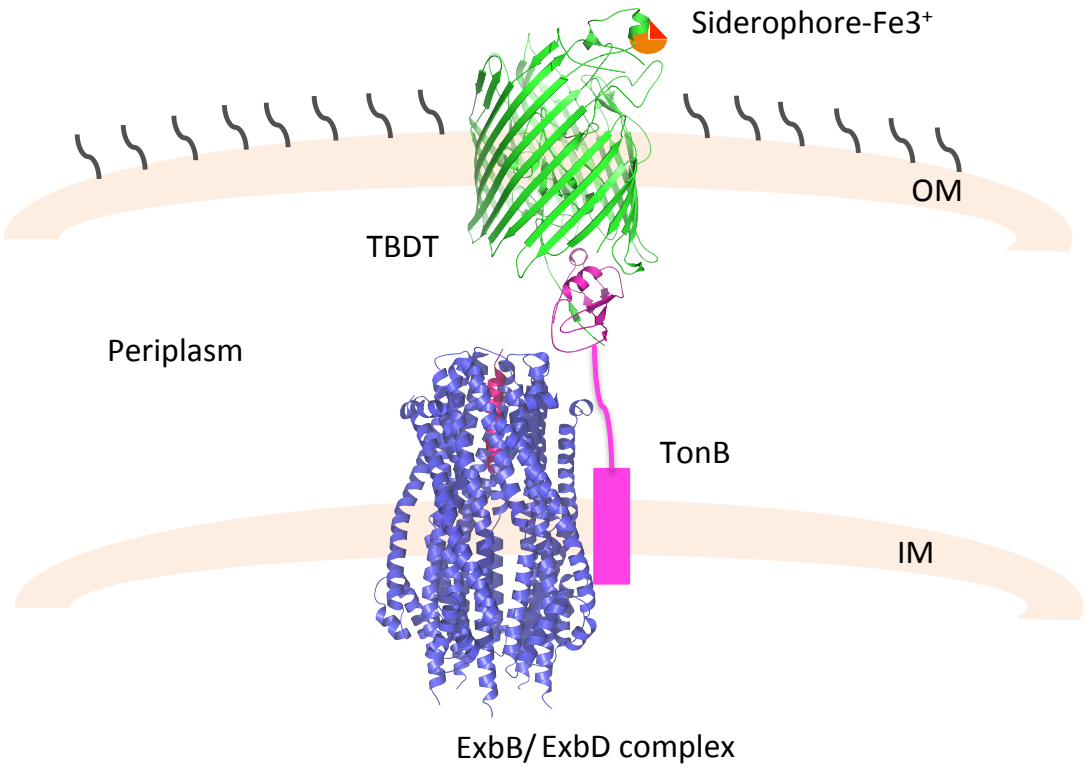

Figure 1.7: Schematic representation of TBDT mediated transport. Transport of the siderophore-Fe^{3+}occurs via specific TBTD receptor (green, PDB code: 2GRX). Upon ligand interaction the receptor interacts with the C-terminus of TonB (magenta, PDB code: 2GRX) giving the power stroke for translocation. The ExbB/ExbD complex is depicted in blue (ExbB) and pink (ExbD) (PDB code 5SV1). Picture adapted from [59].

Recently the x-ray structure of the starch utilization system (SusCD) became available, reveling a diverse example of TBDT [60]. In fact, the SusCD complex from Bacteroides thetaiotaomicron solved by Glenwright et al., disclosed a novel substrate-binding mechanism [60]. SusD is a lipoprotein that acts as a lid on the top of SusC, a typical 22-β stranded TBTDs (Figure 1.8). In absence of the ligand, SusD is in an open and motile state to then switch to a closed conformation upon ligand binding. The ligand is located in between the interface of SusC and SusD [60]. As for the case of the canonical TBDTs, the plug domain is pushed away from the barrel to interact with the TonB-ExbB-ExbD complex and complete the translocation.

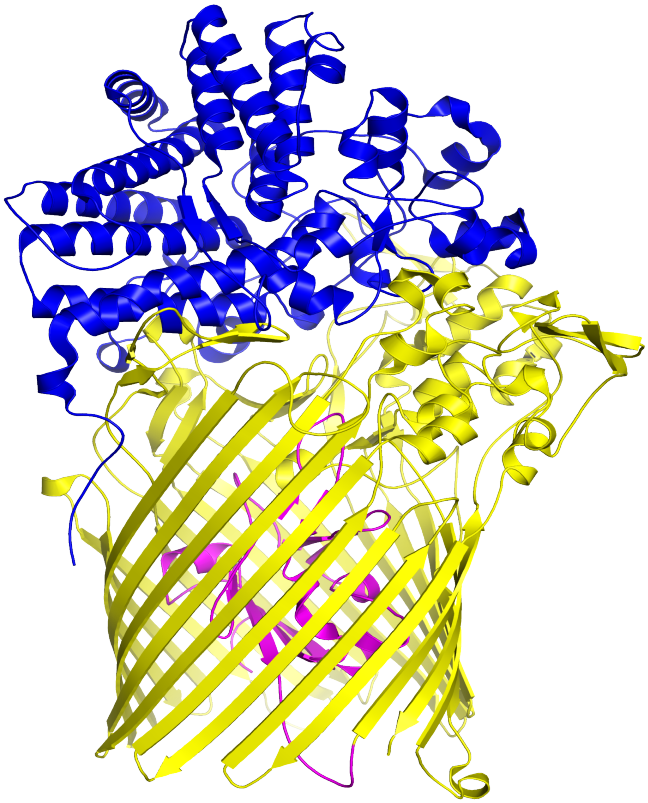

Figure 1.8: SusCD complex from *Bacteroides thetaiotaomicron.* SusC, TonB dependent transporter, in complex with the lipoprotein SusD. SusC is colored in yellow, the inner plug in magenta and SusD in blue (PDB code: 5FQ6).

1.1.5 OMPs with enzymatic activity

To date, only few outer-membrane proteins have been characterized as enzymes [61],[62]. Those OMPs have adapted to modify the outer-membrane structure as a response to external stimuli and threats [61]. For instance, OmpT porin from *E. coli,* a well-characterized member of the omptine family, is involved in the catalysis of antimicrobial peptide [63]. The x-ray structure of OmpT showed a 10 β-sheets barrel with the catalytic residues (D83, D85, D210, H212) placed at the level of the extracellular loops (Figure 1.9 A) [64]. The structural organization of the catalytic pocket is stabilized due to the interaction with the LPS, so that the LPS is considered as a cofactor of OmpT [65]. *In silico* modeling analysis have suggested that a molecules of water, located in between the residues D83 and H212, it is directly involved in the hydrolysis of the peptide bound of two consecutives basic amino acids [66].

PagP and PagL from *E. coli* are another example of enzymatic OMPs. Both porins are monomeric and 8-β-stranded and are involved in the modification of the LPS [67],[68]. Specifically, PagP and PagL undertake the palmitoylation and the deacylation of the Lipid A, respectively[69],[70]. Such modification have been linked to an increase (palmytoylation) and a decrease (deacylation) of LipidA endotoxicity [71].

OMPLA, a monomeric 12-β-stranded porin, is also involved in the LPS modification. OMPLA is a calcium-dependent phospholipase able to hydrolyze

glycerophospholipids in the outer leaflet of the outer-membrane [72]. Interestingly the monomeric form of this protein is inactive [73]. Activation of OMPLA occurs via dimerization and it is triggered by alteration of the LPS asymmetry [73],[74] (Figure 1.9 B).

Further, LpxR and LpxQ have too been identified as OMP enzymes. They are involved in the acyloxyacylation and oxidation of the Lipid A, respectively [75],[76]. No structural information is yet available for either of those enzymes.

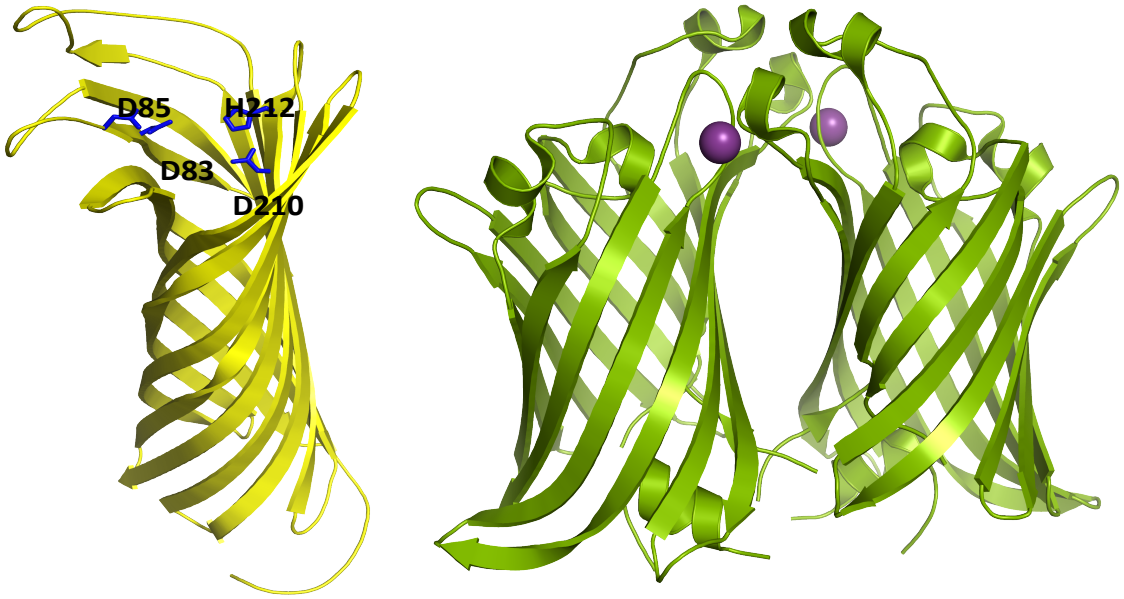

Figure 1.9: OMPs enzymes. (A) Crystal structure of OmpT is colored in yellow (PDB code: 1I78). The amino acids proposed as catalytic domain are shown in sticks and colored in blue. (B) Dimer of OMPLA (colored in pea-green) (PDB code: 1QD6). The calcium molecules are depicted as spheres and colored in purple.

1.1.6 Biosynthesis of OMPs

The biosynthesis of OMPs starts, like any other protein, in the cytoplasm. Several proteins, often associated to form multi-protein complexes, are involved in the OMPs assembly [77],[78]. Chaperones, both in the cytoplasm and in the periplasm, keep the precursors of the OMPs (pre-OMPs) unfolded [79],[80], the SEC complex allows the pre-OMPs to pass through the IM and finally the β- barrel assembly machinery, also known as BAM, fold and insert the OMPs in the OM (Figure 1.10)[81].

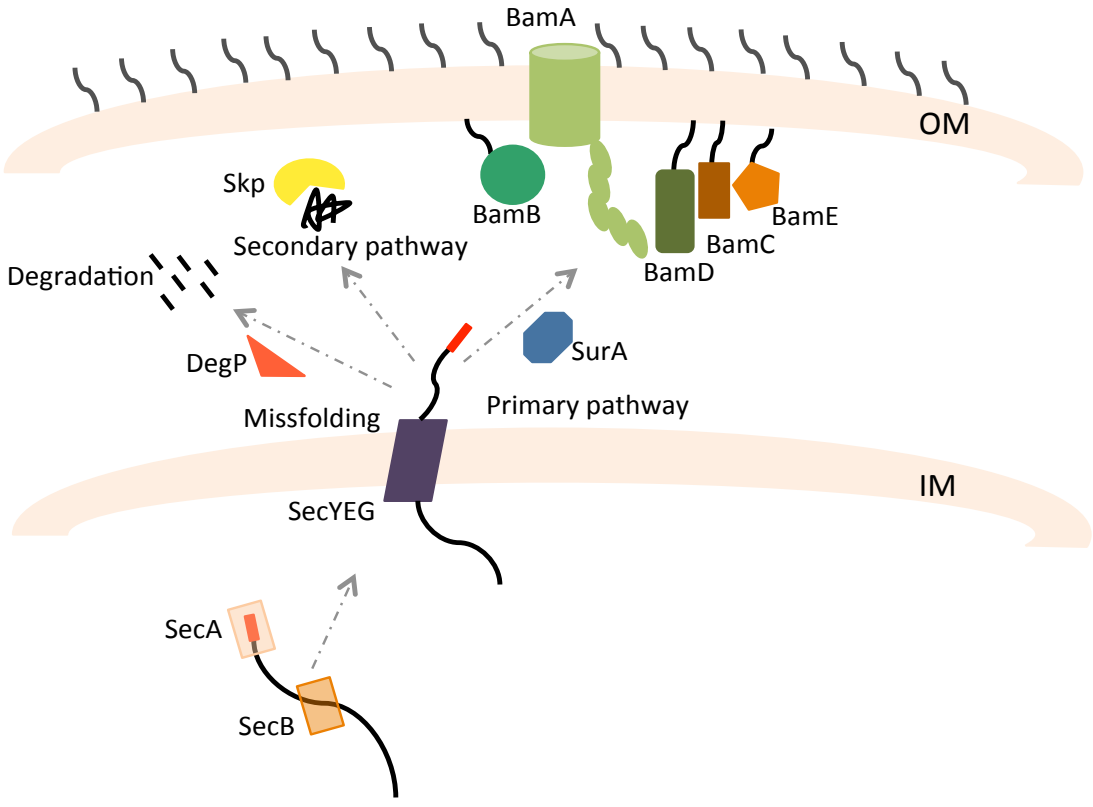

Figure 1.10: Cartoon representation of the OMPs assembly. The pre-OMPs are targeted to the IM via the SecAB complex, and reached the periplasm through the secYEG translocone. Here several chaperons bind the pre-OMPS and deliver them to the BAM complex. Figure adapted from [81]

The majority of OMPs contains a signal peptide that allows the bacteria to recognize and target the protein to the correct translocon. The signal peptide is a three-part sequence, located at N-terminus of the pre-OMPs and it is usually 18-20 amino acids long [82]. The three motifs that comprised the signal peptide are identified as n-region (at the N-terminus of the sequence), h-region (composed of hydrophobic amino acids) and c-region (at C-terminus of the sequence, often contains an A-A consensus)[83].

A two proteins complex, SecAB, is responsible to deliver the pre-OMPs to the SEC translocon [84]. SecA is an ATP-powered protein, whose role is to carry the pre-OMPs to the translocon, while the chaperon SecB which bounds the pre-OMPs in specific sequences, usually masked in the folded protein, keeps them unfolded [85].

Although the majority of the proteins cross the IM maintaining an unfolded conformation, fully folded proteins can also translocate through the IM, by using an alternative translocon, known as twin-arginine-translocase (TAT) [86]. In *E. coli* the TAT system consists of three inner membrane proteins, TatA, TatB and TatC. The signal peptide, that target the proteins to the TAT complex includes the consensus sequence Ser/Thr-Arg-Arg-(X)-Phe-Leu-Lys (with X being any polar amino acid)[86]. When the proteins reach the TAT complex, a H^+ proton gradient drives the proteins through the translocon to the periplasm [87].

The SecYEG translocon is a multi-protein complex composed of the three proteins SecY, SecE and SecG [88]. A homologue of the bacteria SEC translocon, the translocon Sec61αβγ, has been identified in Eukaryotes [89]. Although the mechanism of translocation through the SEC complex has not been fully understood, it is clear that SecA plays a major role [90]. During translocation, in fact, SecA partially insert itself through the translocon pore and through several cycle of binding and hydrolysis of ATP gives the energy necessary for the pre-OMPs to translocate [91][90].

In the SEC pathway, once the protein has crossed the IM, a signal peptidase cleaves the signal peptide and releases the pre-OMPs in the periplasm. The pre-OMPs are recognizes by different chaperons (SurA, Skp, FkpA and Spy) whose role is to keep the pre-OMPs unfolded, avoiding their aggregation [92][93]. In case of misfolded proteins, a particular chaperone with protease activity, DegP, binds and hence degrades the pre-OMPs [94]. Once the chaperons bind the pre-OMPs, they are delivered to the BAM complex.

In *E. coli* the BAM machinery is a multi-protein complex composed of BamA, an outer-membrane protein, and four lipoproteins, BamBCDE, linked to the inner leaflet by a N-terminus modification [95], [96]. BamA is a 16-β-stranded barrel with an extended periplasmic domain comprising of five repetitions of a POTRA (polypeptide-translocation-associated) domain (Figure 1.11) [97],[98]. The POTRAs present a β-α-α-β-β architecture and although structurally identical they share low sequence identity. The POTRAs domain mediates BamA and BamB

interaction. Deletion of the last three POTRAs (P3-5) is lethal for *E. coli*, but not for *Neisseria gonorrhea* [99], which implies that the importance of the single POTRAs on the bacterial viability is species-specific.

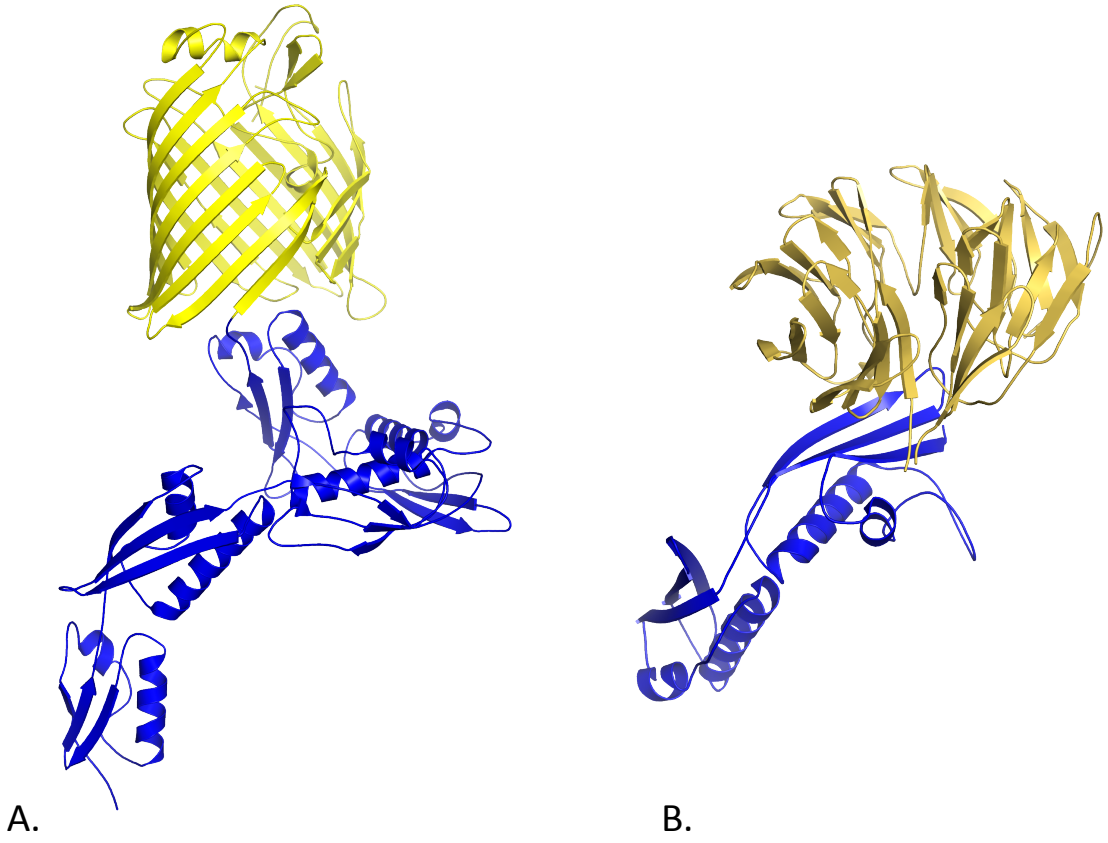

Figure 1.11: Crystal structures of BamA and BamB. (A) BamA structure is colored in yellow and POTRAs domains in blue. (B) The lipoprotein BamB in complex with P3-5 POTRAs domains of BamA (PDB codes: 4K3B and4XGA, respectively).

BamA interacts to BamC and BamE through BamD. While deletion of BamB, BamC and BamE is tolerable, deletion of BamA and BamD severely impairs the OMPs assembly leading to the bacteria death. BamA and BamD the only essential components of the BAM system [96].

Although the BAM complex has been structurally characterized, its mechanism of action has yet to be fully understood. Several *in vitro* studies, have demonstrated that most of the OMPs can spontaneously (but slowly) fold and insert themself into an artificial lipid bilayer [100] [101]. These results have brought to the idea that, *in vivo*, the BAM complex might increase the kinetic of the OMPs insertion in the OM, making the process more favorable [81]. A BAM-assisted model has therefore been proposed to explain the OMPs assembly. According to this model, the BAM complex plays a dual role: (1) to direct the OMPs to the OM and (2) to destabilize the OM and consequently facilitate the OMP insertion [102]. Nevertheless, another model, known as "BAM budding model", has also been introduced to explain the BamA-mediated insertion [103]. According to such model, the unfolded OMP would use the first β strand (β1) of BamA as a template to start the folding process. The growing OMP would therefore insert inside the BamA β-barrel, forming a BamA-preOMP intermediate complex. Eventually a lateral opening of BamA would lead the fully folded OMP to "bud" and insert into the outer-membrane [104]. Although more studies need to be conducted to elucidate this convoluted mechanism, it is likely that both mechanisms play an important role in the OMPs biogenesis and insertion [105].

1.1.7 Antibiotic resistance: role of the OM and OMPs

Antibiotic resistance has now become a real concern for public health. Particular alarming is the increasing pace at which resistance pathogens are emerging, while the Pharma industries are struggling to find new classes of antibiotics [106].

Gram-negative bacteria show "intrinsic" resistance due to the presence of the OM that act as barrier against external agents. However, hydrophobic antibiotics, such as aminoglycoside and chloramphenicol can penetrate the bacterial cell by slowly diffuse through the OM [107]. As a resistance mechanism, bacteria can modify the OM composition and hence alter its permeability. For instance, the pathogenic bacteria, *Salmonella enterica* [108], has showed the ability to adjust the composition of the LPS, following the host colonization. This mechanism is due to the presence of a two components regulatory system *PmrB-PmrA,* that regulates the expression of genes involved in the modification of the LPS [109],[110]. Such modifications include the incorporation of aminoarabinose and phosphoethanolamine to the Lipid A, which decrease the negative charge of the LPS. PmrBA system is activated by the presence of antibiotics polypeptides, such as Polymixins B or colistins, and cationic antimicrobial peptides (CAMPs)[110],[111]. Those antibiotics bind to the anionic surface of the outer-membrane and hence gain access to the bacterial cells. In polimixins-resistant strains a mutation in the PmrA gene lead to the expression of a constitutively active PmrA and therefore to an high level of amminoarabinose and phosphoethanolamine in the Lipid A, impairing the binding of polimixins [111],[112].

The number and the types of channels also determine the level of permeability of the OM, and therefore they play an important role in antibiotic resistance. It is well established that antibiotics, such as β-lactams, cefalosphorins and fluoroquinolones can cross the OM via general (non-specific) porins [113]. In pathogens, such as *P. aeruginosa,* the absence of general channels is associated with low susceptibility to antibiotics [40].

Mutations affecting the size and conductivity of the channel, modification of the level of porins expression, alongside with the complete loss of one or more general porins, are examples of how the bacteria are able to modify the OM permeability when exposed to antimicrobials agents (acquired resistance) (Figure 1.12) [114],[115].

Mutation of genes encoding for porins can lead to an altered porin expression, hence impaired antibiotic uptake. In *P. auroginosa* point mutation and/or insertion element within the gene encoding for OprD have been shown to cause an early termination of the translation process and therefore a total loss of the porin. Clinic isolates carrying such mutation exhibit high level of resistance to carbapenems. Likewise, in *E. Cloacae*, mutation of the promoter regulating the expression of Ompk35 leads to a significantly reduction of the expression levels (up to 20-fold less expressed), causing a decreased ertapenem susceptibility.
Antibiotics resistance can also be linked to mutations within genes involved in the regulation of porins, as well as efflux pumps, expression [116]. *MarA, SoxS* and *Rob* are transcriptional regulators highly conserved in the Gram-negative bacteria

[117],[118],[119]. Those genes are activated by several external stimuli, such us oxidative stress, pH changes and antibiotics [120]. Once activated, they up-regulate the expressions of efflux pumps, such as TolC-AcrAB and small RNAs like *micF* and down-regulate the expression of porins such as OmpF [121],[122][123]. Point mutation, insertion element and deletion of those genes lead to a MDR phenotype and to an increased minimum inhibitory concentration (MIC) for different classes of antibiotics[116], [124],.

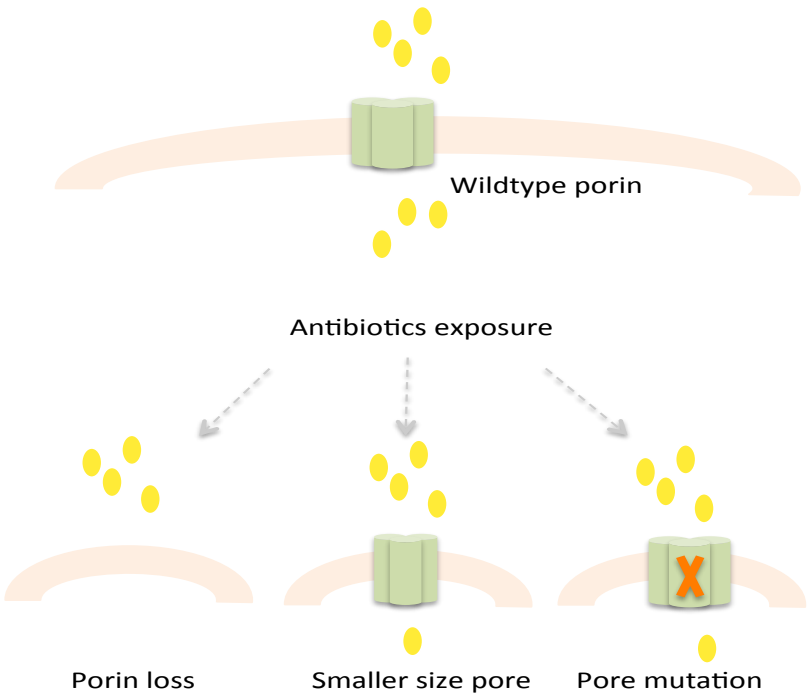

Figure 1.12: Schematic representation of porins regulation under antibiotics pressure. Antibiotics exposure leads the bacteria to alter the permeability of the OM, by modifying the expression level of its porins. Picture adapted from [115].

Mutation of amino acids located in the loop 3 has also been associated to a decreasing antibiotic susceptibility [125]. G119D mutation in OmpF and similarly G112D mutation in Omp36 from *Enterobacter aerogene* and D116A mutation in OmpU from *Vibro cholera* have been found in clinic isolates resistant to β-lactams and cefalosphorins [22], [126]. In most organisms, different mechanisms synergistically function to protect the bacterial cell from the effect of antibiotics. In this phenomenon, known as MIC creep, alongside an altered OM the bacteria would increase the expression of efflux pumps (thus decrease the amount of antibiotic inside the cells) and increase the production of enzymes targeting the antibiotics (impeding their functions) [115].

Chapter 2: Major outer-membrane protein (MOMP) from *Campylobacter jejuni*

2.1 Introduction

2.1.1 Campylobacter: an overview

First isolated in 1913 from an aborted lamb, *Campylobacters* were originally wrongly classified in the genus *Vibrio* (*Vibrio fetus*), and they were subsequently identified as a new genus (*Campylobacter)* in 1973 [127]. To date 15 species and 6 subspecies (both commensal and pathogenic) have been annotated [128].

Campylobacter spp. are gram-negative bacteria belonging to the class of ε-proteobacteria [129]. Usually spiral or curve shaped, *Campylobacter spp* are motile by means of a single or bipolar flagellum [129]. They belong to the group of microaerophilic and thermophilic bacteria, meaning that a modified atmosphere with a low concentration of oxygen and a high concentration of CO_2, as well as high temperatures (37-44°C), are necessary for optimal growth [6], [131],[132]. Growth at lower temperatures has been proven to be slow [132].

Particular metabolic characteristics distinguish *Campylobacter* from other gram-negative bacteria [133],[134]. Campylobacter species are incapable of using glucose or other carbohydrates as sources of energy due to the lack of the glycolytic enzyme 6-phosphofructokinase [135]. Thus, organic acids, as well as amino acids, such as serine, proline and glutamic acid represent their main source of energy [136][137][138]. In certain strains of *C. jejuni*, however, an L-fucose pathway has been identified but not yet fully characterized [139]. Accordingly, gluconeogenesis appears to be fundamental for the production of glucose and

glucose-derivatives that are essential for lipopolysaccharide (LPS) and capsule biosynthesis and hence campylobacter virulence [134].

2.1.2 Campylobacter jejuni infection

C. jejuni and, to a lesser extent, *Campylobacter coli* have been recognized as the main cause of bacterial gastroenteritis (campylobacteriosis) in both developed and undeveloped countries [140],[141],[142]. In recent years, other *Campylobacter* species, including *C. concisus*, *C. ureolyticus*, *C. upsaliensis* and *C. lari,* have been associated with gastrointestinal infections and have been classified as "emerging pathogens" [143]. Although *C. jejuni* has been isolated from a wide range of organisms, avians (poultry in particular) are considered to be the main reservoir [144]. Undercooked, contaminated poultry represents the primary source for human infections. Contaminated water and unpasteurized milk can also lead to infections, while human-to-human contamination is rare [145]. Motility, cell adhesion and cell invasion are critical factors that mediate *C. jejuni* virulence. In particular, the flagellum plays a central role in host colonization [146]. Classified as a Type 3 secretion system (T3SS), this motile structure has been shown to be responsible for the secretion of virulence factors inside the cytosol of its host [147]. Additionally, several proteins located on the surface of the bacteria contribute to the adhesion to the epithelium, enhancing *C. jejuni* virulence [148]. Usually the symptoms of the infection arise within 3 days after ingestion of contaminated food, with symptoms lasting, on average, 5-6 days. Commonly, people (in most cases children) infected with *C. jejuni* experience

abdominal cramps, bloody or watery diarrhea, weight loss and fever [144]. *Campylobacter* infections are normally self-limiting, however, in immunocompromised patients, or when the symptoms persevere, the use of antibiotics is required. Untreated campylobacteriosis can progress to irritable bowel diseases (IBDs) such as Crohn's syndrome and ulcerative colitis [149]. In rare cases, infected individuals can also develop paralysis through Guillan-barre syndrome (GBS) or, its related form, Fisher syndrome (FS) [150],[151],[152]. GBS is a neuropathy affecting the peripheral nerves, leading to paralysis of the lower and, occasionally, the upper part of the body. GBS preceded by campylobacteriosis is caused by a so-called molecular mimicry mechanism [153][154][155]. This is due to the fact that the lipooligosaccharide (LOS) structure of *C. jejuni* resembles the organization of the human ganglioside (Figure 2.1). Therefore during the infection, antibodies against *C. jejuni* can cross react with the peripheral nerves resulting in their demyelization [153]. Recent studies have also suggested that components of *C. jejuni* capsule and heat shock proteins (HSP) might have a role in GBS susceptibility associated with *C. jejuni* [156].

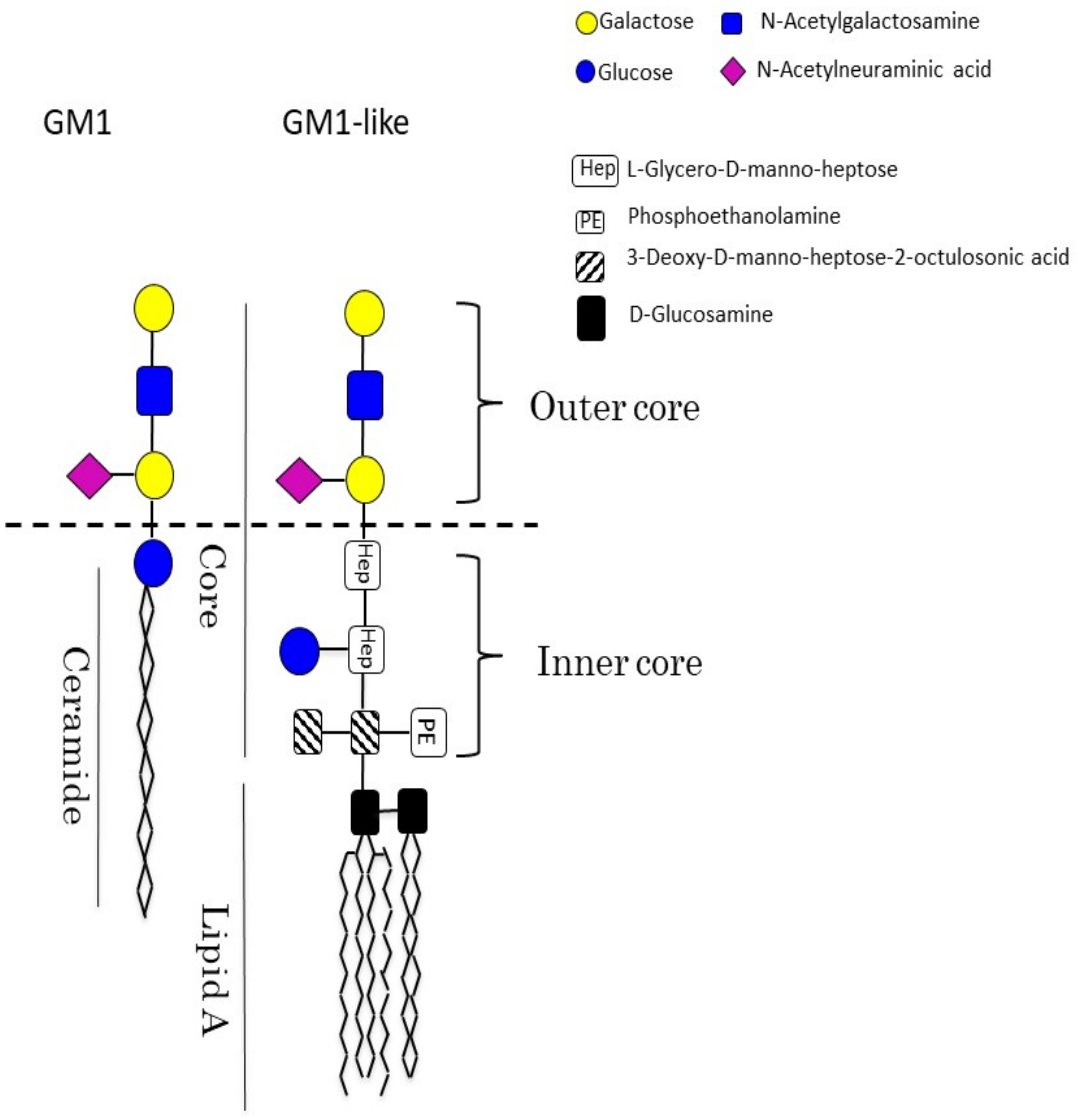

Figure 2.1: Mimicry mechanism in GBS associated to *C. jejuni*. Schematic representation of human ganglosides GM1 and *C. jejuni* LOS. Figure adapted from [29].

2.1.3 Campylobacter jejuni antibiotic resistance

Antibiotic resistance in *C. jejuni* has become a real concern in public health. As *Campylobacter* contamination among people is rare, the use of antibiotics in animal farming is considered to be the main cause of resistance [157]. Although the European Union has prohibited the addition of antibiotics in animal feed for non-therapeutic purpose (i.e. growth promotion of livestock), in other part of the world, the use of antibiotics as growth agents is still allowed [158]. *C. jejuni* strains isolated from contaminated poultry have shown resistance to different classes of antibiotics such as fluoroquinolone (FQ), macrolide [159], β-lactam and tetracycline [160][161][162] (Figure 2.2). A multi-drug resistance (MDR) phenotype has also been observed [163][164]. The macrolide erythromycin (Ery) is used as first choice treatment when campylobacteryosis is diagnosed. However, as campylobacteryosis is indistinguishable from other enteric infections, Ciprofloxacin – an FQ with a broad spectrum activity against Gram-negative bacteria – is often preferred [160].

Antibiotic resistance in *C. jejuni* (as in other bacteria) is caused mainly by three mechanisms: (i) Low OM permeability (ii) target alteration (ribosome, gene mutation) and (iii) active efflux of antibiotics (CmeABC)[165],[166],[167]. Most antibiotics enter the cell via non-specific porins. In general, porins govern the translocation of antibiotics depending on the charge and the size of their pores [14]. In *E. coli*, two outer membrane proteins, OmpC and OmpF are predominant. In resistant clinical isolates, expression of OmpF (higher conductance) is down regulated whilst expression of OmpC (lower conductance) is up regulated,

therefore translocation of antibiotics is decreased [125]. Unlike *E. coli*, *C. jejuni* has only one major outer membrane protein (MOMP), which has a molecular weight limit of 360 Da, thus molecules with higher molecular weight cannot permeate inside the cell [168]. Additionally, being cationic selective, MOMP represent a barrier for translocation of anionic antibiotics [168].

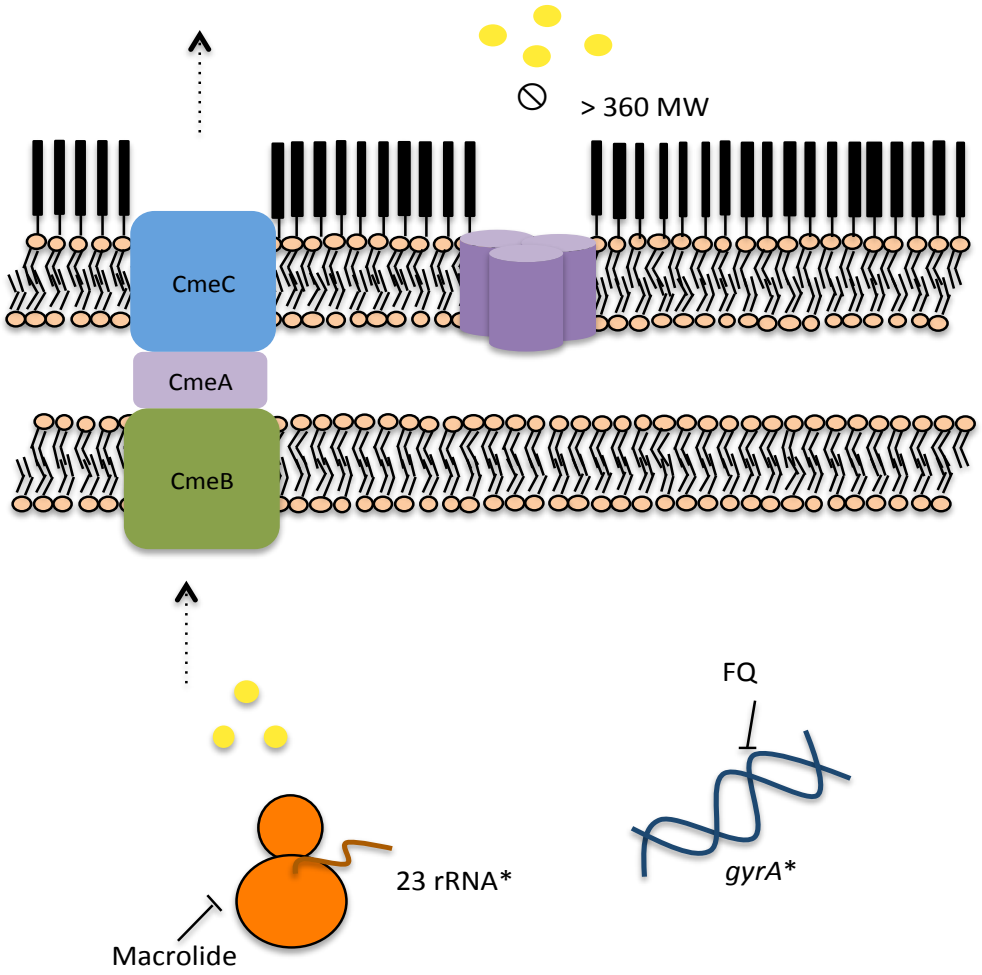

Figure 2.1: *C. jejuni* antibiotic resistance. Schematic representation of *C. jejuni* mechanisms of antibiotic resistance.

2.1.4 Major outer membrane protein (MOMP)

In the early 80's, Logan and Trust identified a putative porin encoded by *PorA,* of an apparent molecular weight of 45 KDa located in the outer membrane of *C. jejuni* [169]. This protein was largely expressed in the OM, and therefore named as major outer membrane protein (MOMP). Predictions of the tertiary structure suggested that MOMP resembled the typical architecture of an outer-membrane porin, with an 18 β-strands barrel connected by loops and turns [170]. The presence of β-sheets structures was suggested by circular dichroism (CD) analysis [171],[172]. Additionally, examination of the amino acid composition showed that MOMP was comparable to the two major porins in *E. coli*, OmpC and OmpF. The N-terminal of MOMP, however, displayed significant differences [173]. MOMP, in vivo, adopts a trimeric arrangement, as shown in electron microscopic (EM) experiments [174]. In solution, detergents and temperature have been suggested to influence oligomerization. Extraction with increasing concentrations of SDS and heating over 60 °C leads to dissociation of the trimer into folded monomers. Both folded monomer and the trimer can be identified by SDS-PAGE at 35 kDa and 140 kDa, respectively. Increasing the temperature up to 96 °C has been shown to cause a shift from a folded to an unfolded monomer, which is, instead, identified at 45 kDa [171]. A similar behavior was described for the trimeric porin PhoE from *E. coli*[175]. Both oligomeric states displayed pore activity when tested in single channel experiments (with a conductance of 400 pS for the monomer and 1200 pS for the trimer) [176]. *In vitro*, MOMP has been shown to participate in the adhesion of *C. jejuni* to human epithelial cells [177],[178],[179].

Surface exposed antigens stimulate the immune system to produce antibodies [180]. In chicks, maternal antibodies have been proven to serve as protection against *C. jejuni* infections [181]. This inspired the idea to use *C. jejuni* surface proteins as a target to develop vaccines. However, in chickens and mice models, immunization using CmeC subunit, the lipoprotein CjaA and PEB1 antigen (all surface-exposed proteins), have failed to protect from *C. jejuni* colonization [182],[183],[184]. On the contrary, MOMP-derived vaccines have shown promise. MOMP contains antigenically variable regions at the level of the loops and conserved regions present in the β-strands [170]. Islam and co-workers have already shown the protective effect of a recombinant MOMP-vaccine tested in mice models[185]. This study can be used as a starting point to generate a vaccine for human use. Given that *C. jejuni* live attenuated vaccines could potentially trigger auto-immune diseases, the use of a MOMP-derived vaccines would represent a safer alternative.

2.1.5 Aims

Although MOMP from *C. jejuni* has been extensively studied over the last three decades, only recently its crystal structure has became available (the structure was solved by Dr. Gregor Wallat for Naismith's lab). Being *C. jejuni* a fastidious organism to cultivate, Dr. Wallat successfully over-expressed and purified MOMP from *E. coli.*

However, the LPS of *C. jejuni*, differs from the one of *E. coli*, with a smooth or a rough O-antigen phenotype. To address concern about the effect of the LPS on the

organization of the MOMP structure, we set up to purify, solve the X-ray structure of MOMP natively expressed in *C. jejuni* and to compare it to the structure obtained by Dr. Wallat. We also aimed to functionally characterize MOMP (both native and recombinantly expressed) and explore the role of the calcium found at the constriction zone of MOMP. (Dr Wallat solved the structure at the end of his PhD, no analysis was carried out).

2.2 Material and Methods

2.2.1Campylobacter jejuni culture

Campylobacter jejuni 85H strain [45] was grown according to Bolla *et al.* [171]. The *C. jejuni* strain was spread onto a blood agar plate and incubated for 24 hours at 42 °C. Bacteria were rinsed with 1 ml of 2YT medium and agitated for 15 minutes. Subsequently, 250 µl of the recovered bacteria were spread onto 4 Columbia agar plates supplemented with the appropriate amount of *Campylobacter* selective antibiotics supplement (Oxoid), and incubated for 48 hours at 42 °C. The plates were rinsed with 1 ml of 2YT medium and left rocking for 15 minutes. The recovered bacteria were subsequently inoculated onto 40 plates of Columbia agar (antibiotic-free) and incubated for 48 hours at 42 °C. Each plate was then rinsed using 5 ml of 10 mM Tris-EDTA (TE) buffer pH 7.4 and agitated for 15 minutes at room temperature. The bacterial suspension was recovered and the OD_{600} checked to be around 2. The bacteria were pelleted by centrifugation at 10,000xg for 30 minutes at 4 °C. The pellet was re-suspended in 200 ml of 200 mM Glycine-HCl pH 2.2 and agitated for 15 minutes. Bacteria were harvested by centrifugation at 10,000xg for 30 minutes and washed twice with 100 mM Tris-HCl pH 7.4. Cell paste was then immediately processed for further purification or stored at –80 °C.

2.2.2 MOMP 85H purification

Cells were re-suspended in 300 ml of lysing buffer (Appendix A.1) and lysed by using two passes at 30 Kpsi through a high-pressure cell disruption for micro volumes (Constant System Ltd). Unbroken cells were removed by spinning the cell lysate at 10,000xg for 30 minutes at 4 °C. Membranes were recovered by ultracentrifugation of the supernatant at 100,000 x g for 1 hour at 4 °C. The pellet was then homogenized in 10 mM Tris-HCl pH 7.4 and 0.1% (w/v) of sodium lauryl sarcosinate (Sigma) and left rocking for 30 minutes at 4 °C. The outer membrane was recovered by ultracentrifugation at 100,000xg for 1 hour at 4 °C. The supernatant containing the inner membrane proteins fraction was discarded and the pellet was homogenized with 20 mM sodium phosphate buffer pH 7.4 and 1% of n-octylpolyoxyethylene (Octyl-POE) (Bachem AG) and left rocking at 4 °C for 30 minutes. Solubilized outer membrane proteins were recovered by ultracentrifugation at 100,000xg for 1 hour at 4 °C. At this stage, the pellet was discarded and the supernatant was loaded onto a MonoQ HR ion exchange column (GE Healthcare) and equilibrated with 5 column volumes (CV) of buffer A (30 mM Na_2HPO_4, 10 mM NaCl and 0.6% Octyl-POE). The bound proteins were eluted stepwise with 5, 12, 20, 70 and 100% of buffer A supplemented with 1 M NaCl (Appendix A.1). The chromatography was performed on ÄKTA Explorer 10 system (GE Healthcare). Each fraction was examined with SDS-PAGE and Western blot with specific antibodies to test both purity and identity. Eluted fractions containing MOMP were collected and concentrated to 5 ml and injected onto a Superdex 200 16/60 GL (GE Healthcare) column equilibrated with 2 CV of 10 mM Tris-HCl pH 8.0, 150 mM NaCl and 0.45% (w/v) of tetraethylene glycol monooctyl

ether (C_8E_4) (Bachem). Fractions containing MOMP were combined and concentrated to 10 mg ml^{-1}.

2.2.3 MOMP 85H crystallization

Initial crystallization trials were carried out using several commercial screens (Appendix B). The screens were dispensed into a 96-well sitting drop plate (Intelli-Plate®, ARI) using a Gryphon robot, at a protein:reservoir ratio of 1:1 and 1:2. First hits appeared within a week. Crystals were manually optimized by the hanging-drop vapor diffusion technique.

MOMP 85H was crystallized in 0.05 M calcium chloride, 0.05 M barium chloride, 0.1 M Tris-HCl pH 7.5 and 32% (v/v) PEG 400. Different ranges of pH and PEG concentrations were tested in order to obtain larger crystals. The best crystals grew in 0.05 M calcium chloride, 0.05 M barium chloride, 0.1 M Tris-HCl pH 8 and 30% (v/v) PEG 400 (Table 2.1). Crystals were harvested and flash cooled in liquid nitrogen prior data collection. No cryoprotectant was added.

Table 2.1. Optimization of MOMP crystallization conditions.

0.1 M Tris-HCl+
0.05 M $CaCl_2$+ 0.05 $BaCl_2$

PEG 400 (v/v)

	pH 7	**pH 7.5**	**pH 8**	**pH 8.5**
30%	A1	A2	A3	A4
31%	B1	B2	B3	B4
32%	C1	C2	C3	C4

2.2.4 Data collection, Structure determination and refinement

X-ray data from a crystal of MOMP purified from *C. jejuni* 85H were collected in house using a Rigaku Micromax™-007HF Cu anode with VariMax optics and a Rigaku Saturn 944+CCD detector and processed with Xia2 [186]. The structure was solved to a resolution of 2.9 Å by molecular replacement using the recombinant MOMP structure (PDB code: 5LDV) as a search model using the program MR Phaser [187] . The model was manually built in Coot [188] and refined with REFMAC5 [189]. Eventually, 15 TLS groups were used in the final refinement cycle. The webserver "CheckmyMetal" [190] was used to validate the presence of calcium molecules at the constriction zone of the protein.

2.2.5 Single channel conductance measurements of MOMP

A planar lipid bilayer was formed using the solvent free lipid bilayer technique [191]. Briefly, the cuvettes used for experiments consist of two separate chambers, named *cis* and *trans*. A 25-µm thick Teflon film (Goodfellow) with an aperture of 40–100 µm diameter is located in between the chambers (Figure 2.3). The aperture in the Teflon film was made by using a high voltage cathode discharge (ElectrotechniProducts). The aperture was pre-painted with 1 µl of 1% hexadecane in hexane using a pipette tip. The chambers were filled with electrolyte solution consisting 1 M KCl, 10 mM MES pH 6.0 to a total solution volume of 2.5 ml. Then, 5% solution of diphytanoyl phosphatidylcholine (DPhPC, Avanti Polar Lipids) was added to both chambers. At this point, the solution was slowly pipetted up and down to allow the formation of the bilayer. MOMP was added to the *cis* side (which is the electrical ground) of the chamber at a final concentration of 2-3 ng ml^{-1} and the channel insertion was eased by quickly mixing the solution contained in the chamber while applying a trans-membrane potential of –199 mV. Electrical recordings were made through a pair of $Ag/AgCl_2$ electrodes (World Precision Instruments) attached to an Axon Instruments 200B amplifier (Axon Instruments Inc.). A low pass Bessel filter at 10 kHz was used to filter the data and saved with a sampling frequency of 50 kHz. Data analyses were performed using Clampfit 10.0 software (Axon Instruments Inc).

Single channel measurements were also performed in presence of divalent ions. In this case, the buffer was supplemented with 10 mM of $CaCl_2$, $MgCl_2$ or $ZnCl_2$.

Additionally, measurements were taken in the presence of 10 mM of the chelating agent ethylene glycol-bis (β-aminoethyl ether)-N,N,N',N'-tetraacetic acid (EGTA). The protein was incubated overnight with 10 mM EGTA.

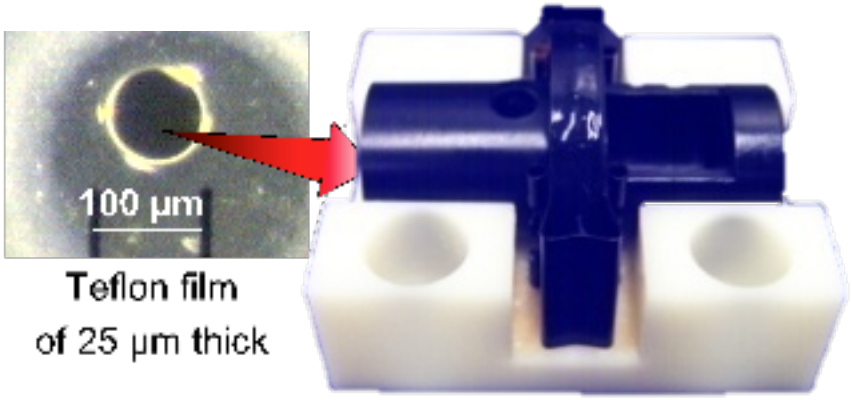

Figure 2.2: Single channel experiments cuvette. Picture of the cuvette used for single channel experiments. On the left particular of the Teflon film aperture placed between the two chambers.

2.3 Results

2.3.1 Campylobacter jejuni 85H culture preparation

Campylobacter jejuni bacteria were spread onto selective blood-agar plates and grown under microaerophilic condition at 42 °C. At an OD_{600} of 2, the bacteria were harvested by centrifugation. Due to a particular pigment produced by Campylobacter, the cell paste displayed a pink coloration.

2.3.2 MOMP extraction and purification

MOMP from the native *Campylobacter jejuni* was purified as described in Bolla *et al*. [173] and yielded 1 mg of protein per 3 g of cell paste. A canonical two step extraction protocol was used in order to separate inner and outer-membrane proteins. MOMP purification was carried out using an anion-exchange chromatography followed by size exclusion chromatography. The anion-exchange chromatogram showed two peaks eluting at 22% and 70% buffer B. Fractions from both peaks were run on an SDS PAGE, and visualized using Coomassie blue stain. The SDS-PAGE showed that the expected two bands, at 45 kDa and at 50 kDa, were present in the fractions eluting at 22% buffer B (Figure 2.4 A lane 1-4). Mass-spectrometry analysis identified the band at 45 kDa as MOMP, and the band at 50kDa as Omp50 (see chapter 3). The majority of MOMP, however eluted at 70% buffer B (Figure 2.4 A lane 5-9). Only the fractions containing MOMP (and not Omp50) where used for further purification. During the size exclusion chromatography Octyl-POE was exchanged to C_8E_4, a more suitable detergent for

crystallography experiments. The eluted protein was then concentrated to 10 mg ml^{-1}. SDS -PAGE was run to evaluate the purity of the protein (Figure 2.4 B). Gel bands were sent for mass spectrometry (MS) to confirm the identity of the protein.

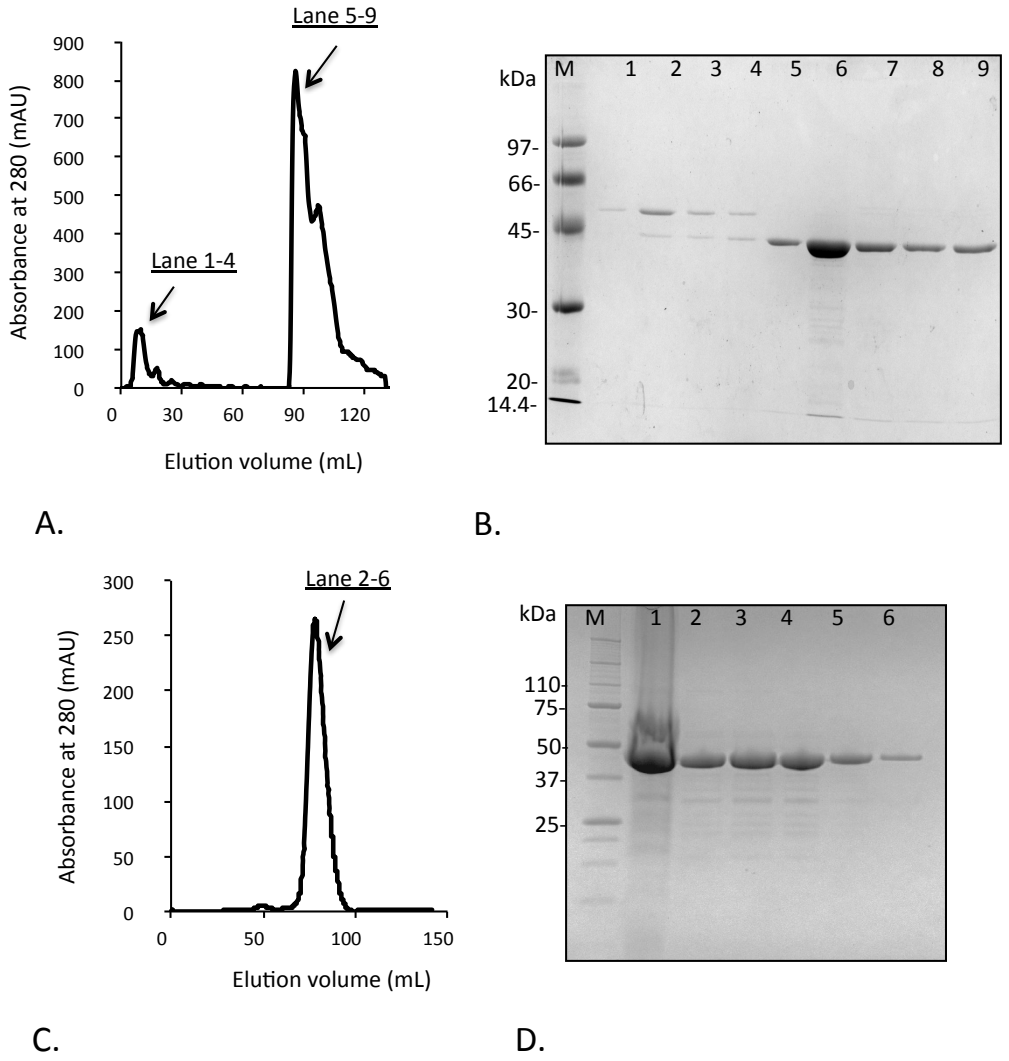

Figure 2.3: MOMP purification. (A). Profile of the anion-exchange chromatography. Two peaks are present: one on the left elutes at 22% buffer B, and the second on the right elutes at 70% buffer B. (B). SDS-PAGE of chosen fractions from the anion-exchange chromatography. M is the ladder, lanes 1-4 show two bands: one at 50 kDa (Omp50) and one at 45 kDa as confirmed by mass spectrometry. C. Profile of the SEC performed using a 16/600 200pg (GE) column. The elution volume of MOMP was compared to the elution volumes of molecular weight (MW) markers (Bio-rad) (used to calibrate the column) in order to analyse its oligomeric state. MOMP was found to be trimeric. (D) SDS-PAGE of chosen fractions from the SEC. M is the ladder, lane 1 is the sample before SEC and lanes 2 to 6 are fractions from the main peak.

2.3.3 MOMP crystallization and structure determination

The MOMP crystals appeared after three days. Crystals were found in condition B3 of the Mem Gold I crystallization screening (Molecular dimension). After optimization using the hanging drop vapor technique, the largest crystals were found in 0.05M Calcium chloride, 0.05 M barium chloride, 0.1 M Tris-HCl pH 8.5 and 30% PEG 400 (Figure 2.5). The crystals were analyzed with an in house X-ray source and found to diffract to 2.9 Å. A dataset was collected and processed using Xia2 [186] in the space group $P2_12_12_1$. Analysis of the Matthew's coefficient (Matthew's coefficient of 2.64) suggested that three molecules were present in the asymmetric unit (AS). The structure was solved by molecular replacement using MR Phaser from the CCP4 suite [187]. As search model was used the recombinantly expressed MOMP (PDB code: 5LDV). The quality of the structure was assessed using Molprobity. Data collection and refinement statistics are shown in table 2.2.

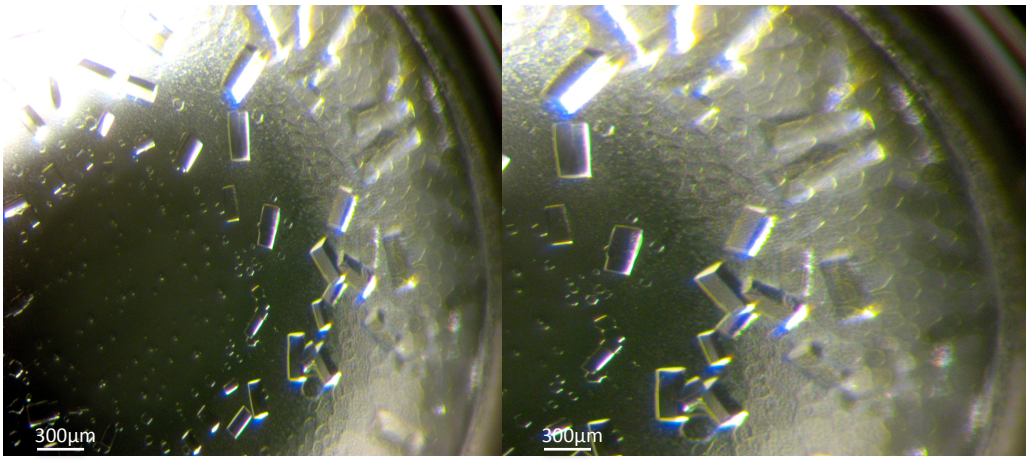

Figure 2.4: MOMP crystals. Crystals of MOMP under visible light. Crystals grew using hanging drop vapor technique.

Table 2.2. Data collection, refinement and validation statistics.

Space group	**$P2_12_12_1$**
Cell dimensions a,b,c (Å)	**94.4, 99.4,172.2**
Cell dimensions α,β,γ (°)	**90, 90, 90**
Resolution (Å)	**47.75-2.9(3.06-2.9)**
R_{merge}	**0.14 (0.86)**
Completeness (%)	**99.9 (99.8)**
Multiplicity	**7.3 (7.2)**
I/σ(I)	**12.9 (3.0)**
CC 1/2	**0.9 (0.7)**
Refinement	
R_{factor}/R_{free} (%)	**23.9/27.1**
N° of unique reflections	**36693**
N° of residues	**405**
Water	**5**
Rmsd	
Bonds length (Å)	**0.01**
Bonds angles (Å)	**1.9**
MolProbity	
Ramachandran outliers (%)	**0**
Ramachandran favored (%)	**95.41**
Clash score	**1.7**
Molprobity score	**1.68**

**(Values in parentheses are for the highest-resolution shell)*

2.3.4 Crystal structure of MOMP

MOMP is a homotrimer composed of 18-β-stranded monomers, with a characteristic elliptical shape. Each monomer consists of 405 amino acids. Common for porins, the β-strands (β) are linked together by long extracellular loops (L) and short periplasmic turns (T) (Figure 2.6 A). As predicted by the software SignalP 4.0 [192], the signal peptide of the native MOMP was cleaved between Ala22 and Thr23. Consequently, the Thr23 is the first residue in the tertiary structure and as such was renumbered to Thr1.

L3, L4, L6 fold back inside the barrel forming the so-called constriction zone (Figure 2.6 B). As is common for porins, the constriction zone of MOMP is characterized of negatively charged residues (located in the L3) interacting with positively charged residues located in the wall of the barrel, at the front of the loop. L2 is involved in the stabilization of the trimer. Accordingly, analysis performed using the web server PDBePISA showed that several hydrogen bonds were formed between L2 and the β- sheets of the adjacent monomer, in particular with β4, β5, β6 and β7.

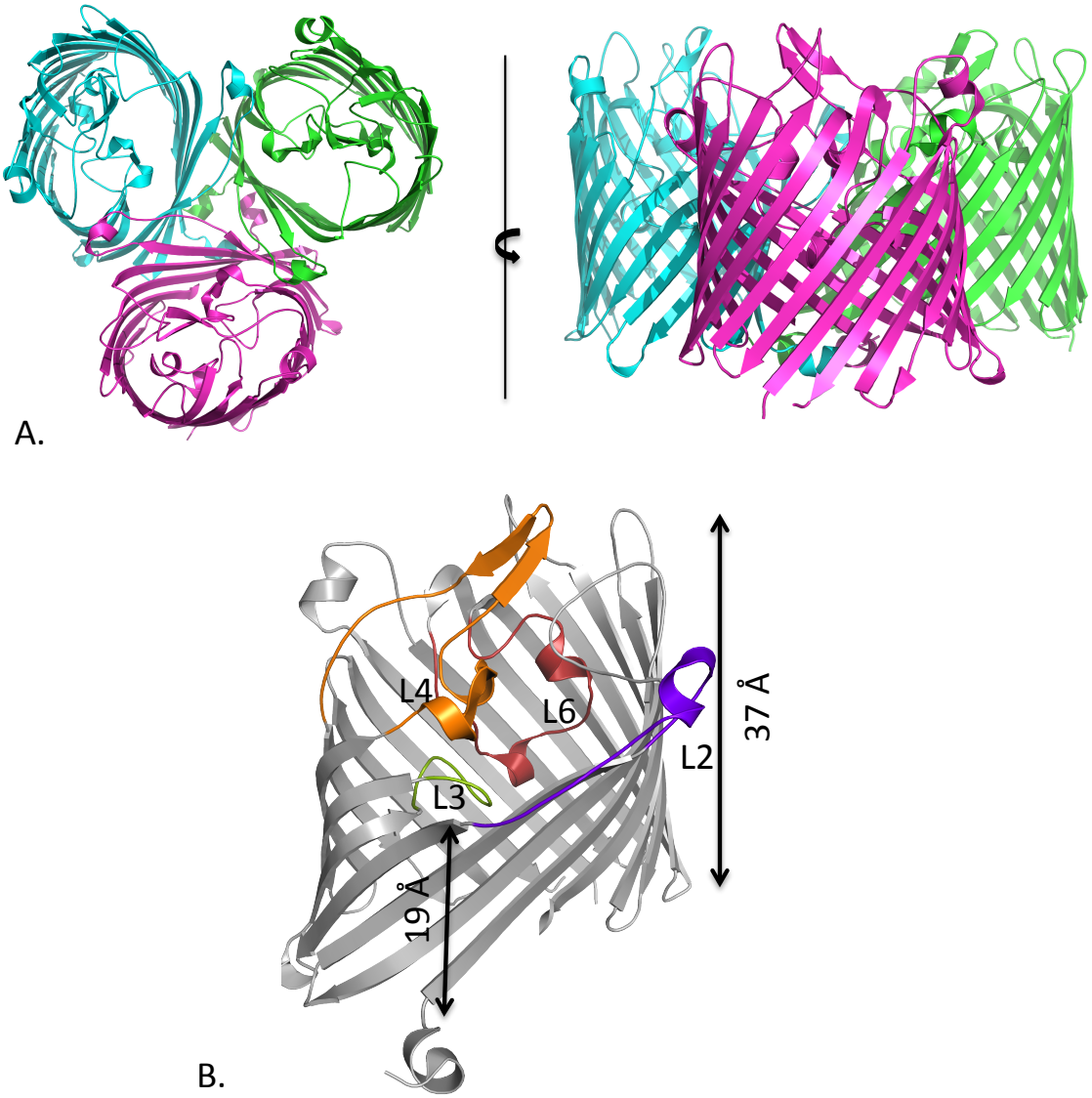

Figure 2.5: Crystal structure of MOMP. (A) Cartoon of MOMP trimer view from the extracellular space (left) and from the side (right) of the membrane. The three chain are colored in magenta, green and cyan. (B) Monomer of MOMP, with highlighted loops involved in the formation of the constriction zone and L2. L3 is colored in green, L4 in orange, L6 in cherry red and L2 in purple. Major and minor axis measure approximately 37 and 19 Å, respectively.

8 amino acids (Thr1 to Lys8) at the N-terminus form an α-helix that points away from the barrel wall, toward the adjacent monomer. In this way, the three α-helices (one for each monomer) form a triangle that faces the periplasmic space (Figure 2.7).

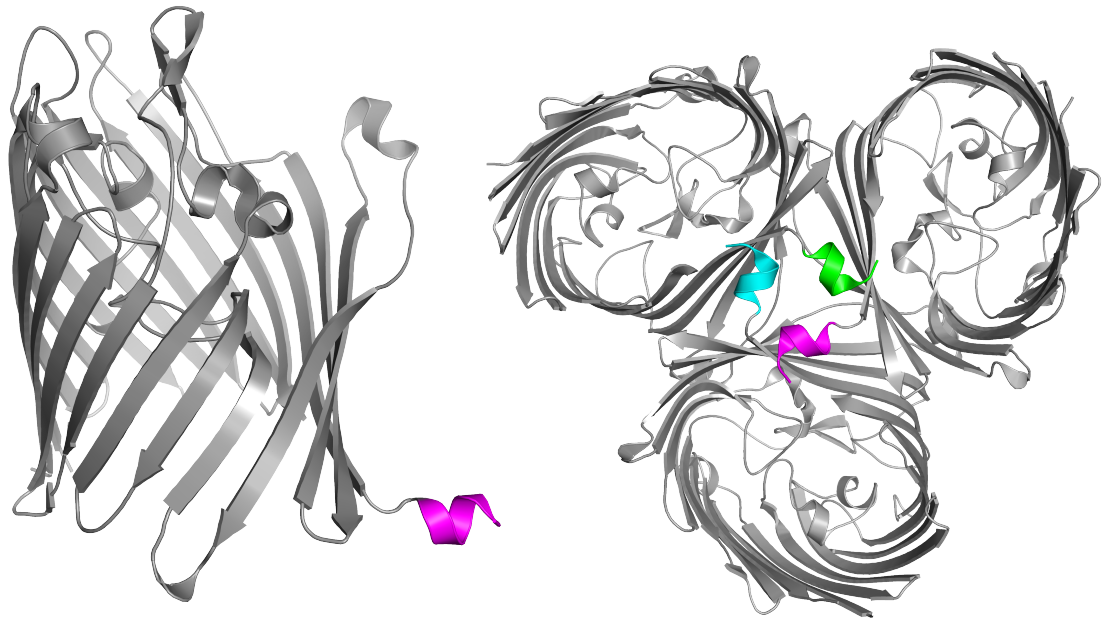

A. B.

Figure 2.6: N-terminus of MOMP. (A) In grey is depicted the MOMP monomer, in magenta the N-terminus. (B) Periplasmic view of the N-terminus complex (color scheme as in 2.5) in MOMP trimer.

2.3.5 The electrostatic potential of MOMP

The electrostatic potential of MOMP was analyzed using CCP4mg program [193]. The eyelet, viewed from the extra-cellular (EX) (Figure 2.8 A) and periplasmic (PE) (Figure 2.8 B) side, exhibited a clear separation of positive and negative charges with Asp116 (L3), Asp 120 (L3) and Asp155 (L4) facing Arg17, Arg19 and Lys43 on the opposite side.

Both the extra-cellular loops and the periplasmic turns of MOMP displayed charged residues (positive and negative), whereas the outside of the barrel, as expected for proteins, embedded in a hydrophobic lipidic bilayer and was uncharged (Figure 2.8 C-D).

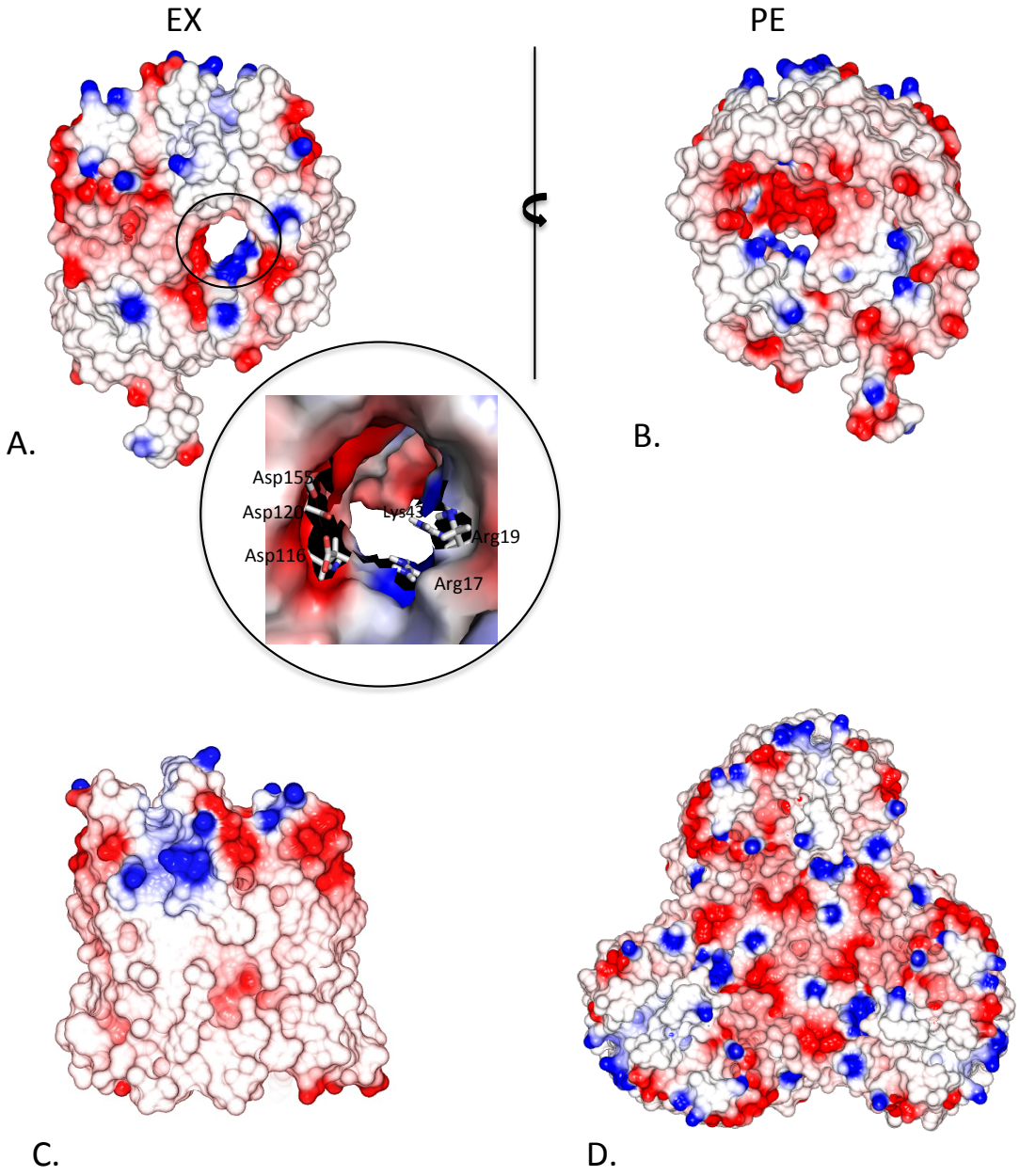

Figure 2.7: Electric potential of MOMP. (A) View of the channel from the extra-cellular space. In the black circle is a zoom in of the eyelet. The charged amino acids forming the eyelet are in sticks. (B) View of the channel from the periplasmic space. (C) View of the channel from the side. (D) View of the trimeric MOMP from the extra-cellular space.

2.3.6 Calcium binding sites in MOMP

Two calcium-binding sites were identified in MOMP, one inside the channel at the level of the constriction zone, and the other one outside the β-barrel at the interfaces between monomers (Figure 2.9 A). At the constriction zone, the metal ion is coordinated by the residues Asp120 (L3) (oxygen and side chain), Gln152 (L4), Asp155 (L4), and Glu288 (L6). A water molecule fills the last position and is in turn coordinated by Asp116 (L3) and Asp289 (L6). The ion has a typical octahedral coordination and creates a bond across L3, L4 and L6 (Fig. 2.9 B). The second calcium ion is instead coordinated by the residues Asp145 (β6) (oxygen and side chain), Asn180 (L4) and Gly72 and Asp77 (both L2) from the adjacent monomer (Figure 2.9 C). The webserver CheckmyMetal confirmed the presence of both the calcium-binding site [190] (Table 2.3).

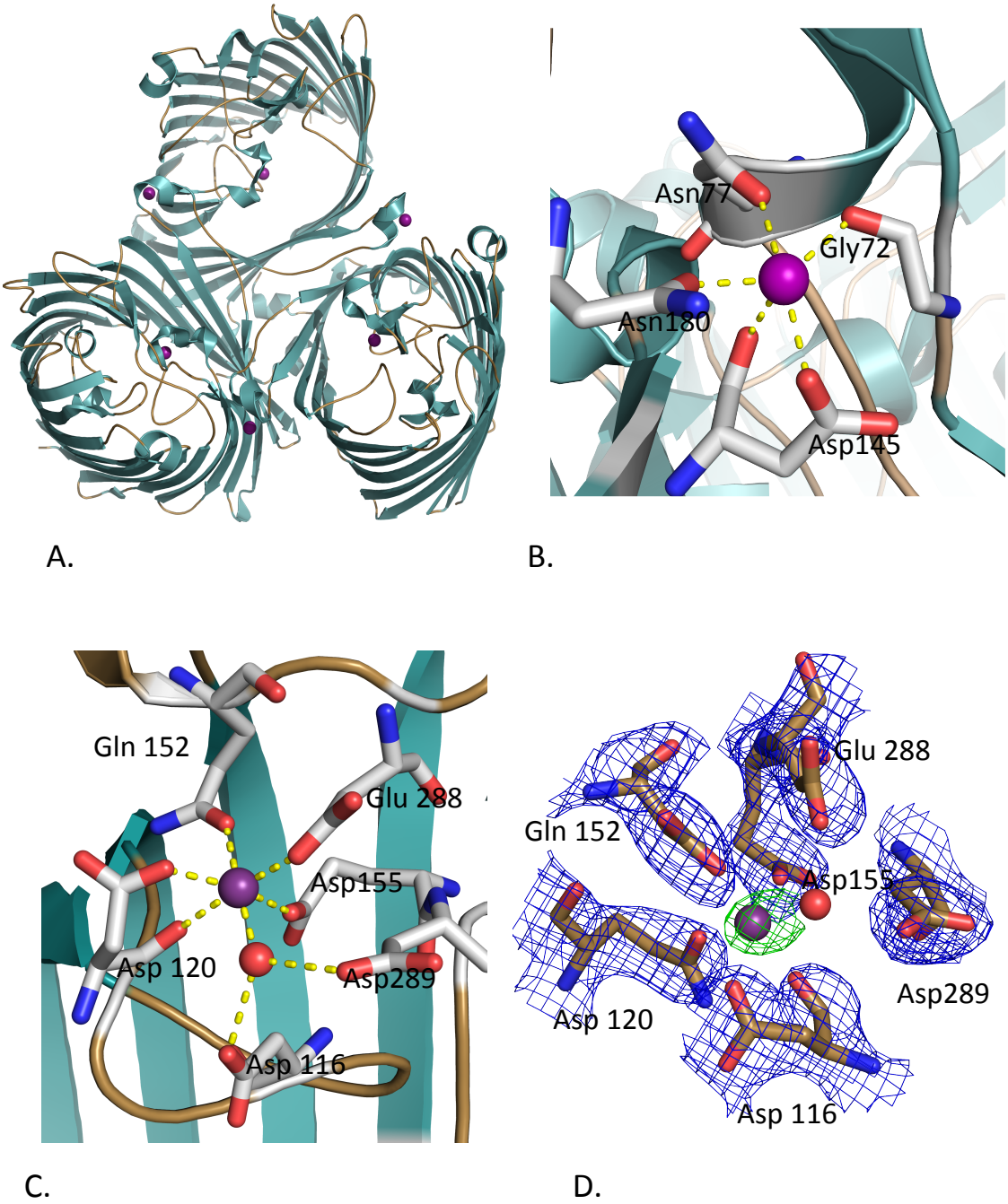

Figure 2.8: Calcium-binding sites in MOMP. (A) Extra-cellular view of MOMP trimer and the calcium binding sites. Theβ-barrel is colored in cyan, the loop in sand and the calcium molecules in purple. Zoom in of the calcium-binding site inside the channel (B) and between monomers. (C) The amino acids involved in the binding are shown in sticks. Calcium is colored in purple and water in red. (D) F_0-F_2 and $2F_0$-F_2 electron density map at 5σ and 2σ, respectively, of the amino acids involved in the calcium binding site at the constriction zone. Calcium is colored in purple and water in red.

Table 2.3. Bond distances of the two calcium binding sites in MOMP.

	Interacting molecule	**Bond length (Å)**
Calcium binding site at the constriction zone		
Asp120 (Oxygen and side chain)	Ca^{2+}	2.33/2.29
Gln152	Ca^{2+}	2.32
Asp155	Ca^{2+}	2.32
Glu288	Ca^{2+}	2.31
H_2O	Ca^{2+}	2.49
Calcium binding site in between monomers		
Asp145 (Oxygen and side chain)	Ca^{2+}	2.29/2.3
Asn180	Ca^{2+}	2.26
Gly72	Ca^{2+}	2.27
Asn77	Ca^{2+}	2.32

2.3.7 Single channel conductance measurements

MOMP conductivity was assessed by single channel measurements in 10 mM Hepes pH 6 and 1 M KCl. MOMP was randomly inserted into the bilayer as either a monomer or a trimer. Consequently, we detected two different levels of conductance, a lower one of 0.7 ± 0.2 nS, and a higher one of 2.2 ± 0.2 nS. These corresponded to the monomeric and trimeric states, respectively. The electrical signature showed that at negative voltages, long upward spikes occurred for both

monomeric and trimeric MOMP. In contrast, at positive voltages, while the monomer trace was noisy (displaying long downward spikes), the trimer trace was silent (Figure 2.10).

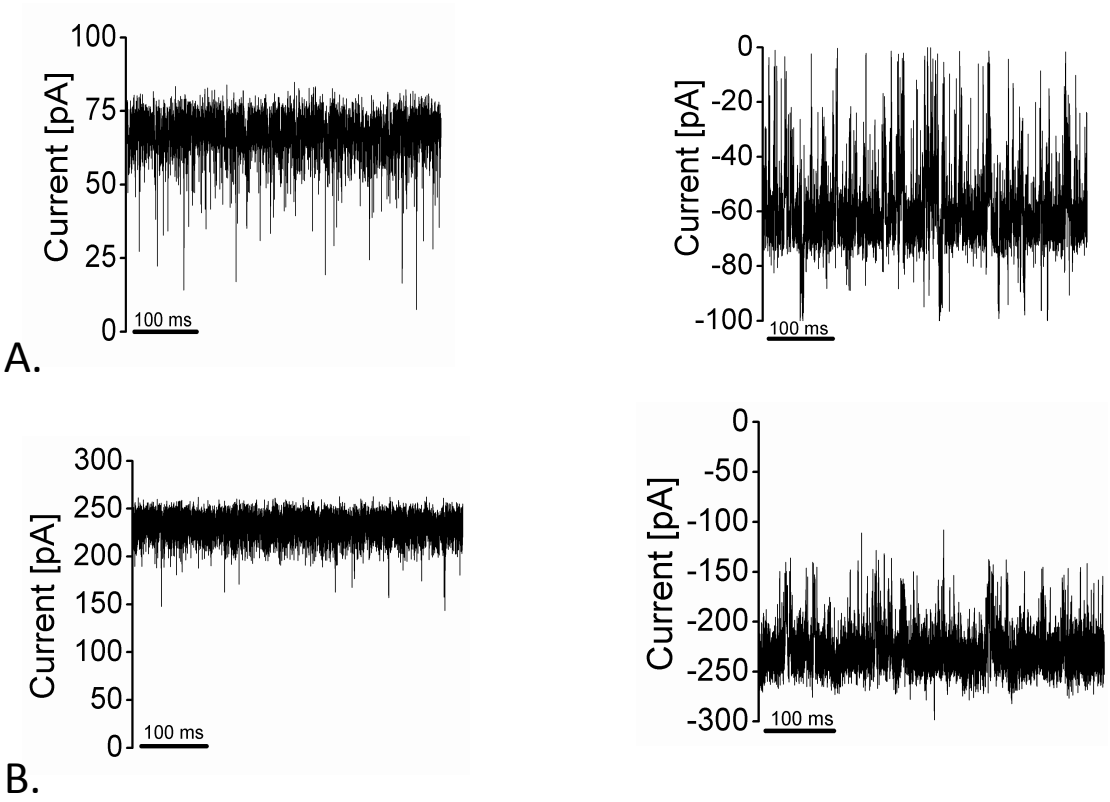

Figure 2.9: Single channel recording of MOMP. Electric trace of (A) MOMP monomer and (B) MOMP trimer at +100 mV (right) and at -100 mV (left).

To elucidate the effect of Ca^{2+} on the channel, conductance measurements were also taken in presence of 10mM $CaCl_2$. Interestingly, the presence of calcium eliminates the long spikes previously observed at negative voltage. The calcium makes the channel stable (at both positive and negative voltage) (Figure 2.11 A). Measurements were also taken after overnight incubation of MOMP with 10mM of the chelating agent EGTA to remove the calcium (EGTA was also added to the

buffer at a final concentration of 10 mM). Not surprisingly, the electrical trace was silent at positive voltage but noisy at negative voltage, as with the native protein (Figure 2.11 B).

In a control experiment, we slowly replaced the buffer containing EGTA with a buffer containing 10 mM $CaCl_2$. As expected the calcium reverted the effect of the chelating agent, resulting in an entirely silent channel.

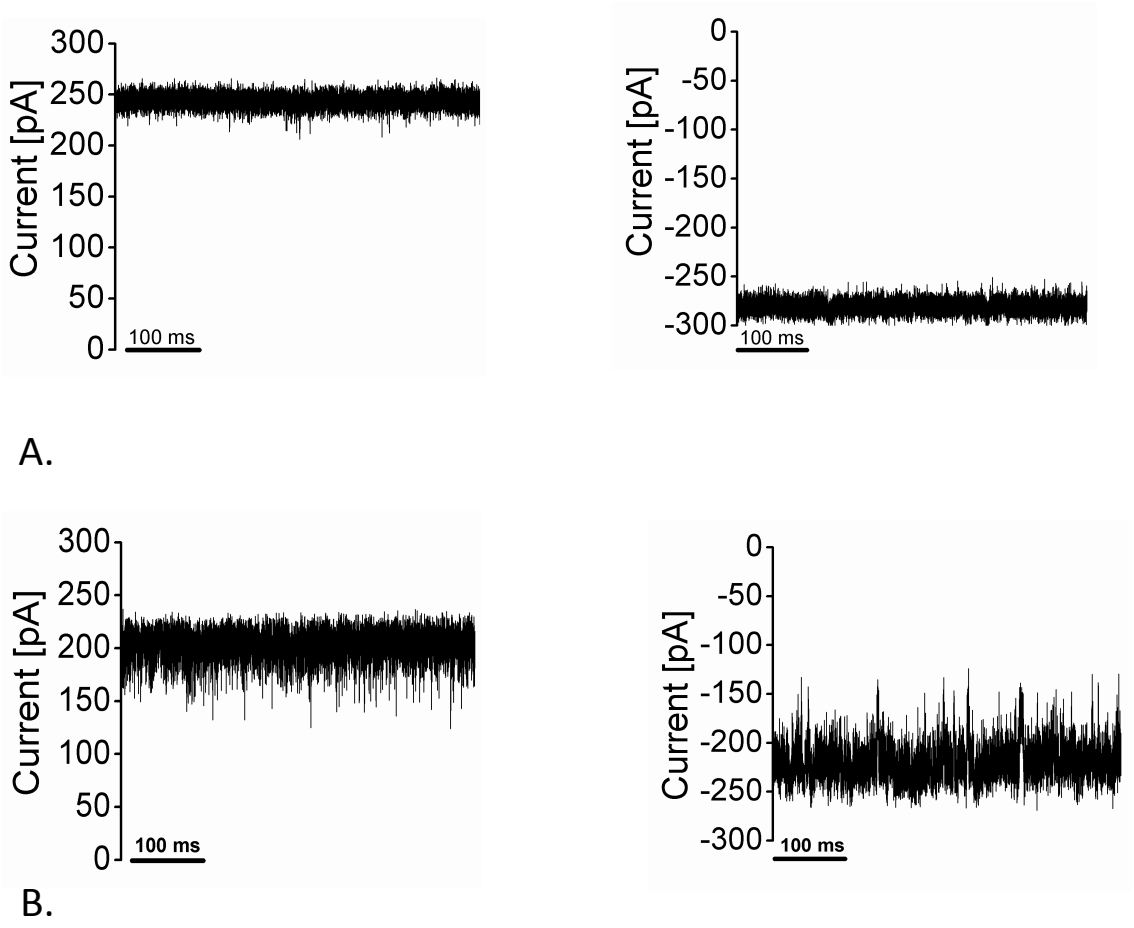

Figure 2.10: Single channel recording of MOMP. Electric trace of MOMP trimer with (A) and without (B) at +100 mV (right) and at -100 mV (left).

In order to assess the specificity of this effect, other divalent ions were tested. In

particular, conductance measurements were taken in the presence of 10mM of either $MgCl_2$ or $ZnCl_2$. Neither the magnesium nor the zinc was able to stabilize the channel. At negative voltage the channel showed the same long spikes detected in absence of calcium (Figure 2.12).

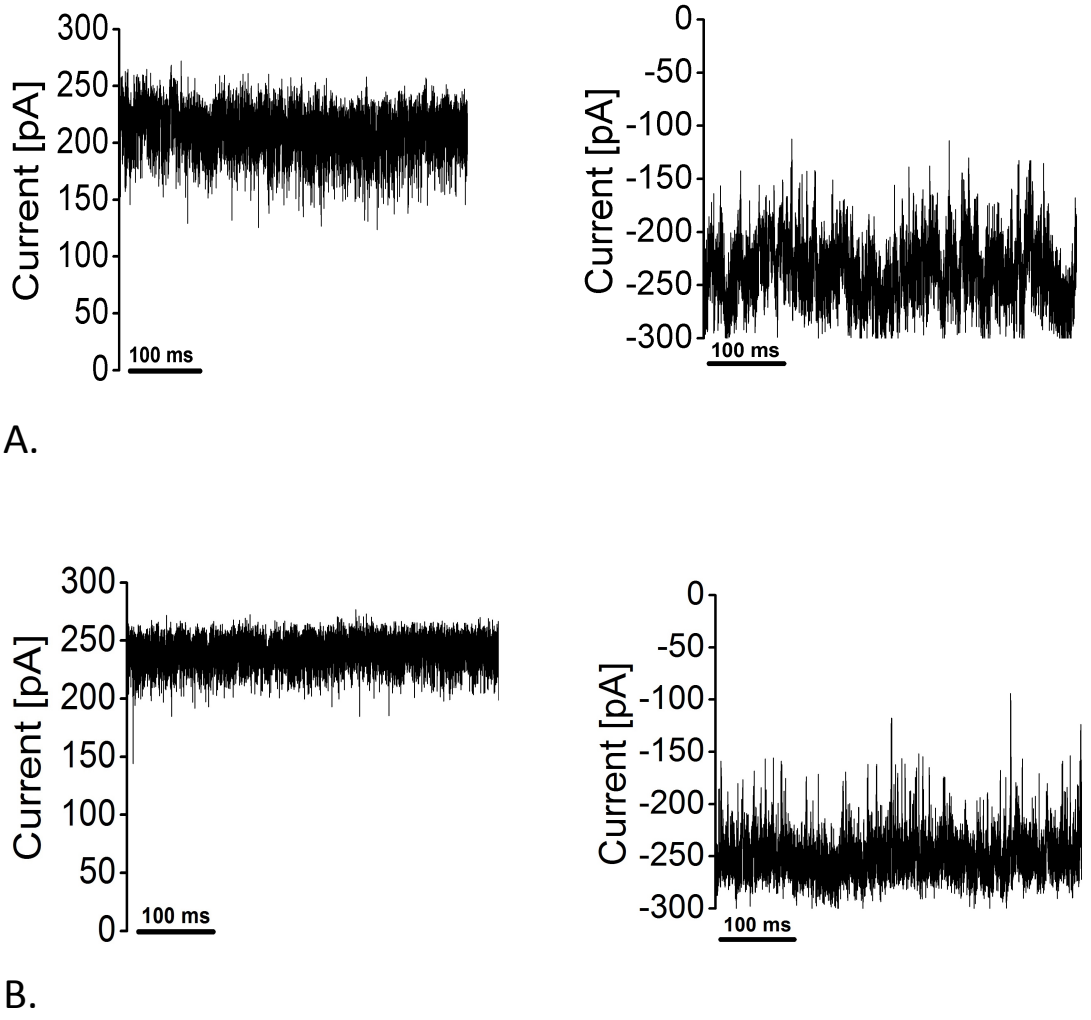

Figure 2.11: Single channel recording of MOMP. Electric trace of MOMP trimer with 10 mM $MgCl_2$ (A) and 10 mM of $ZnCl_2$ (B) at +100 mV (right) and at -100 mV (left).

2.4 Discussion

2.4.1 MOMP crystal structure

In this study, we present the first X-ray structure of the natively expressed MOMP from *Campylobacter jejuni* strain 85 H. Although previous analysis of two-dimensional and three-dimensional crystals of MOMP provided a clear indication of the trimeric arrangement of the protein, similar to that observed for OmpC and OmpF in *E. coli*, they failed to give complete structural data [194]. The crystal packing of the structure we obtained confirmed this trimeric arrangement. Each monomer-monomer interface buries over 1200 $Å^2$ of surface area, while the trimer buries almost 10,000 $Å^2$ of surface area. Overall, the structural features observed in MOMP are common to all the porins characterized so far. A barrel consisting of 18-anti-parallel β-strands joined together by long extracellular loops and short periplasmic turns. The L3 folds back inside the barrel to form the eyelet of the pore, a region characterized of negatively and positively charged residues facing each other that create a strong electric field. L2 stabilizes the trimer as suggested by the several hydrogen bonds formed with the β-strands of the adjacent monomers.

A distinctive feature of MOMP is, instead, the α-helix at the N-terminus, which bends outwards reaching the neighboring subunit and forms an α -helix triangle. To date, only two outer-membrane proteins display such an unusual arrangement at the N-terminal: OprB from *Pseudomonas aeruginosa* [195] and the palmitoyl transferase PagP from *E. coli* [68] (Figure 2.13). The helix in these structures is

not involved in the trimerizazion since both proteins exist as monomer. Interestingly, the sucrose-specific porin (ScrY) from *Salmonella typhimurium* contains a coiled-coil structure at the N-terminal domain [196],[197]. Unlike PagP and OprB, ScrY oligomerises form a homo-trimer. Spectroscopic and biophysical analysis suggested that the ScrY N-terminus α-helical coiled-coil complex might be involved in the oligomer stabilization; however, no structural data of this domain are available [196]. Although the role of the N-terminal α–helix in MOMP has yet to be investigated, PDBePISA analysis suggests it might contribute to the stability of the trimer (Table 2.4).

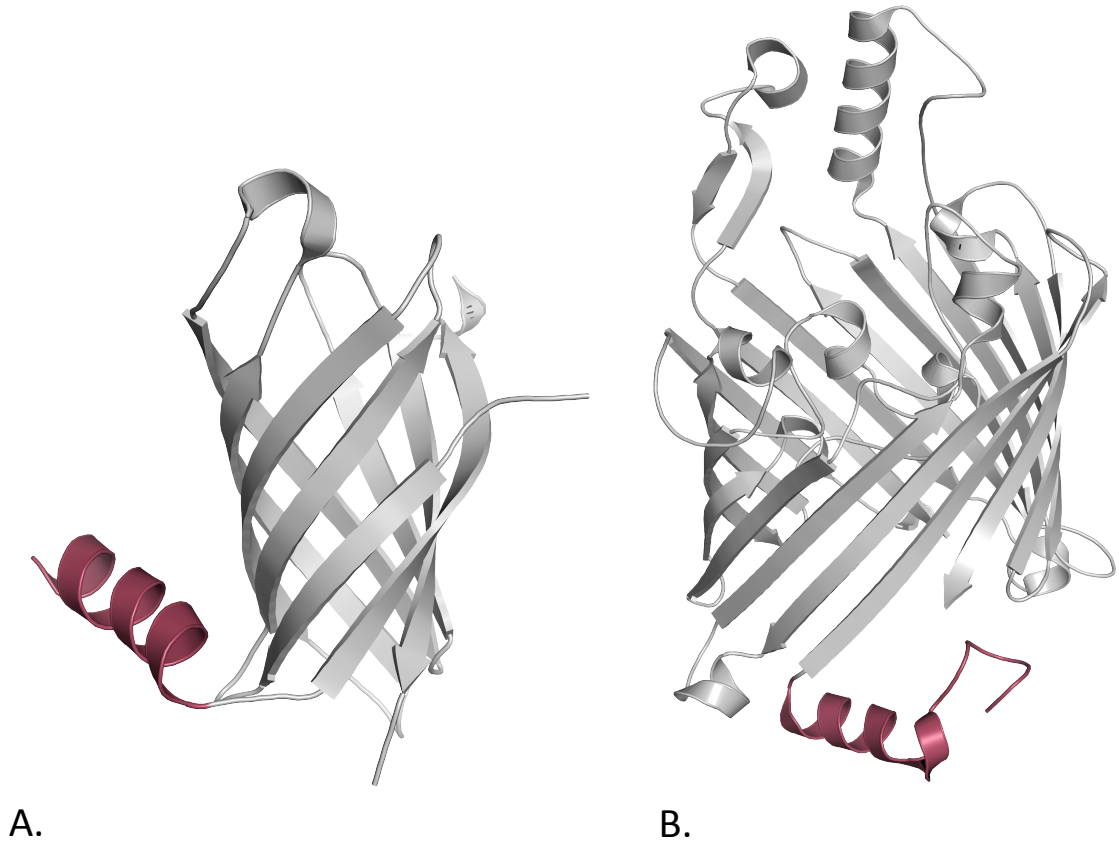

Figure 2.12: α-helices N-terminus. N-terminus of PagP (A) and OprB (B). β-barrels are colored in grey and N-terminus domain in pink.

Table 2.4. **α-helices N-terminus bond distances.** Measurements were generated with PISAePDB.

Residue monomer 1	Residue monomer 2	Bond distance (Å)
Val12 (N)	Thr1 (O)	2.9
Val12 (O)	Thr1 (N)	3.2
Val10	Leu3	3.1

2.5.2 MOMP pore activity analysis in single channel experiments

Single channel measurements indicated that MOMP could randomly insert as either a monomer or a trimer. Previous studies have already shown that in solution MOMP exists as both monomer and trimer depending on the detergents used for the extractions, and that both oligomeric states exhibit pore-forming activity [176]. The trimer exhibits high single channel conductance of 2.2 nS comparable to the *E. coli* osmoporin OmpC (2.5 nS) [198]. In contrast to what has been reported for MOMP, OmpF and OmpC have shown higher stability and in lipid bilayer insert solely as a trimer. While at negative voltage, both monomers and trimers showed the same behavior (long downward spikes), differences were found when a positive voltage was applied. As shown in Figure 2.9, at positive voltage, the trimer was silent, where the monomer was noisy with long upwards spikes However, we are unable to determine if the monomer detected during single channel experiments derived from a trimer with two closed channels or from the dissociation of the trimer in single monomers.

2.5.3 Structural role of the Ca^{2+} at the constriction zone

A unique feature of MOMP, relative to the others OMPs is the calcium ion found at the constriction zone. The calcium holds together a number of key loops (L3, L4 and L6). Previous studies have shown that addition of EDTA to the protein, which would remove any calcium, destabilizes the protein [172]. When we analyzed MOMP behavior in single channel experiments, we observed that the addition of 10 mM $CaCl_2$ gave stable electrical traces, whereas EGTA addition resulted in noisy conductance comparable to the native protein. In a control experiment, we removed the buffer containing EGTA and we replaced it with 10mM $CaCl_2$, this reversed the effect of the chelating agent, restoring a stable trace. This was metal specific as the addition of Mg^{2+} or Zn^{2+} did not result in a stable ion-current profile. In collaboration with the University of Cagliari, we analyzed the structure in the presence and in the absence of calcium. *In silico* measurements of the root mean square deviation (r.m.s.d) and the root mean square fluctuation of the loops (r.m.s.f) showed that in the presence of calcium, the structure is significantly less flexible (r.m.s.d 1.45 Å vs 1.75 Å). Unsurprisingly, when the calcium is removed the instability is mainly focused on the loops involved in its coordination. Therefore, we propose that its role is structural and that the binding of calcium anchors the loops (L3, L4 and L6), hence ordering the eyelet preventing them flickering into the pore and thus eliminating the long spikes observed in ion-current in the absence of calcium.

2.5.4 Functional role of the Ca^{2+} at the constriction zone (Collaboration with the University of Cagliari)

Our collaborators at the University of Cagliari also investigated the effect of the calcium on the permeation of the polar antibiotic ciprofloxacin, a FQ often used to treat cambylobacteriosys. Dr. Silvia Acosta-Gutierrez calculated the free energy profiles for ciprofloxacin translocation for MOMP with and without calcium at the constriction zone. As expected, the two free energy maps significantly differ at the level of the constriction zone where the calcium is bound. In the absence of calcium, ciprofloxacin points at the constriction region with its positive group, towards the negatively charged amino acids that lie on L3. In presence of calcium, the negative charge of those amino acids is shielded and therefore, the ciprofloxacin enters in the opposite orientation, pointing its carboxylic group towards the ion. Additionally, in the presence of calcium, an applied voltage higher than +100mV is required to allow the complete translocation of ciprofloxacin. According to molecular dynamics analysis, the antibiotic follows a different path and has a higher barrier to translocation in the presence of calcium (Figure 2.13).

Similar behavior has already been observed in OmpF from *E. coli* where an ion of magnesium was found bound at the level of the constriction zone [199]. Unlike MOMP, however, OmpF magnesium is just an artifact of crystallization conditions.

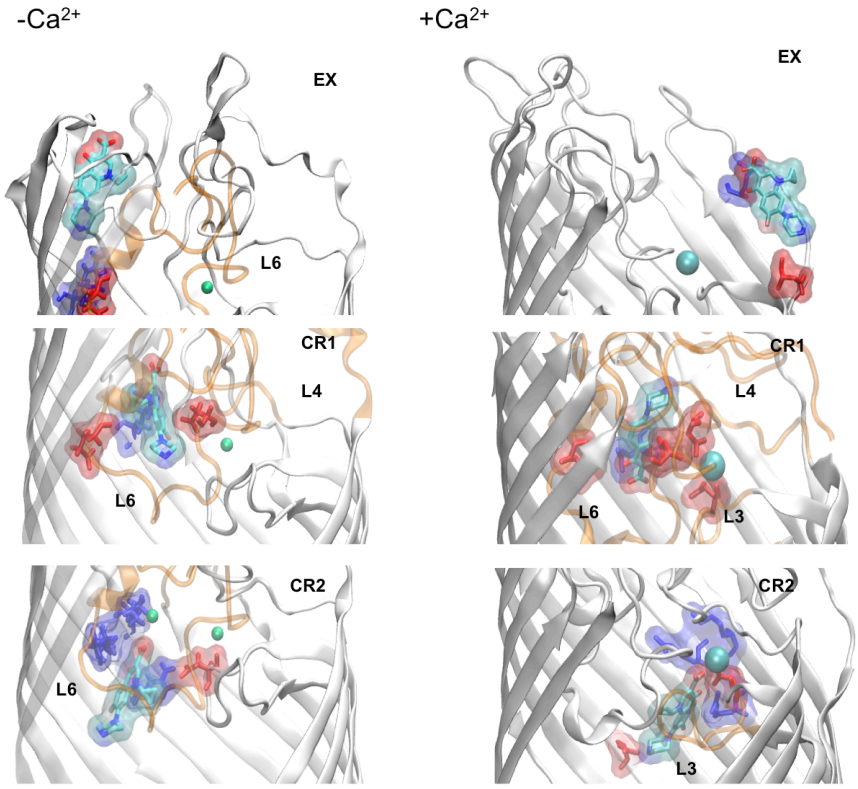

Figure 2.13: "Most statistically relevant conformations for the chosen minima are depicted EX, CR1 and CR2, for both scenarios." "For clarity, β-strands from 9 to 14 have been removed from the cartoon representation of MOMP monomer. Ciprofloxacin is represented in licorice. Interacting loops are highlighted in orange and labeled. Specific charged residues interacting with ciprofloxacin are shown in licorice colored according to its charge". Dr. Silvia Acosta-Gutierrez provided this picture and the caption.

2.5.5 Comparison between recombinant and native MOMP

A structure of MOMP recombinantly expressed in *E. coli* was obtained by Dr. Gregor Wallat (Prof. Naismith's laboratory). We compared the two structures, the recombinant and the natively expressed MOMP and, apart from small differences arising from the different crystal packing, the two structures were structurally identical (r.m.s.d 0.45 Å over 398 Cα position) (Figure 2.15). Both structures have a Ca^{2+} ion bound at the constriction zone. Unlike the recombinant MOMP, the

natively expressed protein was crystallized in the presence of $CaCl_2$. As a consequence, the native structure has an extra calcium ion located at the interface between monomers. The recombinant structure shows a different side chain conformation suggesting that in the recombinant protein this site does not exist and it is an artifact.

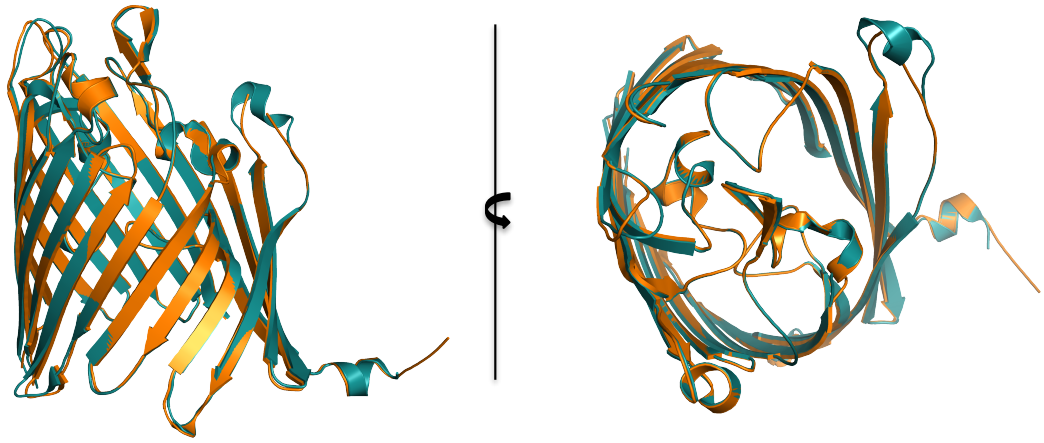

Figure2.14: Superimposition of MOMP native (cyan) and MOMP recombinant (orange). View from the side (left) and from the top (right). The two structures were found to be structurally identical with a r.m.s.d of 0.45 Å over 398 Cα position.

2.5.6 MOMP: general or specific-substrate porin?

As a general rule, 18 β-stranded porins are classified as substrate-specific. To date, aside from MOMP, the only structures of trimeric 18 β-stranded porins available are the structure of the maltoporin LamB from *E.coli* [200] and the sucrose-porin SrcY from *Salmonella tiphymurium* [33]. A distinctive feature of both LamB and SrcY is a cluster of aromatic amino acids (greasy slide) that guides the molecules of sugar through the porin channel [201],[202],[196]. Although

LamB and SrcY share only 20% of sequence homology (Protein Data Bank), the amino acids that form the greasy slide are highly conserved. Analysis of the amino acids sequence and structure revealed that no greasy slide is present inside the channel of MOMP. Furthermore, taking into account the fact that *C. jejuni* is not able to use sugars as a source of carbon [133], it is unlikely that MOMP belongs to the class of sugar-specific porins. Moreover, a closer analysis of the size and charge of the pore, as well as the conductivity, led to the conclusion that MOMP has a greater resemblance to a general porin (pore size and conductivity of MOMP lies in between pore size and conductivity of OmpC and OmpF from *E. coli*), rather than a specific porin. We therefore suggest that, although structurally different to the general porins described so far (18 β-strand rather than 16), MOMP represents the only general porin expressed in *C. jejuni*. In addition, due to the high level of expression of MOMP, we conclude that its role may also be structural, other than merely functional, contributing to the integrity of the outer membrane of *C. jejuni*.

2.6 Conclusion and outlook

Antibiotic resistance in *Cambylobacter* has become a real concern. *C. jejuni* is a fastidious organism that represent the main source of campylobacteriosis worldwide. Unlike *E. coli*, *C. jejuni* has only one major porin, MOMP, highly expressed in the outer membrane (MOMP). Here we present the 2.9 Å structure of MOMP natively expressed in *C. jejuni* 85 H. The structure showed that MOMP is an 18 β- stranded trimeric porin with two calcium binding sites, one inside the channel and the other between monomers. While the calcium between monomers resulted because of an artifact of the crystallization, the calcium found at the constriction zone was bound during expression and remained attached throughout the purification process. In this work, we proved that the calcium at the constriction zone has both a structural and functional role. According to the results obtained in collaboration with Prof. Ceccarelli and Dr. Silvia Acosta-Guitierrez from the University of Cagliari, it is possible that *C. jejuni* utilizes the ion of calcium to modulate the permeations of molecules, and thus antibiotics, through the pore.

Future work should be carried out to clarify if MOMP is indeed a general porin (as we believe) or a substrate-specific porin. Also, co-crystallization trials of MOMP with chosen antibiotics (in presence and absence of EDTA) should be attempted in order to shade more light onto the role of the calcium in drugs permeation.

Chapter 3: Omp50 from *Campylobacter jejuni*

3.1 Introduction

3.1.1 Omp50 from Campylobacter jejuni

Omp50 was first identified as a porin of *C. jejuni* 85H in a report by Bolla *et al.* [203]. Omp50 was predicted to be an 18-β-stranded monomeric porin. Electrophysiology experiments demonstrated the ability of Omp50 to form a pore when inserted in a lipid bilayer [203]. Due to the low conductivity (50-60 pS in 1 M NaCl) exhibited, it was hypothesized that Omp50 could represent a specific porin rather than a general one [203].

The gene encoding for Omp50 (cj1170) is not ubiquitous in *Campylobacter* and therefore is used to differentiate *Campylobacter* species [204]. Cj1170 is transcriptionally regulated in a temperature dependent manner [205] and up-regulated in the presence of the antibiotic erythromycin (Ery) [206]. The effect of Ery on the up-regulation of Omp50 has been linked to its proposed kinase activity [206],[207].

Corcionivoschi *et al.* first suggested Omp50 as a bacterial tyrosine (BY) kinase in *C. jejuni* 11168 strain [207]. BY-kinases belong to a subgroup of kinase able to auto-phosphorylate on several tyrosine [208]. Typically embedded in the inner-membrane, BY-kinases consist of two transmembrane α-helices link together by an external loop (also known as hairpin loop) and of a cytosolic catalytic domain. The catalytic domain contains three different motifs: Walker A, Walker A' and

Walker B motif. In addition to the three motifs, a C-terminus tyrosine cluster (YC) is also found in the catalytic domain [208]. Sequence analysis of Omp50 led to the identification of the Walker A and A' motifs (but no Walker B) motifs were identified in Omp50 sequence and of one tyrosine (Y338) that was reported to be essential for Omp50 kinase activity. Mutation of this tyrosine suppressed the tyrosine kinase pathway in *C. jejuni* 1168, suggesting that Omp50 is the only BY-kinase in this organism. They also identified the enzyme UDP- GlcNAc/Glc 4-epimerase (Gne) as one of Omp50's substrates. It was suggested that Omp50 positively regulates Gne activity by phosphorylating a tyrosine (Y146) in its active site. Considering that Gne is involved in the formation of the lipooligosaccharide (LOS) and the capsule of *C. jejuni*, Omp50 kinase activity has been proposed to have an impact on the permeability of the outer-membrane and therefore on antibiotic permeation.

3.1.2 Aims

Omp50 is a monomeric porin associated to antibiotics (especially macrolides) resistance in *C. jejuni* [206]. To date no structural data about Omp50 are available.

We, therefore, aimed to solve the structure of Omp50 using X-ray crystallography. In order to do so, we first set up to purify Omp50 from the native *C. jejuni*, However, due to the low yield obtained we decided to switch to a recombinant system. We also set up to analyze the pore activity of the recombinantly expressed Omp50 in lipid bilayer by using electrophysiology measurements, and ultimately compared it to the natively expressed.

Following the publication of Corcionivoschi *et al.* [207], we also aimed to investigate the proposed kinase activity of Omp50 with both the recombinantly and native expressed protein.

3.2 Material and methods

3.2.1 Omp50 purification from the native C. jejuni 85H and 11168 strain

C. jejuni cultures were prepared as described in Bolla *et al*. [176]. Purification of Omp50 was performed as described in the Material and Methods section of Chapter 2 (Paragraph 2.3.1).

Omp50 from *C. jejuni* 11168 was produced in collaboration with Prof. Panos Sultanos and Dr. Mahdavi from the University of Nottingham. *C. jejuni* 11168 cultures were also prepared as described in Bolla *et al*. [176].

3.2.2 Omp50 cloning

The Omp50 gene from *C. jejuni* 85H, codon optimized for *E. coli*, was synthesized by Eurofins (Germany). The gene was cloned in two different vectors carrying a TamA signal peptide and a His_6-tag, either at the C-terminus (pTamACterHisTEV) or at the N-terminus (pTamAHisTEV), with a Tobacco etch virus (TEV) protease site placed between the His_6-tag and the gene. Both plasmids carried an ampicillin resistance gene (cloning was performed by Dr. Gregor Wallat).

In order to purify Omp50 from inclusion bodies (IB), Omp50 gene was cloned into a pTacHisTev vector. This vector carries a N-terminus His_6-tag followed by a TEV

recognition site, however, unlike the pTamA vectors, pTacHisTev lacks the signal peptide. Both Omp50 gene and vector were digested using NcoI and HindIII restriction enzymes (both Promega) at 37 °C for 3 hours. Subsequently, 2 µl of alkaline phosphatase (Promega) was added to the vector and incubated for an additional 30 minutes at 37 °C. The Omp50 gene and the pTacHisTev vector were then ligated at room temperature (RT), overnight using a T4 ligase (Promega). The ligation mixture was later used to transform DH5α cells. The transformed cells were plated onto LB agar plates and supplemented with 100 µg/ml of ampicillin. Colonies were picked and grown in 10 ml LB media supplemented with 100 µg/ml of ampicillin at 37 °C and shaken at 200 rpm overnight. Cells were mini-prepped using the commercial kit QIAprep® Spin Miniprep Kit (Qiagen) and the plasmid sent for sequencing (GATC Biotech).

3.2.3 Single base site-directed mutagenesis

Single base site-directed mutagenesis was performed to substitute the tyrosine in position 348 with a phenylalanine using the method described by Dr. Liu [209] (Figure 3.1). Polymerase chain reaction (PCR) was carried out using a *Pfu* DNA polymerase (Promega) and a two stage amplification cycle was chosen. Specific primers were designed with overlapping and non-overlapping regions (Table 3.1). The PCR product was then incubated with 2 µl of DpnI (Promega) (1U/µl) at 37° C for 4 hours. This step ensured the total degradation of the methylated (parental) DNA. To check the amplification efficiency, a small aliquot (5 µl) of the digested sample was analyzed by agarose gel electrophoresis. Consecutively, 50 µl

DH5α *E. coli* cells were transformed with 100 ng of PCR product, plated onto LB agar plates and supplemented with 100 μg/ml of ampicillin. Colonies were picked and grown at 37 °C, 200 rpm overnight in 10 ml LB media supplemented with 100 μg/ml of ampicillin. Then cells were subsequently spun down at 4,000x g for 10 minutes at 4 °C and mini-prepped using a QIAprep® Spin Miniprep Kit (Qiagen). To confirm the presence of the mutation, the plasmid was sent for sequencing (GATC Biotech).

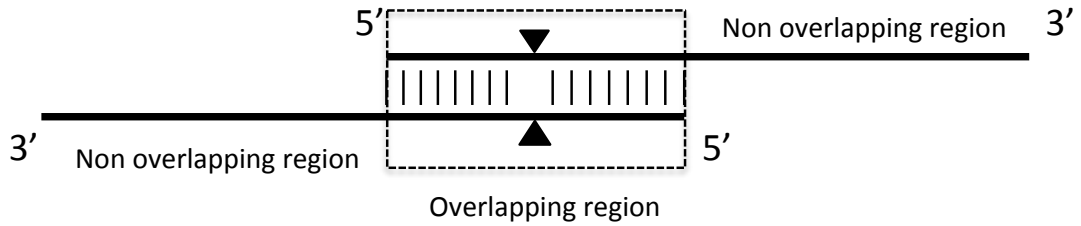

Figure 3.1: Schematic representation of primers used for site-directed mutagenesis. Figure was adapted from [209].

Table 3.1. Primers used to generate Omp50 Y348F.

5'TCTTTGGGCTTCAGTCATGGGAACAATAATCAACTGTCCAGCACGCTG3'
3'AAACCGTGGTTAAAGTTGATGAAATAGAGAAACCCGAAGTCAGTACCC5'

3.2.4 Small-scale expression

For small-scale expression, pTamAHisTev-Omp50 and pTamAHisCter-Omp50 were transformed in different cell lines (BL21(DE3), BL21(DE3)Omp8, C43(DE3), C41(DE3)). 1 µl of DNA was incubated with 50 µl of competent cells and left for 30 minutes on ice, followed by 1 min at 42 °C for heat shock. Cells were then incubated with 400 µl of LB media and left growing for 1 hour at 37 °C, shaking at 200 rpm. Consecutively, cells were plated onto LB-agar plates supplemented with 100 µg ml^{-1} ampicillin and left at 37 °C overnight. Next day, a colony for each cell line was picked and inoculated in 10 ml LB supplemented with ampicillin 100 µg ml^{-1} and was grown overnight at 37 °C and 200 rpm. 100 µl of this starter culture was then used to inoculate 10 ml of fresh media (LB, TB and TPB media were tried for small-scale expression trails) supplemented with 100 µg ml^{-1} ampicillin. This was incubated at 37 °C and shaken at 200 rpm until $O.D_{600}$ reached 0.6-0.7 and subsequently induced with 0.4 mM of isopropyl β-D-1-thiogalactopyranoside (IPTG). After induction, cells were left growing either for 3 hours at 37 °C, or overnight at either 16 °C or 25 °C. Samples were taken and run on an SDS-PAGE to check the expression level. The gel was stained with Coomassie blue stain.

3.2.5 Large-scale expression

The pTamAHisTev-Omp50 construct, transformed in C43(DE3) cell line, was used for large-scale expression. Initially, a 12 L of TPB media supplemented with 100 µgml^{-1} of ampicillin was inoculated with 10 ml of start culture and left grown at

37 °C for 3 hours after induction. Due to the low yield obtained for the purified Omp50, auto-induction media for large-scale was attempted.

The starter culture was prepared by inoculating 100 ml of LB, containing 100 μg ml^{-1} of ampicillin and 1% (w/v) of glucose (Sigma), with one colony of plasmid-transformed C43(DE3). After overnight growth at 37 °C, 10 ml of the start culture was used to inoculate 12x400 ml of ZYP-5052 media supplemented with ampicillin. Adequate aeration is essential to reach an optimum level of protein expression, therefore no more than 400 ml of media was used in 2 L baffled flasks. The culture was incubated at 20 °C and shaken at 250 rpm for 48 hours. Cells were harvested by centrifugation at 6,000x g at 4 °C for 10 minutes (rotor JLA 8.100, Beckman).

3.2.6 Purification of Omp50 Wt and Omp50 Y348F

To purify Omp50 Wt and Omp50 Y348F, 100 g of cell paste was resuspended in 400 ml of lysing buffer and lysed with two passes at 30 kpsi through a high-pressure cell disruption system (Constant System Ltd). Debris were removed by spinning down the lysed cells at 15,000x g at 4 °C for 15 minutes (rotor JA 25.50, Beckman). Total membranes were recovered by ultracentrifugation at 100,000 x g, 4 °C for 1 hour (rotor Ti5.2, Beckman). The pellet was homogenized in 50 mM Na_3PO_4 pH 8, 250 mM NaCl, 10 mM β-mercaptoethanol (BME) and 7 % Octyl-POE. Solubilized membrane were left stirring overnight at 4 °C. The following day, insoluble material was removed by ultracentrifugation at 100,000 x g and 4°C for 1 hour. The supernatant (approximately 200 ml) was then incubated with 5 ml of

nickel nitriloacetic acid (Ni-NTA) resin (Qiagen) at 4°C, stirring for 1 hour. The resin was previously washed twice with water to remove the ethanol used for storage, and ultimately equilibrated with the buffer used for the protein extraction. After 2 hours, the sample was loaded onto a 100 ml gravity flow column (BIO-RAD) and the flow through collected. The resin was washed with 10 CV of washing buffer supplemented with 5 mM BME and eluted with 2 CV of elution buffer also supplemented with 5 mM BME (Appendix A.2). The eluted protein was then dialyzed against 500 ml of dialysis buffer (Appendix A.2) at 4°C for 30 minutes to reduce the concentration of imidazole. A snakeskin membrane (Thermo scientific) with a 10 kDa cut off was used during dialysis. Subsequently, His-tagged TEV protease was added to the protein to a final ratio of 1:10 TEV: protein. The protein was left in dialysis overnight at 4°C. The next day, the sample was filtered through a 0.45 µm filter and applied to a 5 ml His-trap column (Qiagen) using a peristaltic pump. At this point the cleaved protein flowed though the column while the His-tagged TEV remained bound. The cleaved protein was then concentrated to 5 ml, spun down at 14,000 rpm for 15 minutes (centrifuge 5417R, Eppendorf), and loaded onto a 16/60 200 pg superdex column (GE healthcare) that was equilibrated with 2 CV of 10 mM Tris-HCl pH 8.0, 150 mM NaCl and either 0.45% C_8E_4, 1% N,N-Dimethyldodecylamine N-oxide (LDAO) (Sigma), 1% n-Octyl-β-D-Glucopyranoside (OG) (Anatrace) or 1% n-Dodecyl β-D-maltoside (DDM) (Anatrace). The protein was then concentrated to 10 mg ml^{-1}.

3.2.7 Omp50 inclusion bodies (IB) purification

C43(DE3) cell line were transformed with the pTacHisTev plasmid carrying the Omp50 gene. Cells were plated onto LB-agar plates and grown overnight at 3°C. One colony was picked and used to inoculate 20 ml of LB. The starter culture was left overnight at 37°C and 200 rpm. Subsequently, 1 x 2 L of LB media, supplemented with 100 μg ml^{-1} of ampicillin, was inoculated with 10 ml of start culture and left growing at 37°C until $O.D._{600}$ reached 0.6. Cells were induced with 0.4 mM of IPTG and left overnight at 25°C and 200 rpm. Induced cells were harvested at 6000x g, 4°C for 15 minutes. The recovered pellet was resuspended in 50 ml lysis buffer and broken with two passes through a cell disrupter. Inclusion bodies were then recovered by centrifugation at 20,000 rpm, 20°C for 20 minutes (rotor 25.50, Beckman), and the pellet resuspended in the IB buffer supplemented with 1% X100-Triton and left rocking at RT for 15 minutes. The suspension was then spun down again at 20,000 rpm, 20°C for 20 minutes. The recovered pellet was washed twice with IB buffer (no Triton X-100) (Appendix A.2) and then recovered by centrifugation at 20,000 rpm, 20°C for 20 minutes. Finally the protein was extracted resuspending the IB in IB buffer supplemented with 8 M Urea pH 8 and left rocking at RT overnight. The suspension was then clarified by centrifugation at 20,000 rpm, at 20°C for 20 minutes. The supernatant was diluted 10-fold in refolding buffer, supplemented with 1% of either LDAO, Octyl-POE, or Elugent whilst stirring at RT for three days. The suspension was then clarified by centrifugation at 20,000 rpm, at 20°C for 20 minutes and checked by SDS-PAGE.

3.2.8 Crystallization

Initial trials were done using several commercial screens. The screens were dispensed into a 96-well sitting drop plate (Intelli-Plate®, ARI) using a Gryphon robot, at a protein:reservoir ratio of 1:1 and 1:2. First hits appeared within three-four weeks. When necessary, crystallisations conditions were manually optimized by the hanging-drop vapor diffusion technique. In order to improve the quality of the crystals, commercial additive screens were explored, and were also dispensed using the Gryphon robot.

In situ proteolysis of Omp50 was also attempted using different proteases. Stock solution at 1 mg/ml of Subtilis A, Trypsin, Chemotrypsin and Papain were prepared in specific buffers (listed in Appendix A.2) flash frozen in liquid nitrogen and stored at – 20°C. Omp50, at a concentration of 10 mg/ml, was incubated at RT for an hour with different proteases at a final ratio of either 1:10 or 1:100 protein:protease. The reaction was stopped by adding LDS loading buffer (Promega). Omp50 proteolytic products were checked by SDS-PAGE.

3.2.9 Lipid cubic phase (LCP)

To set up LCP plate we used the method described by Caffrey and Porter[210]. Briefly, Omp50, at a concentration of 15 mg/ml, was mixed with monoolein (Molecular Dimension) at a final ratio of 2:3 protein:monoolein. The glass syringe and the tip used to mix the protein and the monoolein was quickly warmed up at 42°C on the top of a heating block. This prevented the monoolein solidifying

during the mixing. Care was taken to avoid bubbles during this process. Once the mixing was completed, the syringe was attached to the Gryphon robot. Previously, several LCP glass plates were prepared as follows. The plates were coated with Rainex and left to dry for a few minutes. Consecutively, the plates were rinsed with milliQ water and dried with a tissue. Once dried, a 96-well spacer was stacked on the top of the each of the glass plates. The distance between the left edge of the plate and the spacer was roughly 0.5 cm, while the distance between the right edge and spacer was roughly 1.5 cm. The plates were placed on the metal base of the Gryphon robot. Several commercial screens were dispensed. For each well, the Gryphon dispensed 800 nl of reservoir and 50 nl of the protein/monoolein mixture. Once the process was completed, the plates were removed from the Gryphon and covered with a glass coverslip and imaged using a Ministrel device (Rigaku).

3.2.10 Single channel conductance analysis of Omp50

Details of the protocol, setup and software used to perform the measurements were essentially the same as described in the Material and Methods section of Chapter 2 (paragraph 2.3.5).

Single channel measurements of recombinantly expressed Omp50 were taken from 1 M KCl, 10 mM MES pH 6. Omp50 was added to the *cis* side of the cuvette at a final concentration of 2 ng ml^{-1}.

3.2.11 Western blot with antibodies anti phosphorylated tyrosine

Omp50, Wzc (positive control) and Omp36 (negative control), all at a final concentration of 1 mg/ml were run on a SDS-PAGE gel. Omp50 and Y348F Omp50 were incubated with 10 mM $MgCl_2$ and 1 mM ATP for 1 hour at RT. A pre-stained ladder (Novex® Sharp Pre-stained, Life Technology) was used for the standard. The gel was run for 35 minutes at 200 V and subsequently transferred for blotting. Six pieces of blotting paper were cut and soaked in different buffers (Appendix A.2). One piece of paper was soaked in anode buffer 1, two pieces were soaked in anode buffer 2 and the last three pieces were soaked in cathode buffer. A piece of polyvinylidene difluoride (PVDF) membrane (Sigma) (same size of the gel) was pre-soaked in 50 ml of methanol (Sigma). The blotting stack was assembled by the placement of the two pieces of blotting paper soaked in the anode buffer 1 at the bottom of the stack, followed by the anode buffer 2 soaked paper, the PDV membrane, the gel and finally the three papers soaked in the cathode buffer. The transfer was performed using a semi-dry transfer cell (Bio-RAD), applying 25 V for 1 hour. A blocking solution was made by dissolving 2.5 g of milk powder in 50 ml PBS. The membrane was placed inside a 50 ml falcon tube filled with the blocking solution and left rolling for 1 hour at 4°C. Then the blocking solution was poured off and replaced with 10 ml PBS supplemented with a 1:1000 dilution of monoclonal anti-phosphotyrosine-peroxidase antibody (Sigma-Aldrich) and left rolling for 1 hour at 4°C. The antibody stock solution was prepared according to manufacturer's instructions. The membrane was then washed 3 times with 40 ml of PBS to remove excess antibody. To develop the western blot, equal amounts (1 ml) of detection reagents (SuperSignal® West Pico

Chemiluminescent substrate, Thermo Scientific) were applied to the membrane prior to imaging with a ChemiDoc imager (Bio-RAD).

3.2.12 Radioactive-thin layer chromatography (TLC)

Radioactive thin-layer chromatography (TLC) was performed in order to investigate the kinase activity of Omp50 and its mutated form, Omp50Y348F. Apyrase and hexokinase (both Sigma) reaction products were used to locate the radioactive spots corresponding to adenosine monophosphate (AMP) and adenosine diphosphate (ADP), respectively. Different reactions were prepared as listed in Table 3.2. Each reaction (20 µl) was incubated with 20 µl of an adenosine triphosphate (ATP) mixture containing 0.3 µCi of [α-^{32}P] ATP (hot ATP) and 0.1 mM of non-radioactive ATP (cold ATP) (both Sigma) for 1 hour at RT. A TLC polyethylenimine (PEI) cellulose membrane (Macherey-Nagel) was prewashed with milliQ water and left to dry on the bench. Following prewash, 1 µl of each reaction was then spotted onto the membrane. In order to obtain well-defined spots, each spot was applied at 0.4 cm interval, and always approximately 3 cm above the bottom of the membrane. Each reaction was spotted in duplicate. The membrane was run in 0.9 M Guanadine-HCl in a TLC glass chamber for 1 hour at room temperature. The membrane was dried on the bench, wrapped in film and exposed to an imaging plate for 15 minutes. The plate was phosphor imaging using a Typhoon FLA 7000 laser scanner (GE Healthcare).

Table 3.2. List of reagents used for the radioactive TLC

	(*) AMP Standard	(**) ADP Standard	ATP Standard	Omp50 WT	Omp50 Mutant
10mM Tris pH8	✓	✓	✓	✓	✓
10 mM $MgCl_2$	✓	✓	✓	✓	✓
150 mM NaCl	✓	✓	✓	✓	✓
0.45% C_8E_4				✓	✓
2 mM D-glucose		✓			
1U/µl Apyrase	✓				
1U/µl Hexokinase		✓			
4,6,8,or 10 µM Omp50				✓	
8 or 10 µM Omp50Y348F					✓
H_20 up to 20 µl	✓	✓	✓	✓	✓

(*) Apyrase+ ATP-> AMP+2P*i*

(**) H*exokinase+ATP+glucose->Glucose-6-phosphate+ ADP*

3.3.Results

3.3.1 Omp50 purification from the native C. jejuni 85H strain

The purification protocol from Bolla *et al* allowed the extraction of both MOMP and Omp50 porins from the outer-membrane of *C. jejun*i (Chapter 2, Figure 2.3). However, the level of the expression and so the final yield of purified Omp50 was very low and not useful for crystallographic studies. Therefore, no further experiments were carried out using Omp50 natively expressed in *C. jejuni* 85 H strain.

3.3.2 Omp50 recombinant expression and purification

Omp50 was overexpressed with either an N-terminus or a C-terminus His_6-tag in several cell lines. The level of expression of Omp50 with the C-terminus His_6-tag was low and therefore no further experiments were carried out with this construct. N-terminus tagged Omp50 showed higher levels of expression and was consequently used for small and large-scale purification. Omp50 was overexpressed in C43(DE3) cell line using TBP media and inducted at high OD_{600} at 37 °C for 3 hours. Omp50 was extracted using Octyl-POE, isolated using nickel resin, TEV cleaved and further purified using size exclusion chromatography. The SEC profile showed a single peak, whose fractions were analyzed by SDS-PAGE and identified as Omp50 by MS; (Figure 3.2 A-B) the purified peak yielded 0.2 mg L^{-1} of protein culture.

In order to improve the final yield, Omp50 was over-expressed in C43(DE3) using

auto-induction media and BME was added during all the steps of the purification. The gel filtration profile showed a single peak. Fractions of the peak were analyzed by SDS-PAGE and protein identity confirmed by MS. The protein showed degradation during the purification process (Figure 3.2 C-D). Final protein yield was 0.6 mg L^{-1} of protein culture.

Refolding was also attempted to increase the final protein yield. Omp50 was extracted from IB using urea. Refolding was carried out by diluting the suspension containing the unfolded Omp50 in refolding buffer containing either Elugent, LDAO or Octly-POE. Unfortunately, none of the buffers used led to a refolded protein. Omp50 precipitated during the refolding process as judged by SDS-PAGE.

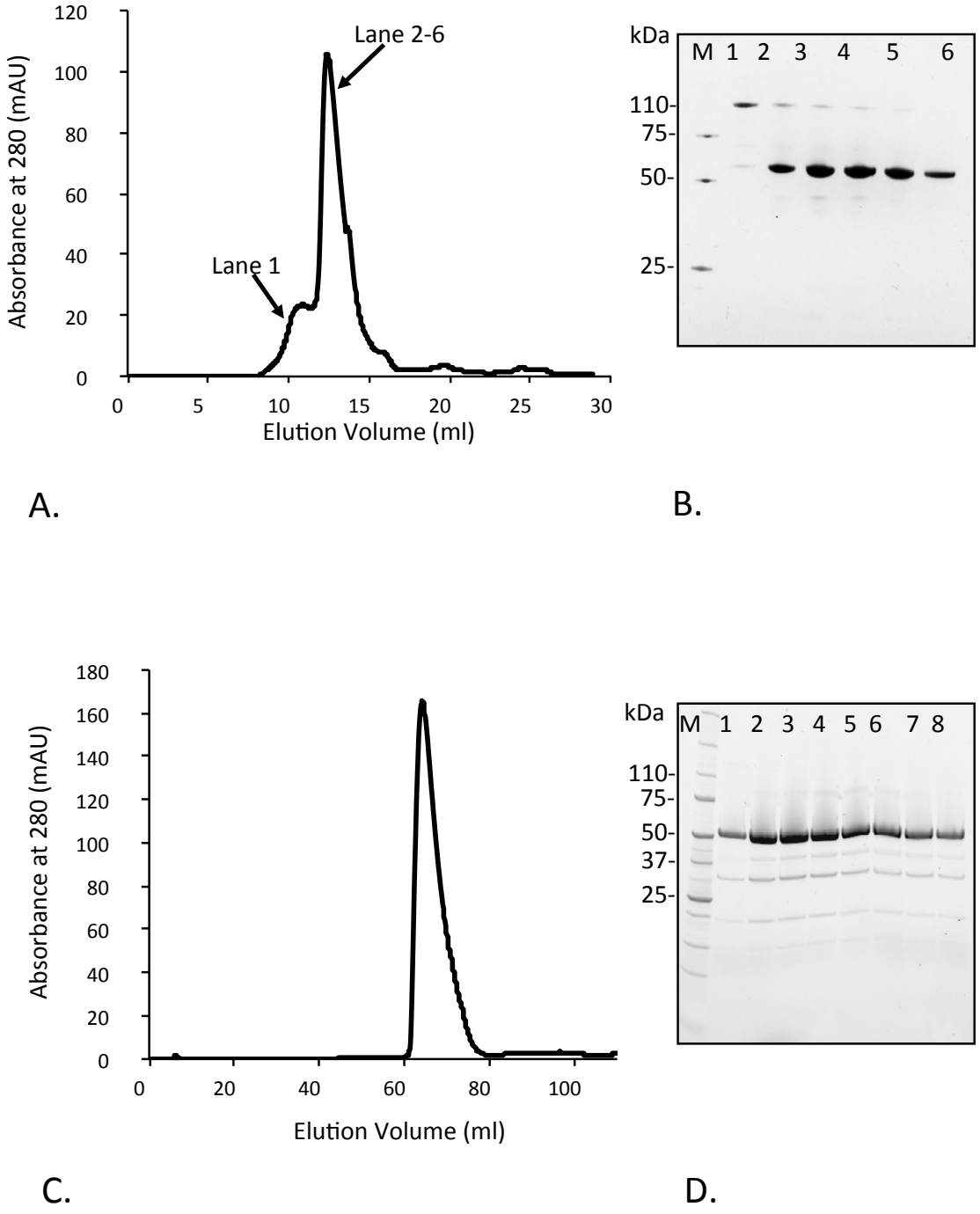

Figure 3.2: Omp50 purification: (A) SEC profile of Omp50 expressed in TBP media. A 10/300 S75 GE column was used for the SEC. (B) SDS-PAGE of chosen fractions from the SEC peak. M is the ladder. Bands at 50 kDa and at 110 kDa are Omp50 monomer and dimer, respectively as confirmed by mass-spec. (C) SEC profile of Omp50 expressed in auto-induction media. A 16/60 S200 GE column was used for the SEC. (D) The SDS-PAGE of chosen fractions from the SEC peak. M is the ladder, bands at 50 kDa are Omp50, while, the lower MW bands are products of degradation of Omp50 as confirmed by mass-spec.

3.3.3 Omp50 crystallization

Crystallization of Omp50 was carried out against several commercial screenings. Most of the drops were clear or were displaying large amounts of precipitation. However, small cubic crystals appeared after approximately 4 weeks (Figure 3.3). The crystals were confirmed to be protein crystals due to absorbance under UV light. When tested, however, they showed no diffraction. Attempts to reproduce and optimized the crystals were unsuccessful. Additive screening also did not improve the reproducibility of the crystals.

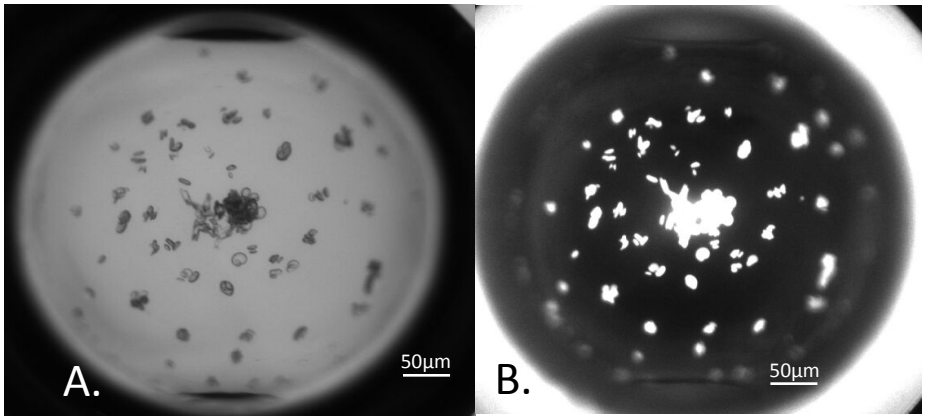

Figure 3.3: Crystallisation of Omp50. Crystals grown using the sitting drop vapor technique. (A) Under visible light (B) Under UV light

Omp50 was subject to limited proteolysis using several proteases at a ratio of 1:10 or 1:100 v/v. The proteolytic products were analyzed by SDS-PAGE in order to identify the most promising degradation pattern (Figure 3.4). The proteolitic products obtained from the digestion with trypsin at a ratio of 1:10 v/v were found to be the largest and the most stable and therefore used for crystallization

trials. Unfortunately, the use of limited proteolysis did not improve the crystallization of Omp50.

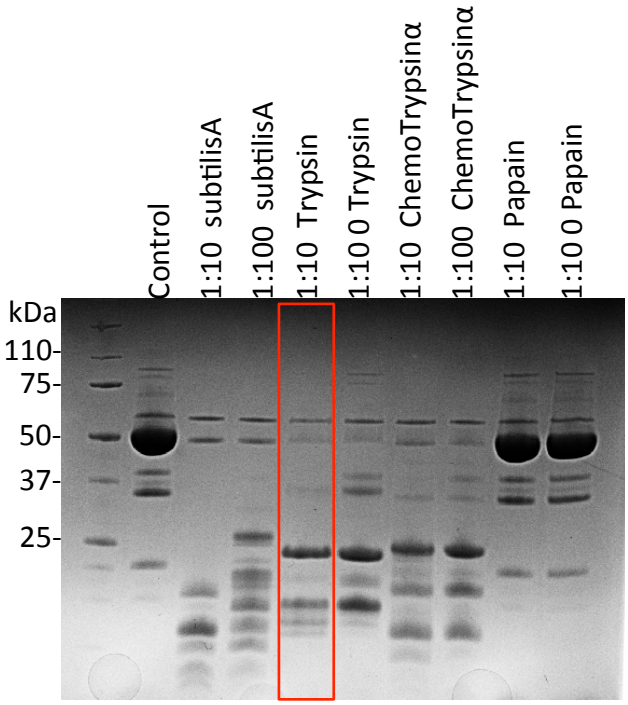

Figure 3.4: SDS gel of Omp50 proteolitic products. SDS gel of the Omp50 products obtained by limited proteolysis using subtilisA, trypsin, chemotrypsin and papain.

3.3.4 Lipid cubic phase (LCP)

In an attempt to get high quality crystals, the LCP technique was used as an alternative to the vapor diffusion technique. Omp50 was mixed with the lipid monooline, and the mixture was used to set up crystal trials against several commercial screenings. In this case, however, the LCP technique was unsuccessful and no crystals were detected.

3.3.5 Single channel conductance measurements of Omp50

Omp50 conductivity was assessed by single channel measurements in 1 M KCl, 10 mM MES pH 6. Omp50 inserted was into the bilayer as a monomer with a conductance of 53±0.2 pS. The insertion of the protein was difficult to achieve and the channel became unstable when a voltage higher than 100 mV was applied. The channel showed a high flickering rate, which is clear from the ion-current trace (Figure. 3.5).

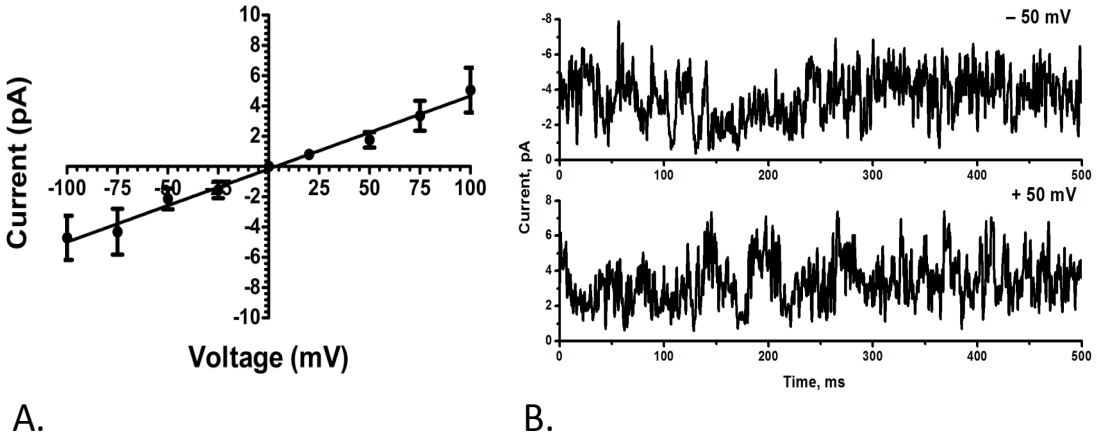

Figure 3.5: Single channel measurement. (A) I-V profile of Omp50. (B) Ion-current trace of Omp50.

3.3.6 Western blot with antibodies anti phosphorylated tyrosine

Omp50 auto-phosphorylation activity was assayed by western blot using an antibody against phosphorylated tyrosine. Wzc- an *E. coli* BY-kinase involved in the capsule biosynthesis- was used as a positive control, while Omp36 – a general porin from *Enterobacter aerogenes* – was used as negative control. Omp50 was analyzed before and after incubation with $MgCl_2$ and ATP. In both cases we could not detect any phosphorylated tyrosine (Fig. 3.6).

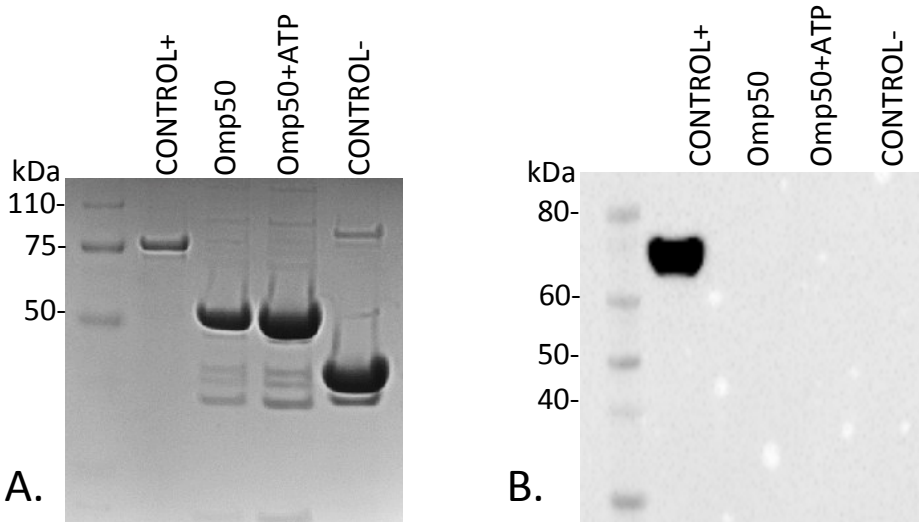

Figure 3.6: WB against phosphorylated tyrosine. (A) SDS gel of the sample tested for tyrosine phosphorylation. (B) WB with ab against phosphorylated tyrosine. Control+ (Wzc from *E. coli*), Omp50, Omp50 incubated with $MgCl_2$ and ATP, control-(Omp36 from *E. a*erogenes).

In collaboration with Prof. Panos Sultanos and Dr. Mahdavi (University of Nottingham), we were able to purify Omp50 from the native *C. jejuni* 11168 strain, the same strain used for the experiments performed by Corcionivoschi *et al*. We repeated the WB with antibodies anti phosphorylated tyrosine, however, also in this case, we did not detect any phosphorylation (Figure 3.7).

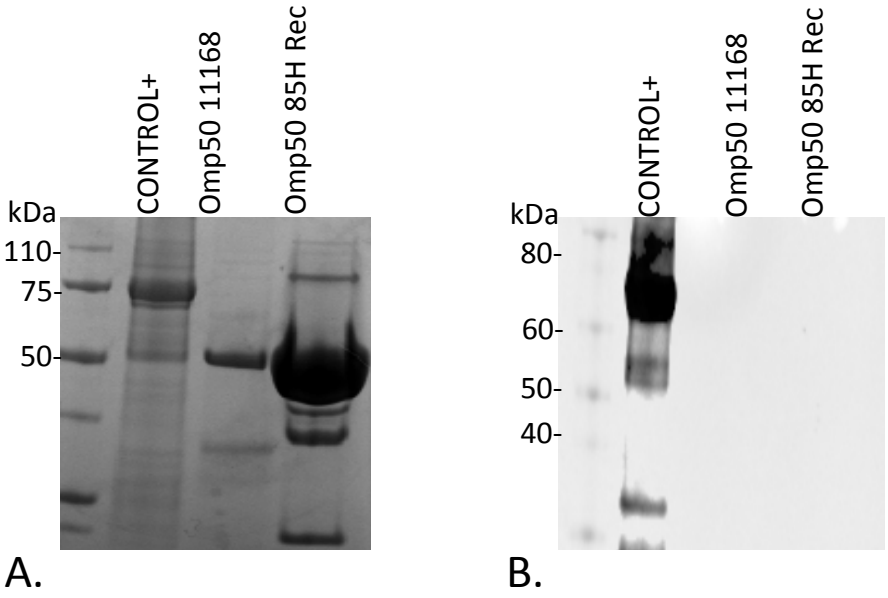

Figure 3.7: WB against phosphorylated tyrosine. (A) SDS gel of the sample tested for tyrosine phosphorylation. (B) WB with ab against phosphorylated tyrosine. Control+ (Wzc from *E. coli*), Omp50 from *C. jejuni* 11168, Omp50 85H.

3.3.7 Radioactive-thin layer chromatography (TLC)

Radioactive TLC was used to determine if Omp50 was able to hydrolyze ATP. Different concentrations of Omp50 were incubated with a mixture of hot and cold ATP and ran on a TLC membrane. To localize the radioactive spots corresponding to AMP, ADP and ATP, standards were also run. The spots corresponding to the reaction products of Omp50 showed that the ATP was not efficiently hydrolyzed. However, we noticed some background that we hypothesized could have been due to a contaminant and not from Omp50 activity. We therefore decided to re-run the experiment in the presence of Omp50Y348F as a negative control, for this mutant, a similar background was observed as in the native protein (Figure 3.8).

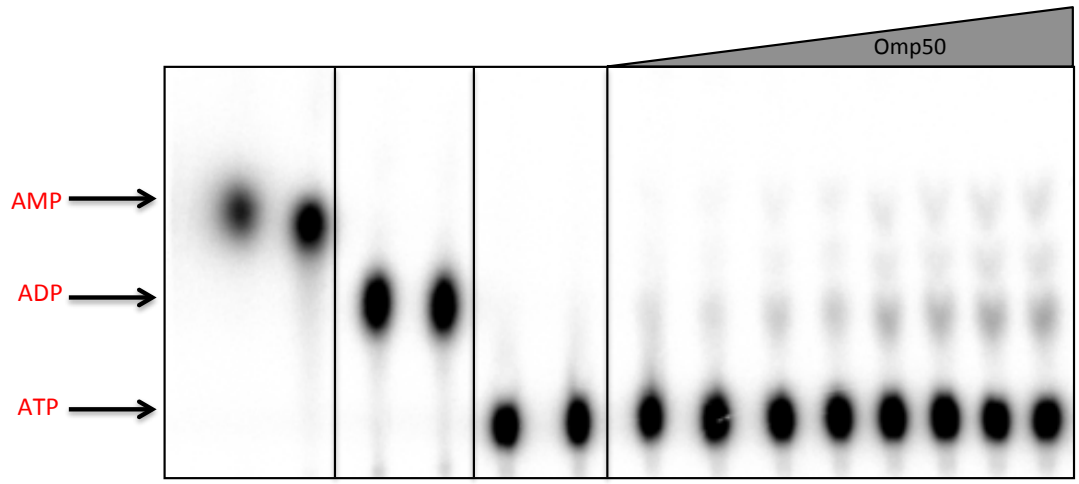

A.

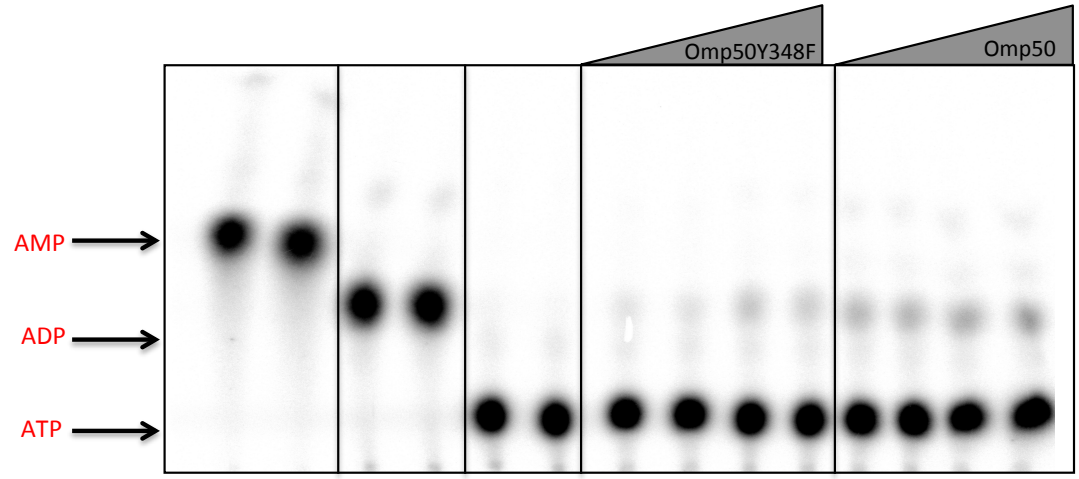

B.

Figure 3.8: Radioactive TLC of Omp50 and Omp50 Y348F. (A) Radioactive spots corresponding (from the left) to AMP, ADP, ATP and products of (4,6,8,10 µM) Omp50 activity. (B) Radioactive spots corresponding (from the left) to AMP, ADP, ATP and products of (8 and10 µM) Omp50 Y348F and (8 and 10 µM) Omp50 activity.

3.4 Discussion

3.4.1 Purification and crystallization of Omp50

Expression and purification of Omp50 was originally attempted using the native *C. jejuni*. Unfortunately, due to the low level of the expression, the amount of protein purified was not sufficient to start crystallization trials. Since *Campylobacter* are fastidious to grow under laboratory conditions, the option of growing a larger quantity of bacteria was rejected and recombinant expression was attempted instead.

Omp50 was recombinantly over-expressed in C43(DE3) *E. coli* cells using auto-induction media. The purified protein was used in crystallization trials and crystals were obtained within a month. However no diffraction was detected. To date, our attempts to reproduce and improve the crystals using various techniques have been unsuccessful.

3.4.2 Homology predictions

Structural homology predictions of Omp50 were generated using the web server Phyre2[211] (Figure 3.9). Omp50 predictions gave high confidence (>96%) based on 18-β-stranded porins (MOMP, Occk9, Occk8, OccaB3, Opdo) (Table 3.3). Interestingly, except from MOMP, all the porins used for the prediction are specific porins [212],[213],[42].

Table 3.3. Phyre2 Omp50 prediction models.

Model	Residues aligned	Confidence %	Identity %
MOMP (*C. jejuni*)	52-469	99.1	16
Occk9 (*P.aeruginosa*)	59-437	98.3	14
Occk8 (*P.aeruginosa*)	62-462	97.8	12
OccaB3 (*A. baumanii*)	58-463	97.7	12
Opdo (*P.aeruginosa*)	62-437	97.6	10

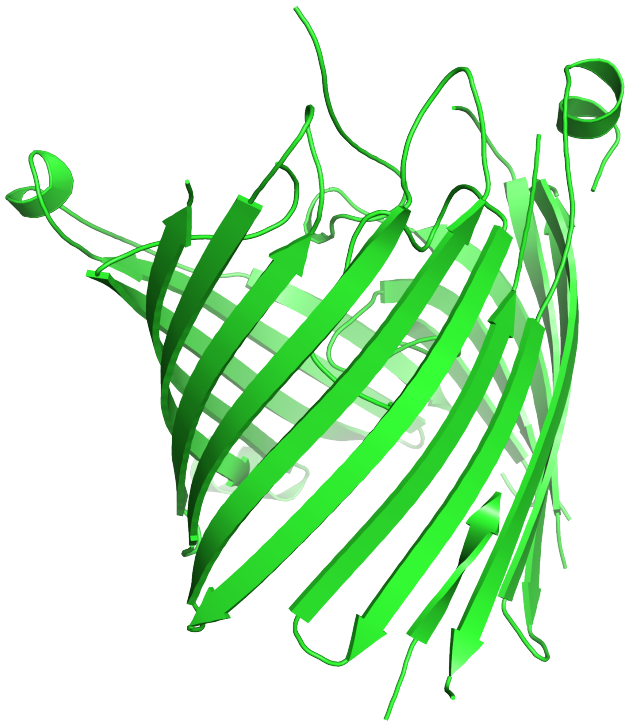

Figure 3.9: 3D homology model of Omp50. Phyre2 homology prediction using MOMP from *C. jejuni* as a model.

3.4.3 Pore activity of Omp50

Single channel experiments revealed that Omp50 recombinantly expressed in *E. coli* exhibits a conductance of 53±0.2 pS. Previously, Bolla *et al.* measured the conductivity of the native Omp50[203], and we found those measurements agree with ours. Omp50 conductance is similar to the conductance of the specific porins from *P. aeruginosa* Occk4 and Occk6 (43±11pS and 71±34pS, respectively)[214]. Conversely, unlike the Occk porins, which showed anion selectivity, Omp50 has been shown to be cation-selective [203].

3.4.4 Omp50 putative tyrosine kinase activity

It was the publication of Corcionivoschi *et al.*[207], that led us to investigate the allegedly kinase activity of Omp50. BY-kinases are typically constituted of two α-helices spanning the inner membrane with the catalytic domain facing the cytoplasm [215],[208],[216]. Omp50, however, has been predicted to be a barrel of 18 β-sheets located in the outer-membrane, hence significantly different from a typical BY-kinase structure. Moreover, while ATP concentration in the cytoplasm ranges from 1-3 mM [217], it has been shown to be absent or considerably low in the periplasmic and in the extra-cellular space [218]. It is a question as to where the ATP for the phosphorylation of Omp50 and its substrates would come from.

In our experiments, western blots against phosphorylated tyrosine failed to detect any phosphorylation in Omp50. When we repeated the western blot using Omp50 natively expressed in *C. jejuni* 11168 we could not detect any phosphorylation either.

We also attempted to determine if Omp50 was able to hydrolyze ATP by using radioactive TLC. The TLC results suggested that Omp50 does not have any kinase activity, since no products of ATP hydrolysis were spotted on the TLC membrane. Although some background was noticed while analyzing the results, Omp50 Y348F (predicted to be inactive) gave a similar background.

Taking into consideration our results, the predicted structure of Omp50 and the inaccessibility to the ATP needed for the phosphorylation process, we think that Omp50 it is unlikely to be a BY-kinase.

3.5 Conclusion and future work

We have shown that we can over-express Omp50 using a recombinant system and purify a suitable quantity of protein for crystal trials. Reproducible Omp50 crystallization, however, was hard to achieve. Future work will be to test a broader range of detergents and buffers to improve the crystallization process.

We also have shown that Omp50 recombinantly expressed in *E. coli* is able to form pores when inserted in a lipid bilayer, and displayed the same conductivity as the natively expressed porin.

While analyzing the *in vitro* kinase activity of Omp50 we did not see any evidence for activity. Therefore our results are in disagreement with Corcionivoschi [207] studies.

Chapter 4: Omp35 and Omp36 from *Enterobacter aerogenes*

4.1 Introduction

4.1.1 Enterobacter aerogenes infections and antibiotic resistance

Enterobacter aerogens are facultative anaerobic and opportunistic bacteria belonging to the family of *Enterobacteriacea*, frequently isolated from the respiratory and urinary system of hospitalized patients [219],[220]. *E. aerogens* infections have been associated with high levels of morbidity and mortality [221]. For example, in Nepal in 1999, *E. aero*gens infections led to an outbreak of septicemia in a neonatal intensive care, causing the death of 12 new borns [222].

Moreover, an increased number of *E. aerogenes* strains, isolated from nosocomial patients, have exhibited a multi-drugs resistance (MDR) phenotype. MDR *E. aerogens* strains have been identified all over Europe [220]. The expression of an extended-spectrum β-lactamase [223], TEM-24 [224], chromosomal cephalosporinase, and recently acquired carbapenemases confer resistance to β-lactams [225], carbapenems along with resistance to the first generation cephalosporin [226],[227]. In France, a pan-drug resistant clone of *E. aerogenes* (EA1509E) has been isolated from a nosocomial patient, that was found to be resistant to all the clinical relevant antibiotics with the only exception of gentamycin [228]. Similarly in Belgium, several patients (aged from 7 to 85 years) were infected with a clone of MDR *E. aerogenes* susceptible only to gentamycin and imipenem [229].

In general, MDR is a complex mechanism regulated at different levels. Several genes, including *MarA, RamA, SoxS* are involved in regulation of MDR, specifically, by up-regulating the expression of efflux pumps and down-regulating the expression of porins [230],[231]. Mutations and overexpression of these genes have been linked to a high level of antibiotic resistance [230]. In particular, an overexpression of *MarA* has led to a 2- to 16- fold increase in resistance to carbapenems and fluoroquinolones in *E. aerogenes* ATCC 13048 strain [230].

4.1.2 Enterobacter aerogenes porins

Two major general porins are found in *E. aerogenes,* Omp35 (OmpF-like porin) and, Omp36 (OmpC-like porin)[232]. Omp35 is a trimeric porin usually expressed under low osmolarity conditions. Pore activity of Omp35 has been confirmed by single channel measurements of conductivity and cation selectivity have been reported; these values are similar to what has been observed for OmpF from *E. coli (*4.22 nS measured at pH 7*)* [232]. Omp36 is a trimeric porin (homologous of OmpC from *E. coli* and OmpK36 from *K. pneumonia*) expressed under high osmolarity conditions [233].

In MDR *E. aerogenes* isolates, porin expression was observed to be significantly altered[234][235]. In ertapenem-resistant isolates the expression of Omp35 is down regulated and eventually completely suppressed [236]. In ertapenem and imipenem-resistant isolates, along with Omp35, Omp36 expression is also suppressed [235]. In clinical isolates, mutations of the L3 in Omp36 have been

associated with antibiotic resistance [233]. Most strikingly substitution of a glycine to an aspartic acid in position 112 has been shown to decrease the uptake of β-lactams and cephalosporin[11].

4.1.3 Aims

Alterations of the expression level and mutations at the level of the constriction zone of Omp35 and Omp36 have been linked to an increased antibiotic resistance in *E. aerogenes isolates.*

In order to analyze how clinically relevant antibiotics translocate via Omp35 and Omp36, we aimed to structurally and functionally characterize both porins. Firstly, we aimed to over-express Omp35 and Omp36 in *E. coli*, to purify them and ultimately solve their X-ray structure. In addition, we aimed to use the purified porins to measure the rate of permeations of several classes of antibiotics by using liposome swelling assay.

The work of this chapter also aimed to have a better understanding of permeation through the orthologues of Omp35 and Omp36 (OmpF and OmpC from *E. coli*, OmpE35 and OmpE36 from *E. cloacae* and OmpK35 and OmpK36 from *K. pneumonia*). To do so we decided to perform the liposome swelling assay with OmpC and OmpF and to compare the data obtained with data shared by our collaborators.

4.2 Materials and methods

4.2.1 Cloning and expression

Codon optimized genes encoding for Omp35 (ATCC 15038) and Omp36 (ATCC 13048) from *E. aerogenes* were ordered from DNA2.0 (California, USA) and cloned into a pTAMAHisTEV ampicillin-resistant vector. The vector and genes were digested with NcoI and BamHI restriction enzymes at 37°C for three hours. The vector was then treated with alkaline phosphatase (Promega) for an additional 30 minutes at 37°C. Omp35 and Omp36 genes and the vector were ligated at RT, overnight using T4 ligase (Promega). The ligation mixture was later used to transform DH5α cells. The transformed cells were plated onto LB agar plates supplemented with 100 μg/ml of ampicillin. Colonies were picked and grew in 10 ml LB media supplemented with 100 μg/ml of ampicillin at 37°C, 200 rpm overnight. Cells were miniprepped using the commercial kit QIAprep® Spin Miniprep Kit (Qiagen) and the plasmid sent to sequencing (GATC Biotech).

The Omp-constructs were transformed in porin-deficient *E. coli* BL21omp8-competent cells. For the overnight culture, 250 ml of LB culture containing 100 μg ml^{-1} ampicillin was incubated with a colony of each of the constructs at 37°C and shacked at 200 RPM overnight. 10 ml of the overnight culture was used to inoculated 12x 1 L LB containing the same amount of ampicillin and grown at 37°C until OD_{600} ~ 0.6. Cells were then induced with 0.4 mM IPTG and the temperature decreased to 25°C. The cells were grown for 16 hours and harvested by centrifugation at 6,200 g (JLA 8.1000 rotor, Beckman Coulter).

4.2.2. Omp35 and Omp36 purification

Cell pellets were re-suspended in lysis buffer (5-10 ml of buffer per gr of cell paste) (Appendix A.3) and lysed by two passes through a chilled cell disruptor at 30 kpsi. Cellular debris were removed by centrifugation at 10,000 g (JA 25.50 rotor, Beckman Coulter). The total membrane fraction was collected by ultracentrifugation at 100,000 g (50.2 Ti rotor, Beckman Coulter) at 4 °C for 1 hour. The membranes were solubilized in 50 mM Na_3PO_4 pH 8, 250 mM NaCl and 7% Octyl-POE and left stirring at 4°C overnight. Soluble material was then recovered by ultracentrifugation at 100,000 g, at 4°C for 1 hour. The supernatant containing the solubilized protein was incubated with 5ml of Ni-NTA resin (Qiagen, UK) and 10 mM imidazole pH 8 at 4°C for 2 hours. The resin was then washed with 10 CV of washing buffer; 50 mM Na_3PO_4 pH 8, 250 mM NaCl, 1% Octyl-POE and 30 mM imidazole pH 8. The protein was eluted with the same buffer containing 250 mM imidazole. 1 mg of His_6-tagged TEV protease was added to the eluted protein and dialyzed in SnakeSkin tubing (Thermo Scientific) against a buffer containing 10 mM imidazole at 4°C overnight. The dialyzed sample was passed through a 0.45 μm syringe filter and applied to a 5 ml His-trap column (GE Healthcare). The cleaved protein was collected from the flow-through fraction and further purified by gel filtration using a 16/ 60 Superdex 200 pg (GE Healthcare) equilibrated with 2 CV of a buffer containing 10 mM Tris-HCl pH 8, 150 mM NaCl and 0.45% (w/v) C_8E_4. The protein was concentrated to 10 mg ml^{-1}

for crystallization. Purity and integrity were monitored on SDS-PAGE (NuPAGE, Invitrogen) and mass spectrometry.

4.2.3 Omp35 and Omp36 crystallization

Different commercial screens were used for initial trials (Appendix B). The screens were dispensed into a 96-well sitting drop plate (Intelli-Plate®, ARI) using a Gryphon robot, at a protein:reservoir ratio of 1:1 and 1:2. When required hits were optimized by hanging-drop vapor diffusion technique. 30 % (v/v) ethylene glycol was used as cryoprotectant to harvest and cool flash crystals in liquid nitrogen. Listed below (Table 4.1) are the crystallization conditions that gave the crystals used for data collection.

Table 4.1. Omp35 and Omp36 crystallization conditions.

Omp35	0.05 M Magnesium sulfate, 8% (w/v) PEG 8000
Omp36	0.1 M Tris-HCl pH 8.5, 8% (w/v) PEG 8000

4.2.4 Omp35 and Omp36 data collection and structure determination

A data set of both Omp35 and Omp36 was collected at the Diamond Synchrotron Light Source (UK), beam-line i02, i04 respectively. Data were processed using Mosflm [237] and scaled with SCALA. The structures were solved by molecular replacement [187] to a resolution of 2.85 Å (Omp35) and 2.45 Å (Omp36). OmpK36 (ID PDB: 1OSM) was used as search model to solve Omp36 structure, while OmpF (ID PDB: 2OMF) was used as search model to solve Omp35. The

structures were built manually using Coot [188] and refined using REFMAC5 [189]. Data quality was checked by Molprobity [238].

4.2.5 Liposome swelling assay

OmpC and OmpF porins used for the liposome swelling assay were purified by our collaborators from the Jacobs University in Bremen (Grermany). Liposome swelling assay data on OmpE35/36 and OmpK35/36 were obtained by our collaborators from Newcastle University (UK).

Liposome swelling assay was carried out following the procedure described by Nikaido [239] (Figure 4.1). Liposome vesicles were prepared by mixing 100 mg of dihexacetyl phosphate dissolved in 0.5 ml of $CHCl_3$ and 2 ml of L-α-phosphatidyl choline (both Sigma). 250 µl of the mixture was dried under vacuum for 2 hours. 300 µl of distilled water was added to the dried liposomes along with 30 µg of either Omp35, Omp36, OmpC, or OmpF. The solution was then sonicated in a Branson bath-type sonicator for one minute. The resulting mixture was left drying under vacuum overnight. For the blank control, the protein was substituted with buffer. Dried proteoliposomes were resupended in 12 mM stackyose dissolved in 10 mM Hepes pH 7. The mixture was left at room temperature (RT) for two hours before starting the experiments. Consecutively, 5-10 µl of the liposome was quickly mixed with 200 µl of an isotonic solution containing the substrates (nutrient or antibiotic) to be tested. The concentration of the substrate/antibiotic ranged between 8-20 mM (see Table 4.3). The correct concentration was

determined by detecting the concentration at which the blank did not show (or showed less that 5%) any variation of optical density at 400 nm. Permeation of the tested antibiotics through the porins was assayed by determining the variation of optical density at 400 nm. Readings were taken every 5 seconds for one minute. Measurements from the same set of proteoliposome were taken in triplicate.

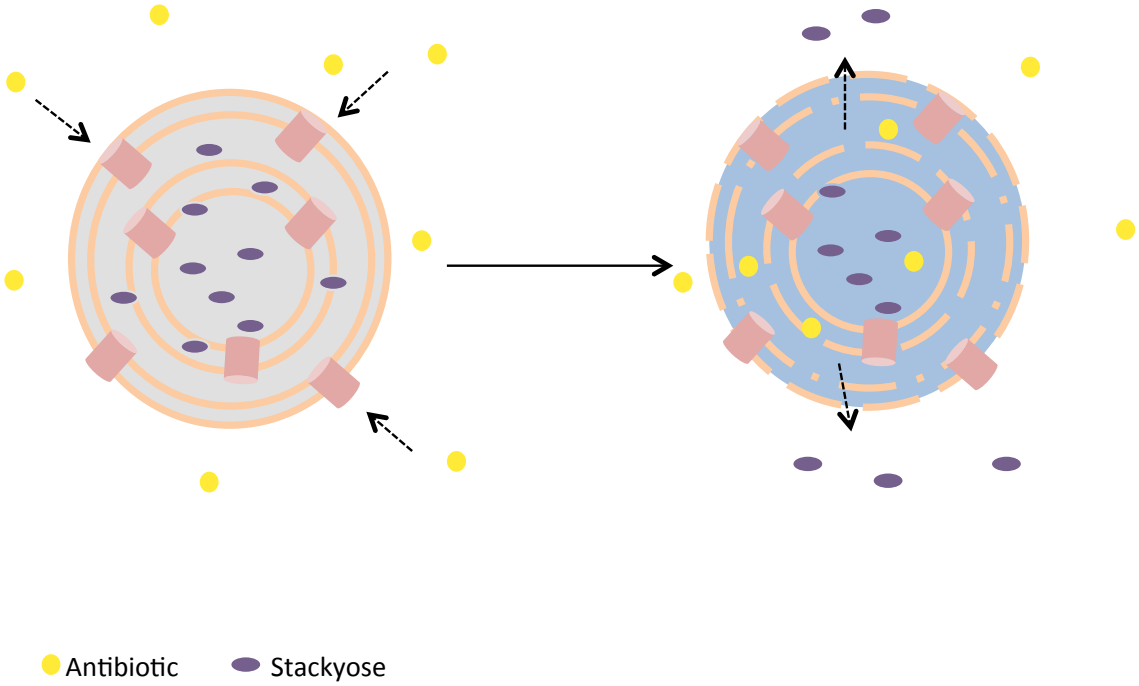

Figure 4.1: Schematic representation of liposome swelling assay. Liposome vesicles, containing the target porins, are mixed in a solution containing the antibiotic to test. If the antibiotic enters the porins, water will follow and cause the liposome vesicles to swell and eventually burst. Picture adapted from [240].

4.3 Results

4.3.1 Omp35 and Omp36 purification

Codon optimized genes for Omp35 and Omp36 were cloned into a pTAMAHisTEV vector, which carries a TamA signal peptide and an N-terminus hexa-histidine tag followed by a TEV cleavable site. ΔOmp8 (DE3) *E. coli* porin-null strain [241] was used to overexpress both proteins. Membranes were solubilized directly in Octyl-POE and the extracted proteins were isolated using nickel resin; TEV cleaved and further purified using size exclusion chromatography. During the size exclusion chromatography Octyl-POE was exchanged to C_8E_4, a more suitable detergent for crystallography experiments. The eluted protein was then concentrated to 10 mg $ml^{-1.}$ The SEC profile showed a single peak for each of the purified proteins (Figure 4.2). Fractions were evaluated by SDS-PAGE and identified by MS. Omp35 and Omp36 purifications yielded 1-1.5 mg of protein per liter of LB media.

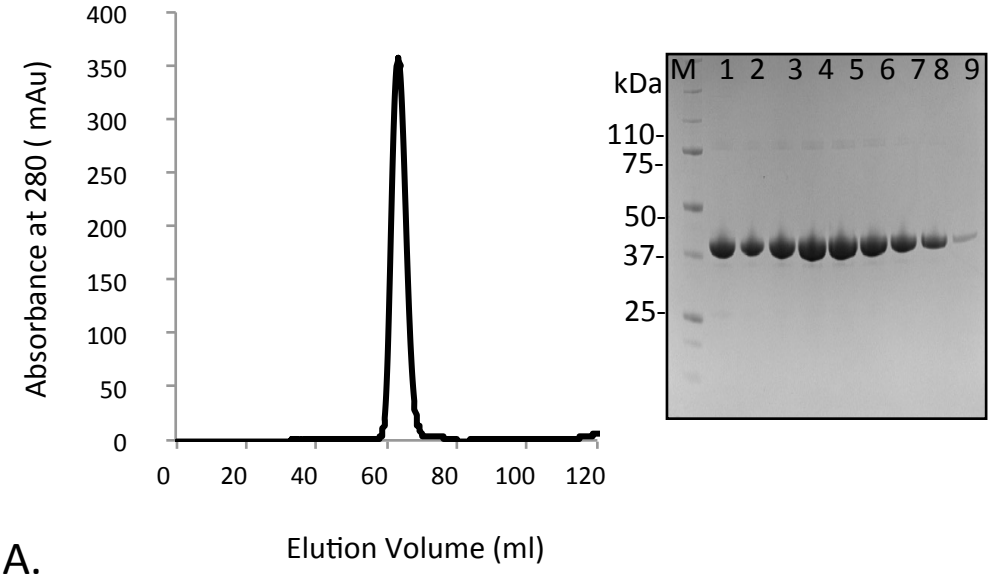

A.

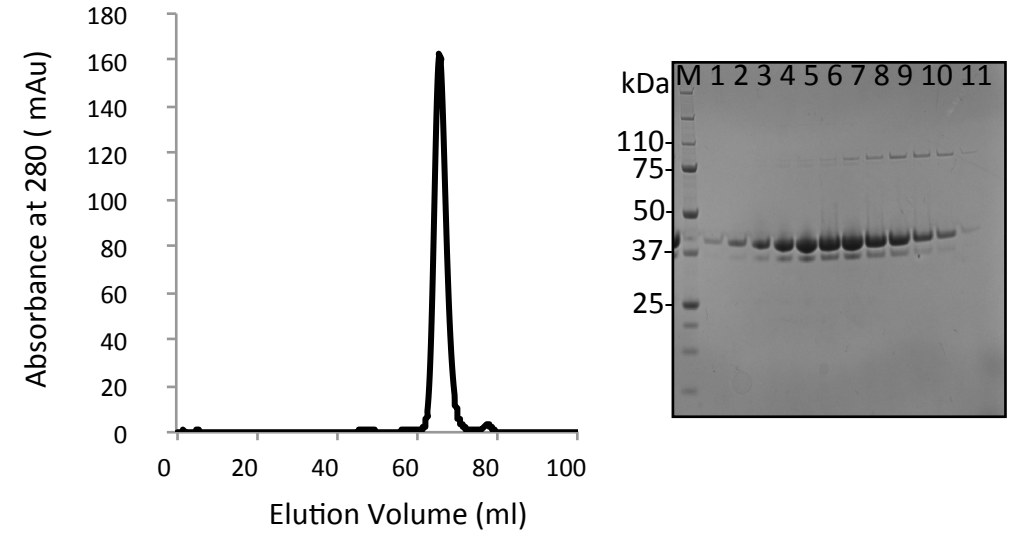

B.

Figure 4.2: Omp35 and Omp36 purification. (A) Shows the SEC profile of Omp35 and the SDS-PAGE gel of the eluted fractions. M is the ladder, line 1-9 are the eluted fractions. (B) Shows the SEC profile of Omp36 and the SDS-PAGE gel of the eluted fractions. M is the ladder and lines 1-11 are the eluted fractions. In lines 7 to 11 is visible an extra band, at 75 kDa. This band was confirmed by mass-spectrometry to be a contaminant. For both Omp35 and Omp36 SEC,a 16/60 200 pg (GE) column was used. The elution volume of both Omp35 and Omp36 was compared to the elution volumes of molecular weight (MW) markers (Bio-rad) (used to calibrate the column) in order to analyse their oligomeric state. Both proteins were found to be trimeric.

4.3.2 Omp35 and Omp36 crystallization and structure determination

Omp35 and Omp36 crystals appeared within a week. When necessary crystals were optimized by hanging drop vapor technique (final crystallization conditions for each protein are listed in 4.1) (Figure 4.3). Crystals were cryo-protected in ethylene glycol and analyzed by synchrotron radiation at Diamond Light Source, beam line iO2, iO4-1 for Omp35 and Omp36, respectively. Omp35 data set was processed to a resolution of 2.85 Å in the space group I222 and solved by molecular replacement using OmpF (PDB code: 1OMF) as the search model. Omp36 data set was processed to a resolution of 2.47 Å in the space group P3 and solved by molecular replacement using OmpK36 (PDB code:) as the search model. Analysis of Mathew's coefficient (Mathew's coefficient: 2.19 and 2.32 for Omp35 and Omp36, respectively) showed a trimeric arrangement in the cell unit. For both structures, the quality of the structures was assessed using Molprobity. Data collection and refinement statistics are shown in table 4.2.

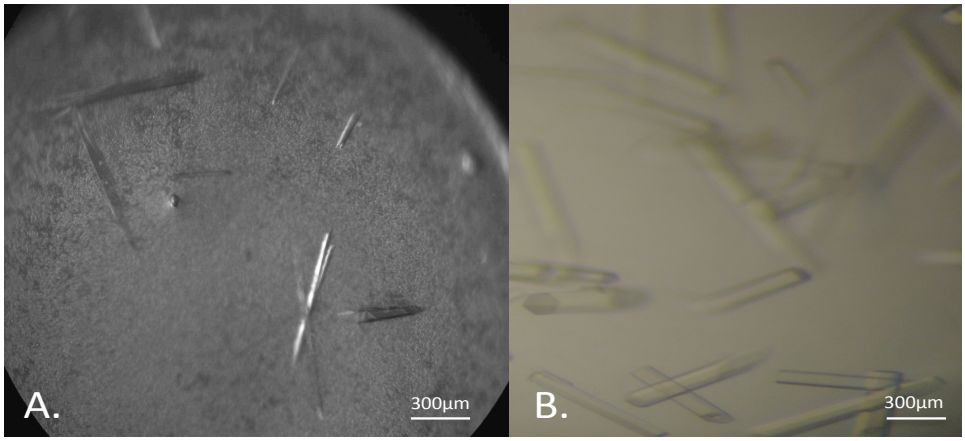

Figure 4.3: Omp35 and Omp36 crystals. (A) Omp35 and (B) Omp36 crystals under visible light.

Table 4.2. Data collection, refinement and validation statistics.

	Omp35	**Omp36**
Beam line	**iO2**	**iO4**
Space group	**I222**	**P3**
Cell dimensions a,b,c (Å)	**111.57, 115.94, 216.66**	**125.09, 125.09, 126.54**
Cell dimensions α,β,γ (°)	**90, 90, 90**	**90,90,120**
Resolution (Å)	**108.56-2.85(3.0-2.85)**	**56.07-2.46 (2.5- 2.46)**
R_{merge}	**0.11 (0.52)**	**0.08 (0.2)**
Completeness (%)	**92.9 (85.5)**	**99.27 (99.0)**
Multiplicity	**2.5 (2.5)**	**3.1 (3.1)**
I/σ(I)	**6.3 (1.3)**	**9.6 (3.8)**
CC 1/2	**0.99 (0.68)**	**0.99 (0.60)**
Refinement		
R_{factor}/R_{free} (%)	**21.33/26.0**	**19.5/23.9**
N° of unique reflections	**33222**	**74780**
N° of residues	**337**	**335**
Water	**-**	**98**
Rmsd		
Bonds length (Å)	**0.010**	**0.015**
Bonds angles (Å)	**1.47**	**1.7**
MolProbity		
Ramachandran outliers (%)	**0.3**	**0.4**
Ramachandran favored (%)	**95.24**	**93.5**
Clash score	**3.1**	**5.5**
Molprobity score	**1.63**	**1.73**

**(Values in parentheses are for the highest-resolution shell)*

4.3.3 Crystal structure of Omp35 and Omp36

The crystal structures of Omp35 and Omp36 show similar architecture as expected from their high degree of sequence identity (%) (Figure 4.4). Each trimer consists of three 16-β-stranded monomers, with long external loops (L1-L7) and short periplasmic turns (T1-T7) (Figure 4.4) As common for porins, L3 folds back into the channel forming the so-called "eyelet" or constriction zone of the pore. Pymol measurements indicated a larger pore diameter for Omp35 (11 Å) when compared to Omp36 (8Å). At the constriction zone of both Omp35 and Omp36, highly conserved negatively charged residues (D100, E110, D114 in Omp35 and Omp36) interact with a cluster of arginine and lysine (also highly conserved) present on the barrel wall facing the loop, creating a transverse electric field (R38, K42, K82, R93, R160 in Omp35 and R37, K41, K82, R93, R166 in Omp36). High levels of heterogeneity are present, instead, at the level of the external loops, especially in L4 and L5. In particular, deletions in L4 and L5 of Omp35 generate shorter loops when compared to L4 and L5 in Omp36 (Figure 4.5).

The electrostatic potential of both structures showed that, the external side of the barrel is uncharged while, inside the barrel, at the level of the constriction zone, there is a clear segregation of charges. Both negatively and positively charged residues are present at the level of the external loops and the periplasmic turns (Figure 4.6).

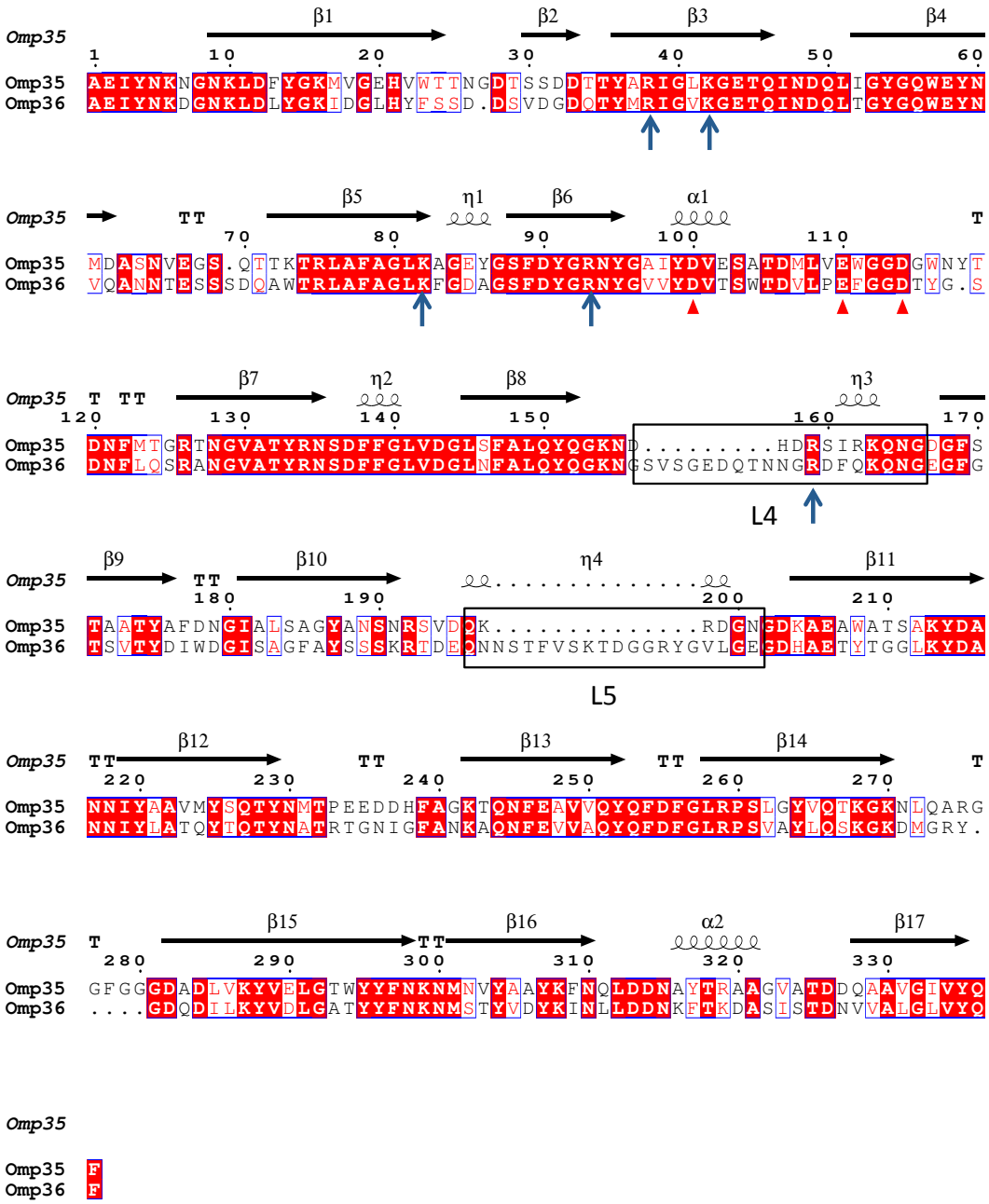

Figure 4.4: Sequence alignment of Omp35 and Omp36. Conserved negatively charged amino acids in L3 are indicated with red triangles. Positively charged amino acids, opposite the L3, are indicated with blue arrows. L4 and L5 are boxed in black.

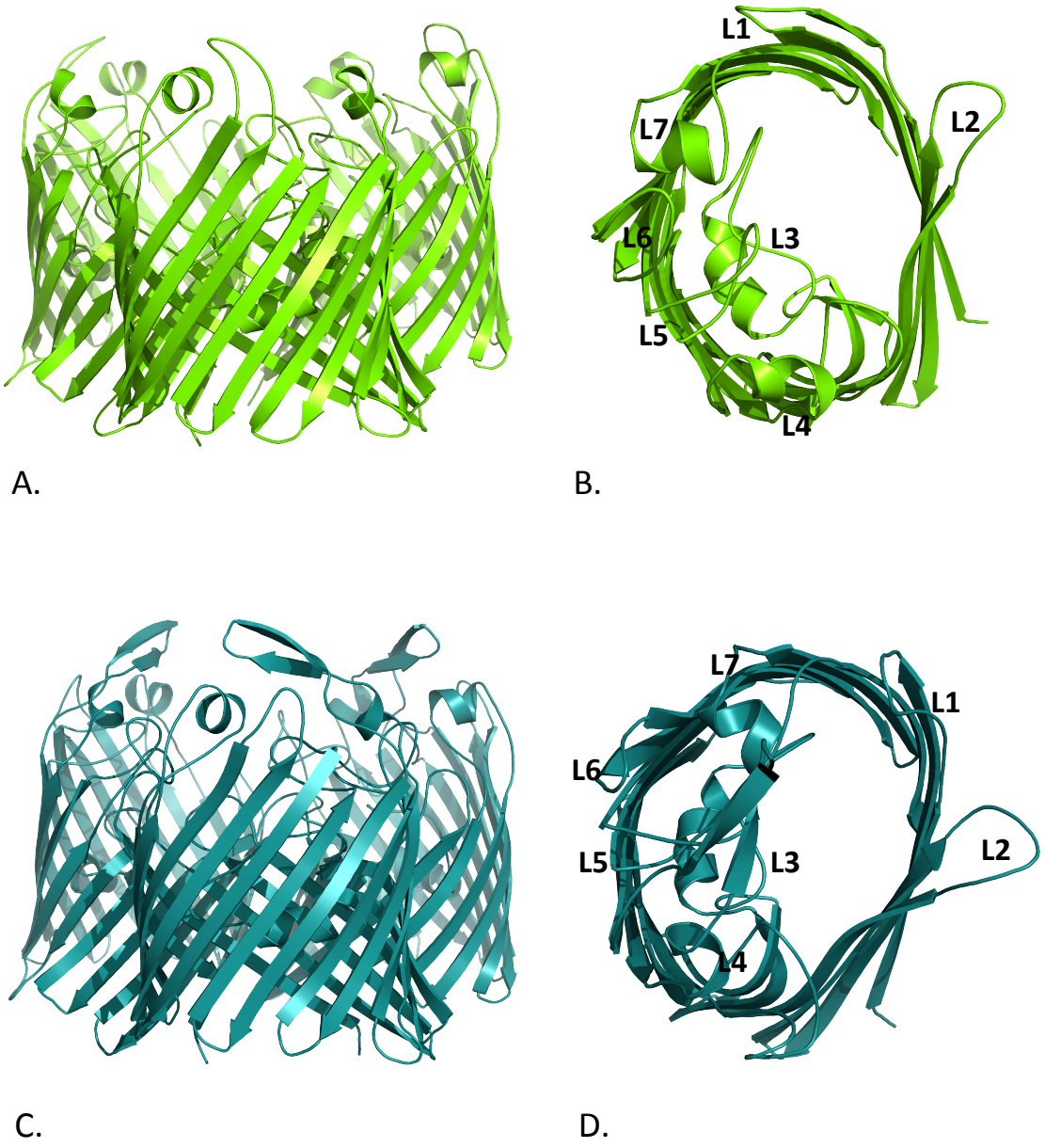

Figure 4.5: Crystal structures of Omp35 and Omp36. (A) Side view of Omp35 trimer. (B) Extracellular view of Omp35 monomer. Loops are labelled in bold. (C) Side view of Omp35 trimer. (D) Extracellular view of Omp35 monomer. Loops are labelled in bold.

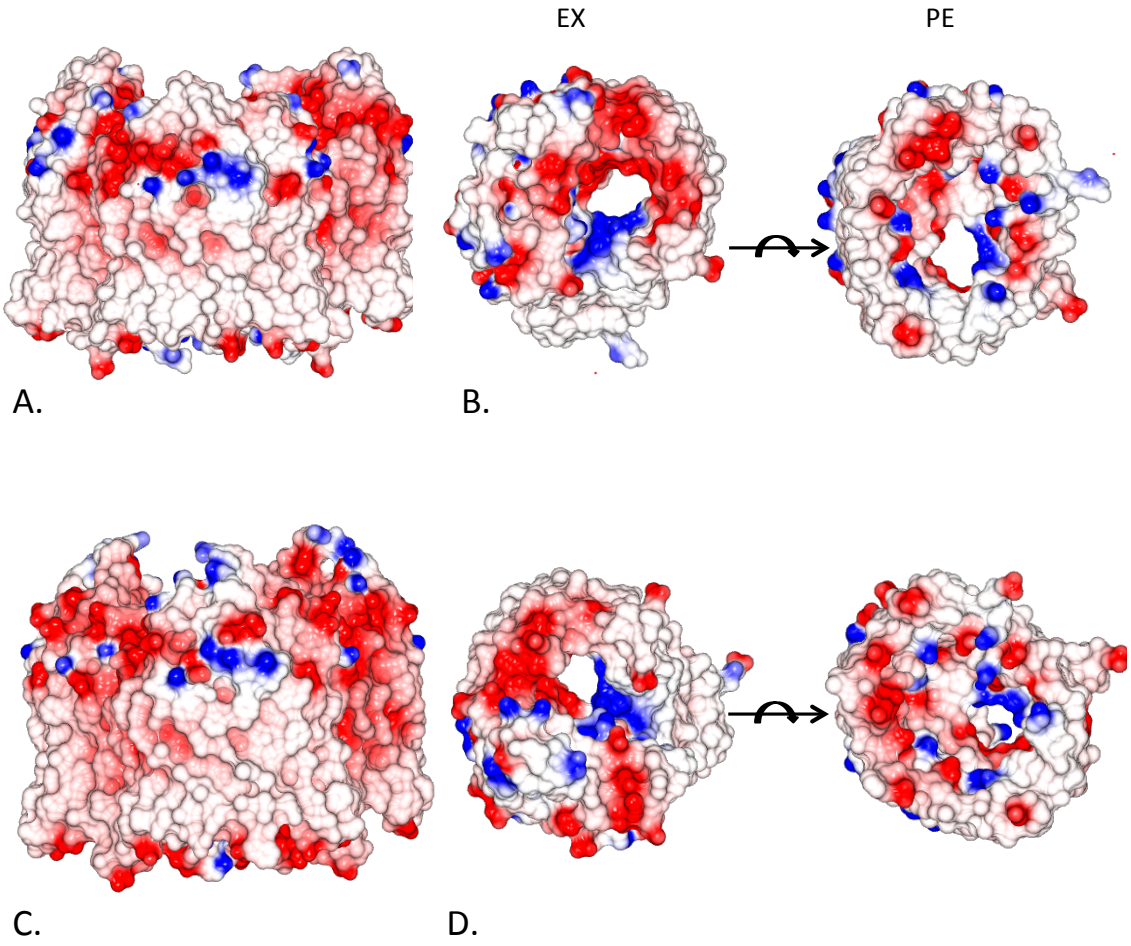

Figure 4.6: Electric potential of Omp35 and Omp36. Side view of Omp35 (A) and Omp36 (B) channel. Extracellular and periplasmic view of Omp35(C) and Omp36 (D) monomer.

4.3.4 Liposome swelling assay

Liposome swelling assay (LSA) was performed in order to analyse the permeation of different substrates (glycine, arginine, glutamic acid and glucose) and antibiotics (penicillins, carbapenems and cephalosphorins) (Table 4.3) through the pore of Omp35 and Omp36. Each measurement was normalised against the permeation rate of the amino acid glycine. Glycine can easily translocate through porins due to its small size. All molecules show higher permeability through Omp35 compared to Omp36. Among the antibiotics tested, the zwitterionic ones (meropenem, imipenem and cefepime) show higher permeability rate, over 40%. On the contrary, negatively charged antibiotics (ceftazidime, cefotaxime, piperacillin and ticarcillin) show less than 30% permeability rate. Overall, meropenem showed the highest rate of permeation while the penicillin-like antibiotics showed the lowest (Figure 4.6).

Table 4.3. Charge and molecular weight of the antibiotics used for the LSA.

Name	Charge	Molecula weight (Da)	Concentration (mM)
Glycine	(+,-)	75	17
Arginine	(+,+,-)	174	17
Glutamate	(+,-,-)	146	12
Glucose	(0)	180	12
	Penicillins		
Ampicillin	(+,-)	349	12
Ticarcillin	(-,-)	382	10
Piperacillin	(-)	517	10
	Carbapenems		
Ertapenem	(+,-,-)	475	15
Imipenem	(+,-)	299	12
Meropenem	(+,-)	383	12
	Cephalosphorins		
Cefotaxime	(-)	454	12
Cefepime	(+,-)	481	8
Ceftazidime	(+,-,-)	546	10

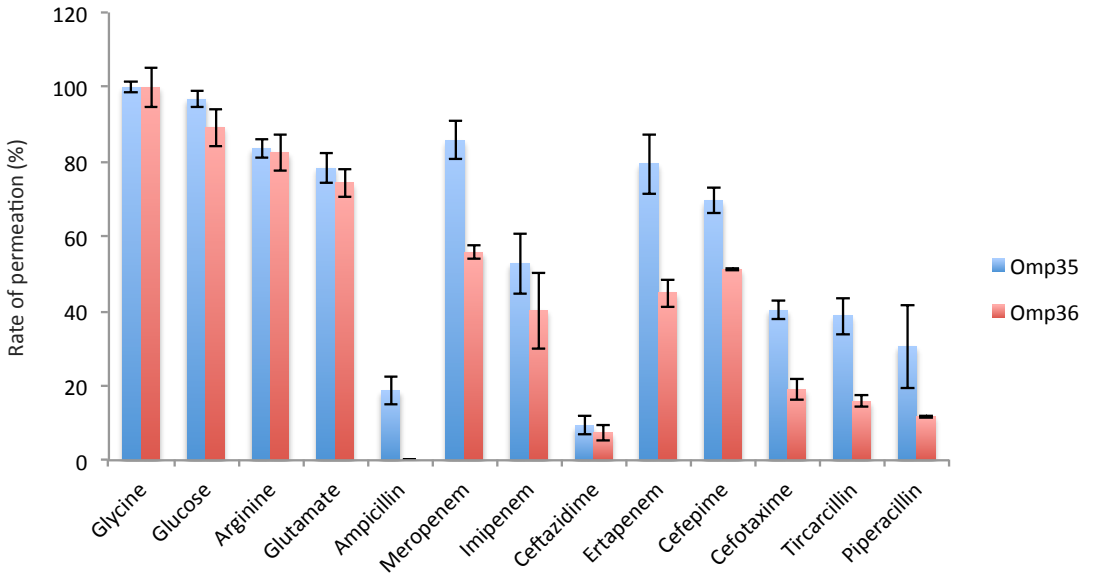

Figure 4.7: Liposome swelling assay chart. Relative permeation rate of several substrates through Omp35 and Omp36. Measurements are taken in triplicate and normalized against glycine permeation (=100). Error bars indicate standard deviation (SD). Concentration of the substrates are listed in Table 4.3. In general, zwitterionic antibiotics (meropenem, imipenem and cefepime) show high rate of permeation (over 40%). On the contrary, negatively charged antibiotics (ceftazidime, cefotaxime, piperacillin and ticarcillin) show lower permeation rate.

4.4 Discussion

4.4.1 Overall structures of E. aerogenes major porins

In this study, we present the X-ray structures of the two major porins from *E. aerogenes,* Omp35 and Omp36. The structures we obtained, showed a trimeric arrangement, as already indicated from the SEC profile. Overall, the structural features observed in Omp35 and Omp36 are common to all the general porins characterized so far in the *Enterobacteriaceae* family. A barrel consisting of 16 anti-parallel β-strands linked together by long extracellular loops (L1-L7) and short periplasmic turns (T1-T7). The constriction zone of the pore encloses highly conserved residues whereas the external loops are different.

.

4.4.2 Structural comparison of OmpC-like and OmpF-like porins in Enterobacteriaceae

General porins from the *Enterobacteriaceae* family (Omp35/36 of *E. aerogenes,* OmpE35/E36 of *E. cloacae,* OmpF/C of *E. coli* and OmpK35/K36 of *K. pneumonia*) share high sequence identity (>70%) and therefore similar structural architecture (Table 4.4).

Table 4.4. Sequence identity and r.m.s.d of OmpC-like and Ompf-like proteins.

	OmpF	OmpE35	OmpK35	Omp35	OmpC	OmpE36	OmpK36	Omp36
OmpF	-	0.62(317)	1.0(312)	1.0(313)	0.93(324)	0.93(322)	1.0(324)	1.0(288)
OmpE35	80	-	0.92(317)	1.0(317)	0.81(325)	0.79(325)	0.85(325)	0.89(288)
OmpK35	58	58	-	0.58(328)	0.90(324)	0.93(325)	0.90(322)	0.90(317)
Omp35	56	56	95	-	0.96(318)	0.96(317)	0.94(314)	0.94(315)
OmpC	64	66	56	57	-	0.51(340)	0.61(339)	0.68(334)
OmpE36	66	67	58	57	88	-	0.60(340)	0.56(335)
OmpK36	64	66	62	62	80	83	-	0.47(335)
Omp36	60	66	61	60	78	81	91	-

Percentage of identity among sequences

R.M.S.D (Cα Carbons)

In both OmpC-like and OmpF-like, a strong transverse electric field is generated by the separation of charged residues on opposite sides of the constriction zone. The acidic residues from the eyelet of OmpF (D113, E117, D121), are conserved in all structures, however some differences are found at the level of the arginine and lysine cluster. From the top of such cluster, R167 is conserved in Omp35 and OmpK35 while it is replaced in others by an uncharged amino acid: L167 in OmpC, OmpE35 and OmpE36, Q167 in Omp36 and S167 in OmpK36. The positively charged residues from the basic ladder inside the CR are conserved in all OmpF-like structures but K80 that is replaced by a tryptophan (W80) in OmpC, and all OmpC-like porins (Omp36, OmpE36 and OmpK36).

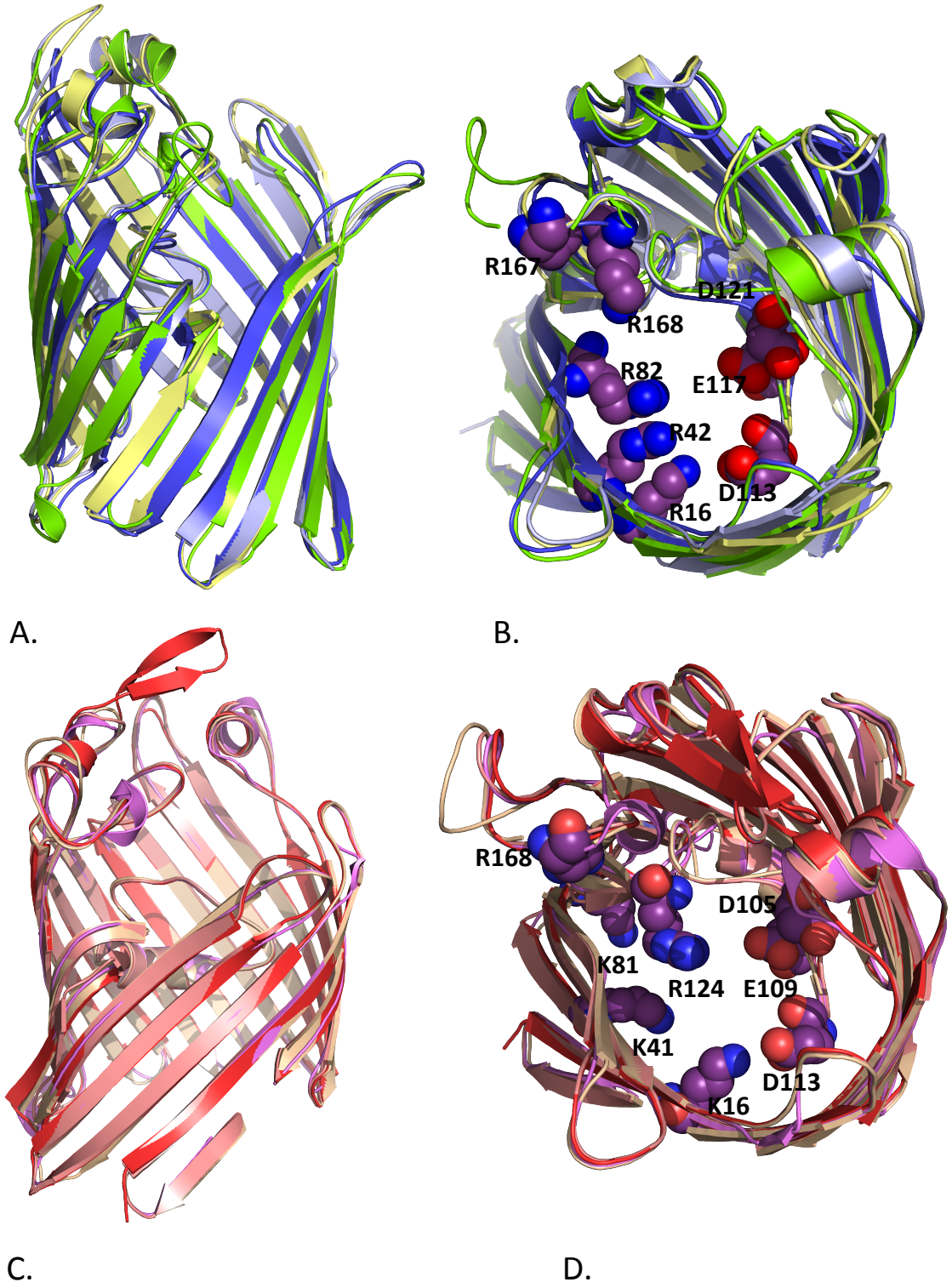

Figure 4.8: Superimposition of OmpF and OmpC orthologs. OmpF-like porins superimposition. (A) View from the side (B) extracellular view. Residues involved in the formation of the electric field are depicted as sphere. OmpC-like porins superimposition. (C) View from the side (D) extracellular view. Residues involved in the formation of the electric field are depicted as sphere.

4.4.3 Liposome swelling assay

We analyzed the permeation of nine clinical relevant antibiotics through the two *E. aerogenes* porins. Zwetterionic antibiotics showed a higher rate of permeation compared to negatively charged antibiotics. As expected from is larger pore, Omp35 has higher permeability than Omp36.

We also analyzed permeations of the above-mentioned antibiotics through the OmpC-like and OmpF-like porins. Once again as might be expected from the pore sizes the antibiotics have a higher permeability through OmpF and orthologues Omp35, OmpE35, OmpK35 than OmpC and orthologues Omp36, OmpE36, OmpK36. The liposome swelling assay results for OmpF permeability are in agreement with previous liposome swelling assay data and with influx rate measurements in intact cells.

The zwitterionic molecules meropenem, imipenem and cefepime exhibited high relative permeability through all porins. Interestingly, ampicillin, had lower relative permeability, resembling more the negatively charged molecules such as ceftazidime, cefotaxime, piperacillin and ticarcillin which displayed very low permeabilities In contrast, ertapenem, which has a net negative charge shows elevated permeability, similar to that of zwitterionic molecules, except via OmpE35 and OmpE36, the only species specific effect that was detected. Overall, meropenem showed the highest porin permeability while piperacillin and ticarcillin had the lowest.

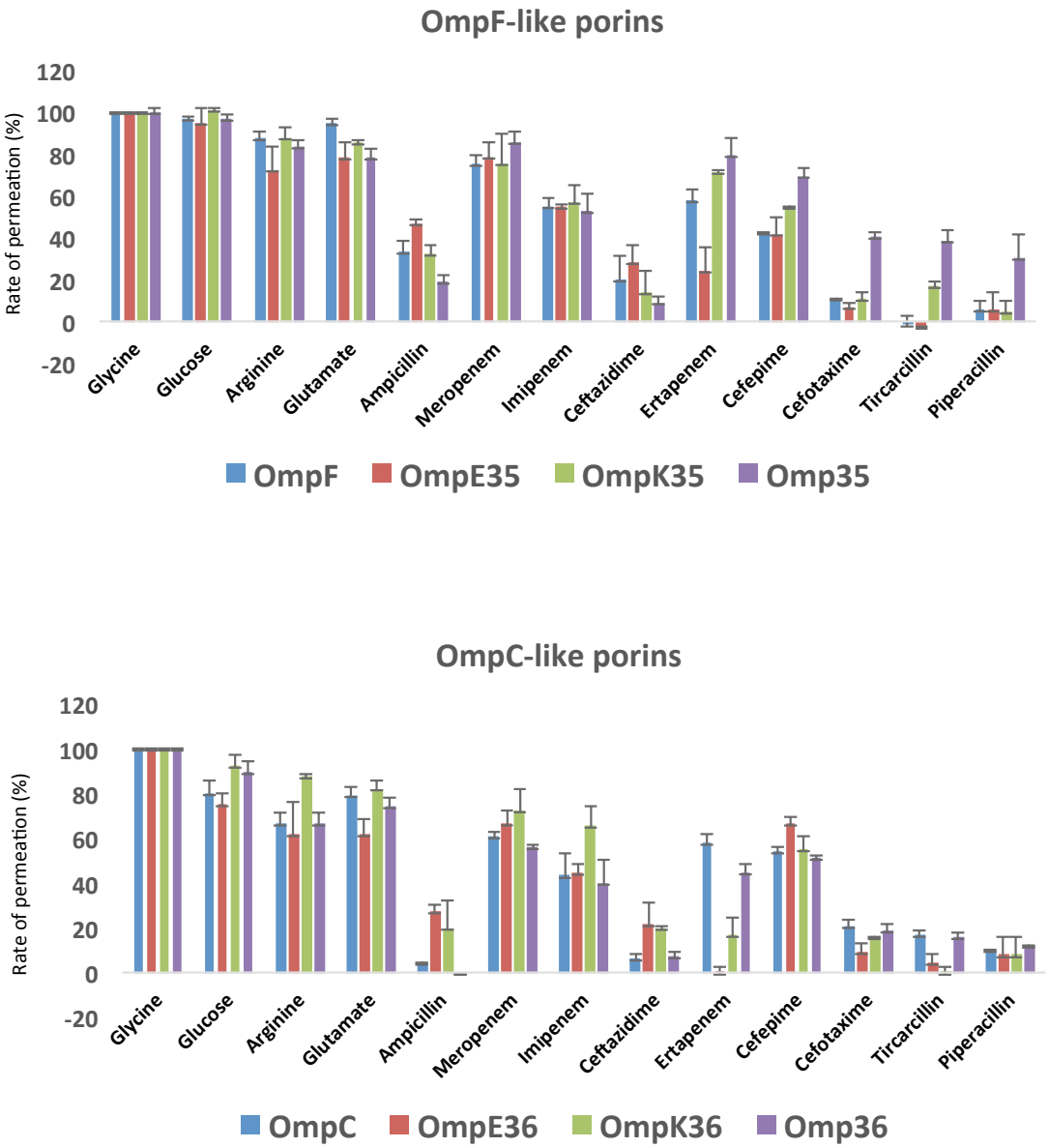

Figure 4.9: Liposome swelling assay of *Enterobacteriacea* orthologs. Relative permeations of several substrates through OmpC and OmpF- like porins. Measurements were taken in triplicate and normalized against glycine permeation (=100). Error bars indicate standard deviations. Overall, OmpF-like (OmpF, Omp35, OmpE35, OmpK35) porins have higher permeability than the OmpC-like (OmpC, Omp36, OmpE36, OmpK36) ones. Among the antibiotics tested, the zwitterionic ones (meropenem, imipenem and cefepime) show high rate of permeation (over 40%) whereas, negatively charged antibiotics (ceftazidime, cefotaxime, piperacillin and ticarcillin) show lower permeation rate.

General porins represent the main path through which polar antibiotics such as fluoroquinolones, penicillins, cephalosporins and carbapenems can enter the bacterial cell [242],[243]. Diffusion of such antibiotics does not occur by a recognition-binding mechanism, but instead is driven by an internal electric field that guides the molecules inside the cell [24]. The importance of such electric field in the constriction zone has been highlighted in multidrug-resistant *E. coli* clinical strains [233]. All atoms *in silico* modeling analysis, obtained in collaboration with Prof. Ceccarelli's team, predicted that molecules with a negative net charge would have a lower permeability than molecules with a net positive charge. In fact, the positive charge would compensate the energy barrier found at the level of the constriction zone. This is in agreement with the cation-selectivity of all OmpF-like and OmpC-like porins, and with the data obtained on accumulation of positive molecules in bacteria [244]. However, our data showed that the negatively charged antibiotic ertapenem exhibits high permeability through all the porins tested. Those data brought us to the conclusion that it is not necessary to have a total positive charge to improve the rate of permeation but instead it is the ability of the molecule to align its dipole moment inside the constriction zone. In particular when the dipole of the molecule is perpendicular to both the long axis of the molecule itself and to the transversal electric field of the pore, permeability is enhanced. In other words the distribution of charges in the molecule is crucial for an increased rate of permeation.

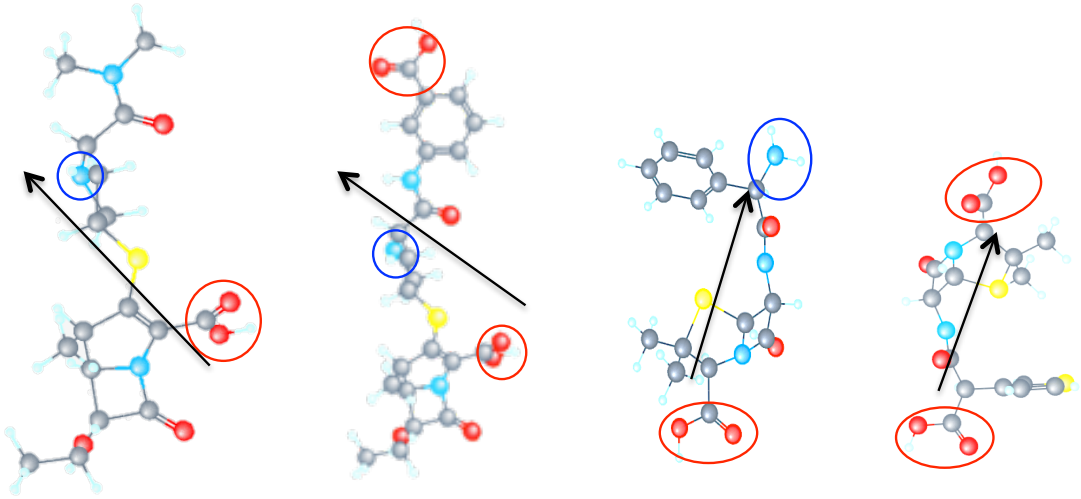

Figure 4.10: Antibiotics molecular structures and dipole moment. Meropenem, ertapenem, ampicillin and ticarcillin molecular structures. Structures were downloaded from PubChem. The dipole moment was calculated and kindly provided by Dr. Silvia Acosta-Gutierrez.

4.4 Conclusions

In this study we presented the X-ray structures of the two major porins in *E. aerogenes*, Omp35 and Omp36. Sequence and structural alignment of Omp35/36 with their orthologs in *E. cloacae* (OmpE35/36) *K. pneumonia* (OmpK35/36) and *E. coli* (OmpC and OmpF) displayed high level of homology. However slight difference were found at the level of the basic ladder, especially for the OmpC-like family.

We also analyzed the permeation of nine antibiotics, currently used in gram-negative bacteria infections, through three sets of orthologs, all showing subtle differences. We observed difference in the rate of permeation among the different antibiotics, with the zwitterionic antibiotics being the most permeable and the negatively charged one the less permeable. In particular we noticed that the ability of a molecules to align its dipole to the electric field at the constriction zone correlated with increased permeation. These results should be taken into account in the design of new drugs.

5. General conclusions and outlooks

In this work, we have presented the structural and functional analysis performed on MOMP and Omp50 from *C. jejuni* and Omp35 and Omp36 from *E. aerogenes*. Both bacteria are pathogenic for humans, causing gastrointestinal and respiratory infections, respectively.

MOMP was expressed in the native *C. jejuni* and its x-ray structure was solved. The structure showed that MOMP was a trimeric porin of 18 β-strand monomers. The obtained structure was compared to the structure of the recombinantly expressed MOMP, and despite differences in the LPS composition between *E. coli* and *C. jejuni,* we found the two structures to be identical. We then focused our attention on the calcium binding site found at the constriction zone. Electrophysiology analysis of MOMP behavior in the presence and absence of calcium led us to conclude that the metal ion is important for the stability of the structure, as it holds together a number of key loops (L3, L4 and L6) involved in its binding. Furthermore, *in silico* data obtained in collaboration with the University of Cagliari gave us some insight on the functional role of the calcium, specifically, highlighting the effect of the calcium on the ciprofloxacin permeation.

It is well established that the constriction zone of porins plays a crucial role in substrates permeation and thus any alterations at this level can lead to impaired diffusions [243]. In MOMP, the presence of the calcium neutralizes the negative charges of the residues D155, D120 and E288 in the eyelet, weakening the electric field and increasing the energy barrier for translocation. Following these

observations, it would be useful to test several antibiotics, using for example liposome swelling assay, and to analyze their permeation rate with and without calcium. This would provide us with more data on how the calcium effects the translocation of different classes of antibiotics and thus improve the design of new ones.

Omp50, also a porin from *C. jejuni*, was also the object of study in this work.
Omp50 purification was first attempted in the native *Campylobacter*, but due to the low expression level and low purity we decided to use a recombinant system. Omp50 was successfully expressed in *E. coli* and the purified porin showed pore activity, when inserted in a lipid bilayer comparable to the protein natively expressed. Crystallization of Omp50 was, however, hard to achieve. Omp50 was also tested in order to find evidences of its proposed kinase activity. None of the experiments we performed, with either the recombinant or the native protein, suggested that Omp50 is able to auto-phosphorylize or is able to hydrolyze ATP. Hence, our data are in disagreement with that proposed by Corcionivoschi *et al* [207].

Lastly, we determined the X-ray structures of Omp35 and Omp36 from *E. aerogenes*, orthologues of the *E. coli* OmpF and OmpC, respectively. The structures we obtained showed that both Omp35 and Omp36 were homotrimer of 16 β-strands monomers. Omp35 and Omp36 structures also showed high levels of homology with OmpC and OmpF from *E. coli*, OmpE35/36 from *E. cloacae* and Ompk35/36 from *K. pneumonie*.

We analyzed the permeation of clinically relevant antibiotics through the OmpC-like (OmpC, Omp36, OmpE36, OmpK36) and the OmpF-like (OmpF, Omp35, OmpE35, OmpK36) porins using liposome swelling assay. We detected difference in the rate of permeation among the different antibiotics. Specifically, in both the OmpC-like and OmpF-like porins, we observed that the zwitterionic antibiotics were the most permeable and the negatively charged one the least permeable. Interestingly, the antibiotic Ertapenem, despite having a net negative charge, showed a rate of permeation over 80%. Further analysis, (in collaboration with the University of Cagliari), led us to conclude that it is not crucial to have a net positive charge to improve the rate of permeation but it is the ability of the molecule to align its dipole moment to the electric field at the constriction zone, instead, correlated with increased permeation.

E. aerogenes strains isolated from hospitalized patients have been shown to be resistant to a wide range of antibiotics [220]. Omp35 and Omp36, *E. aerogenes* major porins, play an important role in the multi-drug resistance phenomenon [235]. Variation in their expression of these two porins and mutation at the level of the constriction zone are the main mechanisms that lead to antibiotic resistance in *E. aerogenes* [235], [236]. The structural and functional analysis we presented in this work represent, a good starting point to better understand translocation of antibiotics through porins of pathogenic bacteria. In order to investigate how (and to what extent) these mutations impair the permeation of different classes of antibiotics when compared to the wild-type, such analysis could also be extended to Omp35 and Omp36 (and also their orthologues) that carry mutations at the level of the constriction zone.

Antibiotics resistance in Gram-negative bacteria has become a threat for public health worldwide. As already discussed in the general introduction of this work, porins play an important role in the translocation of antibiotics and thus in bacteria resistance. It is for this reason that we structurally and functionally characterized the major porins of two pathogenic bacteria. We believe that the data collected in this study will give a better understanding of drug translocation through porins and hence improve the rational design of high permeable antibiotics.

6. Bibliography

[1] H.C. Gram, Gram staining, Fortschritte Der Med. 2 (1884) 185–189. doi:10.1002/0471142735.ima03os23.

[2] Y. Kamio, H. Nikaido, Outer membrane of Salmonella typhimurium: accessibility of phospholipid head groups to phospholipase c and cyanogen bromide activated dextran in the external medium., Biochemistry. 15 (1976) 2561–2570. doi:10.1021/bi00657a012.

[3] C. Alexander, E.T. Rietschel, Bacterial lipopolysaccharides and innate immunity, J. Endotoxin Res. 7 (2001) 167–202. doi:10.1177/09680519010070030101.

[4] C. Galanos, M.A. Freudenberg, Bacterial endotoxins: biological properties and mechanisms of action, Mediators Inflamm. 2 (1993) S11–S16. doi:10.1155/S0962935193000687.

[5] C.R. Raetz, C. Whitfield, Lipopolysaccharide endotoxins, Annu. Rev. Biochem. 71 (2002) 635–700. doi:10.1146/annurev.biochem.71.110601.135414.

[6] M. Caroff, D. Karibian, Structure of bacterial lipopolysaccharides, Carbohydr. Res. 338 (2003) 2431–2447. doi:10.1016/j.carres.2003.07.010.

[7] M.G. Rittig, A. Kaufmann, A. Robins, B. Shaw, H. Sprenger, D. Gemsa, V. Foulongne, B. Rouot, J. Dornand, Smooth and rough lipopolysaccharide phenotypes of Brucella induce different intracellular trafficking and cytokine/chemokine release in human monocytes, J.Leukoc.Biol. 74 (2003) 1045–1055. doi:10.1189/jlb.0103015.

[8] I. Hug, M.R. Couturier, M.M. Rooker, D.E. Taylor, M. Stein, M.F. Feldman, Helicobacter pylori lipopolysaccharide is synthesized via a novel pathway with an evolutionary connection to protein N-glycosylation, PLoS Pathog. 6 (2010). doi:10.1371/journal.ppat.1000819.

[9] C. Dong, K. Beis, J. Nesper, A.L. Brunkan-LaMontagne, B.R. Clarke, C. Whitfield, J.H. Naismith, Wza the translocon for E. coli capsular polysaccharides defines a new class of membrane protein, Nature. 444 (2006) 226–229. doi:10.1038/nature05267.

[10] J.W. Fairman, N. Noinaj, S.K. Buchanan, The structural biology of β-barrel membrane proteins: A summary of recent reports, Curr. Opin. Struct. Biol. 21 (2011) 523–531. doi:10.1016/j.sbi.2011.05.005.

[11] J.W. Fairman, N. Noinaj, S.K. Buchanan, The structural biology of beta-barrel membrane proteins: a summary of recent reports, Curr Opin Struct Biol. 21 (2011) 523–531. doi:10.1016/j.sbi.2011.05.005.

[12] G.E. Schulz, Bacterial porins: structure and function, Curr. Opin. Cell Biol. 5 (1993) 701–707. doi:10.1016/0955-0674(93)90143-E.
[13] R. Koebnik, K.P. Locher, P. Van Gelder, Structure and function of bacterial outer membrane proteins: barrels in a nutshell., Mol. Microbiol. 37 (2000) 239–253. doi:10.1046/j.1365-2958.2000.01983.x.
[14] S.W. Cowan, T. Schirmer, G. Rummel, M. Steiert, R. Ghosh, R.A. Pauptit, J.N. Jansonius, J.P. Rosenbusch, Crystal structures explain functional properties of two E. coli porins, Nature. 358 (1992) 727–733. doi:10.1038/358727a0.
[15] K. Seshadri, R. Garemyr, E. Wallin, G. Von Heijne, A. Elofsson, Architecture of β-barrel membrane proteins: Analysis of trimeric porins, Protein Sci. 7 (1998) 2026–2032. doi:10.1002/pro.5560070919.
[16] G. V. Subbarao, B. van den Berg, Crystal Structure of the Monomeric Porin OmpG, J. Mol. Biol. 360 (2006) 750–759. doi:10.1016/j.jmb.2006.05.045.
[17] H. Schindler, J.P. Rosenbusch, Matrix protein from Escherichia coli outer membranes forms voltage-controlled channels in lipid bilayers., Proc. Natl. Acad. Sci. U. S. A. 75 (1978) 3751–5. doi:10.1073/pnas.75.8.3751.
[18] T. Haltia, E. Freire, Forces and factors that contribute to the structural stability of membrane proteins, BBA - Rev. Biomembr. 1241 (1995) 295–322. doi:10.1016/0304-4157(94)00161-6.
[19] H. Naveed, R. Jackups, J. Liang, Predicting weakly stable regions, oligomerization state, and protein-protein interfaces in transmembrane domains of outer membrane proteins., Proc. Natl. Acad. Sci. U. S. A. 106 (2009) 12735–12740. doi:10.1073/pnas.0902169106.
[20] H. Naveed, J. Liang, Weakly stable regions and protein-protein interactions in beta-barrel membrane proteins., Curr. Pharm. Des. 20 (2014) 1268–1273. doi:10.2174/13816128113199990071.
[21] H. Naveed, D. Jimenez-Morales, J. Tian, V. Pasupuleti, L.J. Kenney, J. Liang, Engineered oligomerization state of OmpF protein through computational design decouples oligomer dissociation from unfolding, J. Mol. Biol. 419 (2012) 89–101. doi:10.1016/j.jmb.2012.02.043.
[22] D. Jeanteur, T. Schirmer, D. Fourel, V. Simonet, G. Rummel, C. Widmer, J.P. Rosenbusch, F. Pattus, J.M. Pagès, Structural and functional alterations of a colicin-resistant mutant of OmpF porin from Escherichia coli., Proc. Natl. Acad. Sci. U. S. A. 91 (1994) 10675–10679. doi:10.1073/pnas.91.22.10675.
[23] A. Basl??, G. Rummel, P. Storici, J.P. Rosenbusch, T. Schirmer, Crystal Structure of Osmoporin OmpC from E. coli at 2.0 Å, J. Mol. Biol. 362 (2006) 933–942. doi:10.1016/j.jmb.2006.08.002.
[24] S. Acosta-Gutierrez, M.A. Scorciapino, I. Bodrenko, M. Ceccarelli, Filtering with Electric Field: The Case of E. coli Porins, J. Phys. Chem. Lett. 6 (2015)

1807–1812. doi:10.1021/acs.jpclett.5b00612.
[25] A. Baslé, G. Rummel, P. Storici, J.P. Rosenbusch, T. Schirmer, Crystal Structure of Osmoporin OmpC from E. coli at 2.0 Å, J. Mol. Biol. 362 (2006) 933–942. doi:10.1016/j.jmb.2006.08.002.
[26] E. Yamashita, M. V Zhalnina, S.D. Zakharov, O. Sharma, W.A. Cramer, Crystal structures of the OmpF porin: function in a colicin translocon., EMBO J. 27 (2008) 2171–2180. doi:10.1038/emboj.2008.137.
[27] R. Dutzler, G. Rummel, S. Albertí, S. Hernández-Allés, P.S. Phale, J.P. Rosenbusch, V.J. Benedí, T. Schirmer, Crystal structure and functional characterization of OmpK36, the osmoporin of Klebsiella pneumoniae, Structure. 7 (1999) 425–434. doi:http://dx.doi.org/10.1016/S0969-2126(99)80055-0.
[28] R. Benz, A. Schmid, R.E.W. Hancock, Ion selectivity of gram-negative bacterial porins, J. Bacteriol. 162 (1985) 722–727.
[29] Y. KOBAYASHI, T. NAKAE, The mechanism of ion selectivity of OmpF-porin pores of Escherichia coli, Eur. J. Biochem. 151 (1985) 231–236. doi:10.1111/j.1432-1033.1985.tb09093.x.
[30] J.H. Lakey, J.P. Watts, E.J.A. Lea, Characterisation of channels induced in planar bilayer membranes by detergent solubilised Escherichia coli porins, BBA - Biomembr. 817 (1985) 208–216. doi:10.1016/0005-2736(85)90022-7.
[31] A. Delcour, Outer membrane permeability and antibiotic resistance., Biochim. Biophys. Acta. 1794 (2009) 808–816. doi:10.1016/j.bbapap.2008.11.005.
[32] T. Schirmer, T.A. Keller, Y.F. Wang, J.P. Rosenbusch, Structural basis for sugar translocation through maltoporin channels at 3.1 A resolution., Science. 267 (1995) 512–514. doi:10.1126/science.7824948.
[33] D. Forst, W. Welte, T. Wacker, K. Diederichs, Structure of the sucrose-specific porin ScrY from Salmonella typhimurium and its complex with sucrose, Nat. Struct. Biol. 5 (1998) 37–46. doi:10.1038/nsb0198-37.
[34] K. Schmid, R. Ebner, K. Jahreis, J.W. Lengeler, F. Titgemeyer, A sugar-specific porin, ScrY, is involved in sucrose uptake in enteric bacteria, Mol. Microbiol. 5 (1991) 941–950. doi:10.1111/j.1365-2958.1991.tb00769.x.
[35] P. Van Gelder, F. Dumas, I. Bartoldus, N. Saint, A. Prilipov, M. Winterhalter, Y. Wang, A. Philippsen, J.P. Rosenbusch, T. Schirmer, Sugar transport through maltoporin of Escherichia coli: Role of the greasy slide, J. Bacteriol. 184 (2002) 2994–2999. doi:10.1128/JB.184.11.2994-2999.2002.
[36] F. Dumas, R. Koebnik, M. Winterhalter, P. Van Gelder, Sugar transport through maltoporin of Escherichia coli: Role of polar tracks, J. Biol. Chem.

275 (2000) 19747–19751. doi:10.1074/jbc.M000268200.
[37] Y.F. Wang, R. Dutzler, P.J. Rizkallah, J.P. Rosenbusch, T. Schirmer, Channel specificity: structural basis for sugar discrimination and differential flux rates in maltoporin., J. Mol. Biol. 272 (1997) 56–63. doi:10.1006/jmbi.1997.1224.
[38] R. Dutzler, Y.-F. Wang, P. Rizkallah, J. Rosenbusch, T. Schirmer, Crystal structures of various maltooligosaccharides bound to maltoporin reveal a specific sugar translocation pathway, Structure. 4 (1996) 127–134. doi:10.1016/S0969-2126(96)00016-0.
[39] C.K. Stover, X.Q. Pham, a L. Erwin, S.D. Mizoguchi, P. Warrener, M.J. Hickey, F.S. Brinkman, W.O. Hufnagle, D.J. Kowalik, M. Lagrou, R.L. Garber, L. Goltry, E. Tolentino, S. Westbrock-Wadman, Y. Yuan, L.L. Brody, S.N. Coulter, K.R. Folger, A. Kas, K. Larbig, R. Lim, K. Smith, D. Spencer, G.K. Wong, Z. Wu, I.T. Paulsen, J. Reizer, M.H. Saier, R.E. Hancock, S. Lory, M. V Olson, Complete genome sequence of Pseudomonas aeruginosa PAO1, an opportunistic pathogen., Nature. 406 (2000) 959–964. doi:10.1038/35023079.
[40] R.E.W. Hancock, F.S.L. Brinkman, Function of *Pseudomonas* Porins in Uptake and Efflux, Annu. Rev. Microbiol. 56 (2002) 17–38. doi:10.1146/annurev.micro.56.012302.160310.
[41] H. Nikaido, Molecular basis of bacterial outer membrane permeability revisited., Microbiol. Mol. Biol. Rev. 67 (2003) 593–656. doi:10.1128/MMBR.67.4.593.
[42] S. Tamber, M.M. Ochs, R.E.W. Hancock, Role of the novel OprD family of porins in nutrient uptake in Pseudomonas aeruginosa, J. Bacteriol. 188 (2006) 45–54. doi:10.1128/JB.188.1.45-54.2006.
[43] J. Trias, H. Nikaido, Protein D2 channel of the *Pseudomonas aeruginosa* outer membrane has a binding site for basic amino acids and peptides., J. Biol. Chem. 265 (1990) 15680–15684.
[44] T.F. Moraes, M. Bains, R.E.W. Hancock, N.C.J. Strynadka, An arginine ladder in OprP mediates phosphate-specific transfer across the outer membrane., Nat. Struct. Mol. Biol. 14 (2007) 85–87. doi:10.1038/nsmb1189.
[45] E. Eren, J. Vijayaraghavan, J. Liu, B.R. Cheneke, D.S. Touw, B.W. Lepore, M. Indic, L. Movileanu, B. van den Berg, Substrate specificity within a family of outer membrane carboxylate channels, PLoS Biol. 10 (2012). doi:10.1371/journal.pbio.1001242.
[46] S. Galdiero, A. Falanga, M. Cantisani, R. Tarallo, M. Elena Della Pepa, V. D'Oriano, M. Galdiero, Microbe-Host Interactions: Structure and Role of Gram-Negative Bacterial Porins, Curr. Protein Pept. Sci. 13 (2012) 843–854. doi:10.2174/138920312804871120.

[47] F. Orlik, C. Andersen, C. Danelon, M. Winterhalter, M. Pajatsch, A. Bock, R. Benz, CymA of Klebsiella oxytoca outer membrane: Binding of cyclodextrins and study of the current noise of the open channel, Biophys. J. 85 (2003) 876–885.

[48] B. van den Berg, S. Prathyusha Bhamidimarri, J. Dahyabhai Prajapati, U. Kleinekathöfer, M. Winterhalter, Outer-membrane translocation of bulky small molecules by passive diffusion, Proc. Natl. Acad. Sci. U. S. A. 112 (2015) E2991-9. doi:10.1073/pnas.1424835112.

[49] N. Noinaj, M. Guillier, T.J. Barnard, S.K. Buchanan, TonB-dependent transporters: regulation, structure, and function., Annu. Rev. Microbiol. 64 (2010) 43–60. doi:10.1146/annurev.micro.112408.134247.

[50] A.D. Ferguson, E. Hofmann, J.W. Coulton, K. Diederichs, W. Welte, Siderophore-Mediated Iron Transport : Crystal Structure of FhuA with Bound Lipopolysaccharide, Science. 282 (1998) 2215–2220. doi:10.1126/science.282.5397.2215.

[51] S.K. Buchanan, B.S. Smith, L. Venkatramani, D. Xia, L. Esser, M. Palnitkar, R. Chakraborty, D. van der Helm, J. Deisenhofer, Crystal structure of the outer membrane active transporter FepA from Escherichia coli., Nat. Struct. Biol. 6 (1999) 56–63. doi:10.1038/4931.

[52] L. Moyniè, A. Luscher, D. Rolo, D. Pletzer, A. Tortajada, H. Weingart, Y. Braun, M.G.P. Page, J.H. Naismith, T. K??hler, Structure and function of the PiuA and PirA siderophore-drug receptors from Pseudomonas aeruginosa and Acinetobacter baumannii, Antimicrob. Agents Chemother. 61 (2017). doi:10.1128/AAC.02531-16.

[53] D.P. Chimento, R.J. Kadner, M.C. Wiener, The Escherichia coli outer membrane cobalamin transporter BtuB: Structural analysis of calcium and substrate binding, and identification of orthologous transporters by sequence/structure conservation, J. Mol. Biol. 332 (2003) 999–1014. doi:10.1016/j.jmb.2003.07.005.

[54] V. Braun, Energy-coupled transport and signal transduction through the Gram-negative outer membrane via TonB-ExbB-ExbD-dependent receptor proteins, FEMS Microbiol. Rev. 16 (1995) 295–307. doi:10.1111/j.1574-6976.1995.tb00177.x.

[55] E. Fischer, K. Günter, V. Braun, Involvement of ExbB and TonB in transport across the outer membrane of Escherichia coli: phenotypic complementation of exb mutants by overexpressed tonB and physical stabilization of TonB by ExbB., J. Bacteriol. 171 (1989) 5127–5134. doi:10.1128/JB.171.9.5127-5134.1989.

[56] N. Noinaj, M. Guillier, T.J. Barnard,, S.K. Buchanan, TonB-Dependent

Transporters: Regulation, Structure, and Function, Annu. Rev. Microbiol. 64 (2010) 43–60. doi:10.1146/annurev.micro.112408.134247.
[57] P.D. Pawelek, N. Croteau, C. Ng-Thow-Hing, C.M. Khursigara, N. Moiseeva, M. Allaire, J.W. Coulton, Structure of TonB in Complex with FhuA, E. coli Outer Membrane Receptor, Science (80-.). 312 (2006) 1399–1402. doi:10.1126/science.1128057.
[58] H. Celia, N. Noinaj, S.D. Zakharov, E. Bordignon, I. Botos, M. Santamaria, T.J. Barnard, W. a Cramer, R. Lloubes, S.K. Buchanan, Structural insight into the role of the Ton complex in energy transduction, Nature. 538 (2016) 60–65. doi:10.1038/nature19757.
[59] H. Celia, N. Noinaj, S.D. Zakharov, E. Bordignon, I. Botos, M. Santamaria, T.J. Barnard, W.A. Cramer, R. Lloubes, S.K. Buchanan, Structural insight into the role of the Ton complex in energy transduction, Nature. 538 (2016) 60–65. doi:10.1038/nature19757.
[60] A.J. Glenwright, K.R. Pothula, S.P. Bhamidimarri, D.S. Chorev, A. Baslé, S.J. Firbank, H. Zheng, C. V Robinson, M. Winterhalter, U. Kleinekathöfer, D.N. Bolam, B. van den Berg, Structural basis for nutrient acquisition by dominant members of the human gut microbiota, Nature. 541 (2017) 407–411. doi:10.1038/nature20828.
[61] R.E. Bishop, Structural biology of membrane-intrinsic beta-barrel enzymes: sentinels of the bacterial outer membrane., Biochim. Biophys. Acta. 1778 (2008) 1881–96. doi:10.1016/j.bbamem.2007.07.021.
[62] W.C. Wimley, The versatile beta-barrel membrane protein., Curr. Opin. Struct. Biol. 13 (2003) 404–11. doi:10.1016/S0959-440X(03)00099-X.
[63] K. Sugimura, T. Nishihara, Purification, characterization, and primary structure of Escherichia coli protease VII with specificity for paired basic residues: Identity of protease VII and OmpT, J. Bacteriol. 170 (1988) 5625–5632.
[64] L. Vandeputte-Rutten, R.A. Kramer, J. Kroon, N. Dekker, M.R. Egmond, P. Gros, Crystal structure of the outer membrane protease Ompt from Escherichia coli suggests a novel catalytic site, EMBO J. 20 (2001) 5033–5039. doi:10.1093/emboj/20.18.5033.
[65] K. Brandenburg, P. Garidel, A.B. Schromm, J. Andrä, A. Kramer, M. Egmond, A. Wiese, Investigation into the interaction of the bacterial protease OmpT with outer membrane lipids and biological activity of OmpT:lipopolysaccharide complexes, Eur. Biophys. J. 34 (2005) 28–41. doi:10.1007/s00249-004-0422-3.
[66] M. Baaden, M.S.P. Sansom, OmpT: molecular dynamics simulations of an outer membrane enzyme., Biophys. J. 87 (2004) 2942–2953.

doi:10.1529/biophysj.104.046987.
[67] L. Rutten, J. Geurtsen, W. Lambert, J.J.M. Smolenaers, A.M. Bonvin, A. de Haan, P. van der Ley, M.R. Egmond, P. Gros, J. Tommassen, Crystal structure and catalytic mechanism of the LPS 3-O-deacylase PagL from Pseudomonas aeruginosa., Proc. Natl. Acad. Sci. U. S. A. 103 (2006) 7071–7076. doi:10.1073/pnas.0509392103.
[68] P.M. Hwang, W.-Y. Choy, E.I. Lo, L. Chen, J.D. Forman-Kay, C.R.H. Raetz, G.G. Privé, R.E. Bishop, L.E. Kay, Solution structure and dynamics of the outer membrane enzyme PagP by NMR., Proc. Natl. Acad. Sci. U. S. A. 99 (2002) 13560–13565. doi:10.1073/pnas.212344499.
[69] R.E. Bishop, H.S. Gibbons, T. Guina, M.S. Trent, S.I. Miller, C.R. Raetz, Transfer of palmitate from phospholipids to lipid A in outer membranes of gram-negative bacteria., EMBO J. 19 (2000) 5071–5080. doi:10.1093/emboj/19.19.5071.
[70] J. Geurtsen, L. Steeghs, J. Ten Hove, P. Van Der Ley, J. Tommassen, Dissemination of lipid A deacylases (PagL) among gram-negative bacteria: Identification of active-site histidine and serine residues, J. Biol. Chem. 280 (2005) 8248–8259. doi:10.1074/jbc.M414235200.
[71] J. Geurtsen, L. Steeghs, H.J. Hamstra, J. Ten Hove, A. De Haan, B. Kuipers, J. Tommassen, P. Van Der Ley, Expression of the lipopolysaccharide-modifying enzymes PagP and PagL modulates the endotoxic activity of bordetella pertussis, Infect. Immun. 74 (2006) 5574–5585. doi:10.1128/IAI.00834-06.
[72] N. Dekker, Outer-membrane phospholipase A: Known structure, unknown biological function, Mol. Microbiol. 35 (2000) 711–717. doi:10.1046/j.1365-2958.2000.01775.x.
[73] H.J. Snijder, I. Ubarretxena-Belandia, M. Blaauw, K.H. Kalk, H.M. Verheij, M.R. Egmond, N. Dekker, B.W. Dijkstra, Structural evidence for dimerization-regulated activation of an integral membrane phospholipase, Nature. 401 (1999) 717–721. doi:10.1038/44890.
[74] E.L. Wu, P.J. Fleming, M.S. Yeom, G. Widmalm, J.B. Klauda, K.G. Fleming, W. Im, E. coli outer membrane and interactions with OmpLA, Biophys. J. 106 (2014) 2493–2502. doi:10.1016/j.bpj.2014.04.024.
[75] C.M. Reynolds, A.A. Ribeiro, S.C. McGrath, R.J. Cotter, C.R.H. Raetz, M.S. Trent, An outer membrane enzyme encoded by Salmonella typhimurium lpxR that removes the 3 α-acyloxyacyl moiety of lipid A, J. Biol. Chem. 281 (2006) 21974–21987. doi:10.1074/jbc.M603527200.
[76] N.L.S. Que-Gewirth, M.J. Karbarz, S.R. Kalb, R.J. Cotter, C.R.H. Raetz, Origin of the 2-amino-2-deoxy-gluconate unit in Rhizobium leguminosarum lipid A: Expression cloning of the outer membrane oxidase LpxQ, J. Biol. Chem. 278

(2003) 12120–12129. doi:10.1074/jbc.M300379200.
[77] N.W. Rigel, T.J. Silhavy, Making a beta-barrel: Assembly of outer membrane proteins in Gram-negative bacteria, Curr. Opin. Microbiol. 15 (2012) 189–193. doi:10.1016/j.mib.2011.12.007.
[78] H. Tokuda, Biogenesis of outer membranes in Gram-negative bacteria., Biosci. Biotechnol. Biochem. 73 (2009) 465–73. doi:10.1271/bbb.80778.
[79] Z.X. Lyu, X.S. Zhao, Periplasmic quality control in biogenesis of outer membrane proteins., Biochem. Soc. Trans. 43 (2015) 133–8. doi:10.1042/BST20140217.
[80] D. Missiakas, J.M. Betton, S. Raina, New components of protein folding in extracytoplasmic compartments of Escherichia coli SurA, FkpA and Skp/OmpH., Mol. Microbiol. 21 (1996) 871–884. doi:10.1046/j.1365-2958.1996.561412.x.
[81] M.P. Bos, V. Robert, J. Tommassen, Biogenesis of the gram-negative bacterial outer membrane., Annu. Rev. Microbiol. 61 (2007) 191–214. doi:10.1146/annurev.micro.61.080706.093245.
[82] G. von Heijne, Signal sequences. The limits of variation, J. Mol. Biol. 184 (1985) 99–105. doi:10.1016/0022-2836(85)90046-4.
[83] W. Hemminger, S.M. Sarge, P. Bundesanstalt, Post-Targeting Functions of Signal Peptides, Protein Transp. into Endoplasmic Reticulum. 1 (1998) 1–16. doi:10.1007/BFb0111316.
[84] P. Fekkes, J.G. De Wit, J.P.W. Van Der Wolk, H.H. Kimsey, C.A. Kumamoto, A.J.M. Driessen, Preprotein transfer to the Escherichia coli translocase requires the co-operative binding of SecB and the signal sequence to SecA, Mol. Microbiol. 29 (1998) 1179–1190. doi:10.1046/j.1365-2958.1998.00997.x.
[85] A.A. Lilly, J.M. Crane, L.L. Randall, Export chaperone SecB uses one surface of interaction for diverse unfolded polypeptide ligands, Protein Sci. 18 (2009) 1860–1868. doi:10.1002/pro.197.
[86] P.A. Lee, D. Tullman-Ercek, G. Georgiou, The bacterial twin-arginine translocation pathway., Annu. Rev. Microbiol. 60 (2006) 373–95. doi:10.1146/annurev.micro.60.080805.142212.
[87] T. Palmer, B.C. Berks, The twin-arginine translocation (Tat) protein export pathway., Nat. Rev. Microbiol. 10 (2012) 483–496. doi:10.1038/nrmicro2814.
[88] D.J.F. Du Plessis, N. Nouwen, A.J.M. Driessen, The Sec translocase, Biochim. Biophys. Acta - Biomembr. 1808 (2011) 851–865. doi:10.1016/j.bbamem.2010.08.016.
[89] D. Görlich, T.A. Rapoport, Protein translocation into proteoliposomes

reconstituted from purified components of the endoplasmic reticulum membrane, Cell. 75 (1993) 615–630. doi:10.1016/0092-8674(93)90483-7.
[90] K.J. Erlandson, S.B.M. Miller, Y. Nam, A.R. Osborne, J. Zimmer, T.A. Rapoport, A role for the two-helix finger of the SecA ATPase in protein translocation., Nature. 455 (2008) 984–987. doi:10.1038/nature07439.
[91] J. Zimmer, Y. Nam, T.A. Rapoport, Structure of a complex of the ATPase SecA and the protein-translocation channel., Nature. 455 (2008) 936–943. doi:10.1038/nature07335.
[92] M. Merdanovic, T. Clausen, M. Kaiser, R. Huber, M. Ehrmann, Protein quality control in the bacterial periplasm., Annu. Rev. Microbiol. 65 (2011) 149–68. doi:10.1146/annurev-micro-090110-102925.
[93] J.G. Sklar, T. Wu, D. Kahne, T.J. Silhavy, Defining the roles of the periplasmic chaperones SurA, Skp, and DegP in Escherichia coli, Genes Dev. 21 (2007) 2473–2484. doi:10.1101/gad.1581007.
[94] X. Ge, R. Wang, J. Ma, Y. Liu, A.N. Ezemaduka, P.R. Chen, X. Fu, Z. Chang, DegP primarily functions as a protease for the biogenesis of β-barrel outer membrane proteins in the Gram-negative bacterium Escherichia coli, FEBS J. 281 (2014) 1226–1240. doi:10.1111/febs.12701.
[95] D.P. Ricci, T.J. Silhavy, The Bam machine: A molecular cooper, Biochim. Biophys. Acta - Biomembr. 1818 (2012) 1067–1084. doi:10.1016/j.bbamem.2011.08.020.
[96] A.M. Plummer, D. Gessmann, K.G. Fleming, C.T. Webb, T. Lithgow, The BAM Complex, 2015. doi:10.1007/978-1-4939-2871-2.
[97] L. Sánchez-Pulido, D. Devos, S. Genevrois, M. Vicente, A. Valencia, POTRA: A conserved domain in the FtsQ family and a class of β-barrel outer membrane proteins, Trends Biochem. Sci. 28 (2003) 523–526. doi:10.1016/j.tibs.2003.08.003.
[98] M.P. Bos, V. Robert, J. Tommassen, Functioning of outer membrane protein assembly factor Omp85 requires a single POTRA domain., EMBO Rep. 8 (2007) 1149–1154. doi:10.1038/sj.embor.7401092.
[99] S. Kim, J.C. Malinverni, P. Sliz, T.J. Silhavy, S.C. Harrison, D. Kahne, Structure and function of an essential component of the outer membrane protein assembly machine., Sci. (New York, NY). 317 (2007) 961–964. doi:10.1126/science.1143993.
[100] N.K. Burgess, T.P. Dao, A.M. Stanley, K.G. Fleming, β-Barrel proteins that reside in the Escherichia coli outer membrane in vivo demonstrate varied folding behavior in vitro, J. Biol. Chem. 283 (2008) 26748–26758. doi:10.1074/jbc.M802754200.
[101] N. Dekker, K. Merck, J. Tommassen, H.M. Verheij, In Vitro Folding of

Escherichia Coli Outer-Membrane Phospholipase A, Eur. J. Biochem. 232 (1995) 214–219. doi:10.1111/j.1432-1033.1995.tb20801.x.
[102] N. Noinaj, A.J. Kuszak, J.C. Gumbart, P. Lukacik, H. Chang, N.C. Easley, T. Lithgow, S.K. Buchanan, Structural insight into the biogenesis of β-barrel membrane proteins, Nature. 501 (2013) 385–390. doi:10.1038/nature12521.
[103] N. Noinaj, S.E. Rollauer, S.K. Buchanan, The β-barrel membrane protein insertase machinery from Gram-negative bacteria, Curr. Opin. Struct. Biol. 31 (2015) 35–42. doi:10.1016/j.sbi.2015.02.012.
[104] N. Noinaj, A.J. Kuszak, C. Balusek, J.C. Gumbart, S.K. Buchanan, Lateral opening and exit pore formation are required for BamA function, Structure. 22 (2014) 1055–1062. doi:10.1016/j.str.2014.05.008.
[105] X.C. Zhang, L. Han, How does a β-barrel integral membrane protein insert into the membrane?, Protein Cell. 7 (2016) 471–477. doi:10.1007/s13238-016-0273-6.
[106] S. Vasoo, J.N. Barreto, P.K. Tosh, Emerging Issues in Gram-Negative Bacterial Resistance: An Update for the Practicing Clinician, Mayo Clin. Proc. 90 (2015) 395–403. doi:10.1016/j.mayocp.2014.12.002.
[107] S.I. Miller, Antibiotic resistance and regulation of the Gram-negative bacterial outer membrane barrier by host innate immune molecules, MBio. 7 (2016). doi:10.1128/mBio.01541-16.
[108] J. van der Heijden, L.A. Reynolds, W. Deng, A. Mills, R. Scholz, K. Imami, L.J. Foster, F. Duong, B.B. Finlay, Salmonella rapidly regulates membrane permeability to survive oxidative stress, MBio. 7 (2016). doi:10.1128/mBio.01238-16.
[109] S.M. Richards, K.L. Strandberg, M. Conroy, J.S. Gunn, Cationic antimicrobial peptides serve as activation signals for the Salmonella Typhimurium PhoPQ and PmrAB regulons in vitro and in vivo, Front. Cell. Infect. Microbiol. 2 (2012). doi:10.3389/fcimb.2012.00102.
[110] S.M. Moskowitz, R.K. Ernst, S.I. Miller, PmrAB, a Two-Component Regulatory System of Pseudomonas aeruginosa that Modulates Resistance to Cationic Antimicrobial Peptides and Addition of Aminoarabinose to Lipid A, J. Bacteriol. 186 (2004) 575–579. doi:10.1128/JB.186.2.575-579.2004.
[111] H. Lee, F.F. Hsu, J. Turk, E.A. Groisman, The PmrA-regulated pmrC gene mediates phosphoethanolamine modification of lipid A and polymyxin resistance in Salmonella enterica, J. Bacteriol. 186 (2004) 4124–4133. doi:10.1128/JB.186.13.4124-4133.2004.
[112] Z.D. Dalebroux, S.I. Miller, Salmonellae PhoPQ regulation of the outer membrane to resist innate immunity, Curr. Opin. Microbiol. 17 (2014) 106–

113. doi:10.1016/j.mib.2013.12.005.
[113] A. Bryskier, Antimicrobial agents: Antibacterials and antifungals., ASM Press. (2005) 42–43. doi:10.1093/jac/dkl218.
[114] U.O. Hasdemir, J. Chevalier, P. Nordmann, J.M. Pagès, Detection and prevalence of active drug efflux mechanism in various multidrug-resistant Klebsiella pneumoniae strains from Turkey, J. Clin. Microbiol. 42 (2004) 2701–2706. doi:10.1128/JCM.42.6.2701-2706.2004.
[115] L. Fernández, R.E.W. Hancock, Adaptive and mutational resistance: Role of porins and efflux pumps in drug resistance, Clin. Microbiol. Rev. 25 (2012) 661–681. doi:10.1128/CMR.00043-12.
[116] V. Duval, I.M. Lister, MarA, SoxS and Rob of Escherichia coli - Global regulators of multidrug resistance, virulence and stress response., Int. J. Biotechnol. Wellness Ind. 2 (2013) 101–124. doi:10.6000/1927-3037.2013.02.03.2.
[117] M.N. Alekshun, S.B. Levy, The mar regulon: Multiple resistance to antibiotics and other toxic chemicals, Trends Microbiol. 7 (1999) 410–413. doi:10.1016/S0966-842X(99)01589-9.
[118] T. Nunoshiba, E. Hidalgo, C.F.A. Cuevas, B. Demple, Two-stage control of an oxidative stress regulon: The Escherichia coli SoxR protein triggers redox-inducible expression of the soxS regulatory gene, J. Bacteriol. 174 (1992) 6054–6060.
[119] R.R. Ariza, Z. Li, N. Ringstad, B. Demple, Activation of multiple antibiotic resistance and binding of stress-inducible promoters by Escherichia coli Rob protein., J. Bacteriol. 177 (1995) 1655–1661.
[120] P.J. Pomposiello, M.H.J. Bennik, B. Demple, Genome-wide transcriptional profiling of the Escherichia coli responses to superoxide stress and sodium salicylate, J. Bacteriol. 183 (2001) 3890–3902. doi:10.1128/JB.183.13.3890-3902.2001.
[121] H. Okusu, D. Ma, H. Nikaido, AcrAB Efflux Pump Plays a Major Role in the Antibiotic Resistance Phenotype of Escherichia coli Multiple- Antibiotic-Resistance (Mar) Mutants, J. Bacteriol. 178 (1996) 306–308. doi:10.1128/jb.178.1.306-308.1996.
[122] E. Hartog, L. Ben-Shalom, D. Shachar, K.R. Matthews, S. Yaron, Regulation of marA, soxS, rob, acrAB and micF in Salmonella enterica serovar Typhimurium, Microbiol. Immunol. 52 (2008) 565–574. doi:10.1111/j.1348-0421.2008.00075.x.
[123] R.J. Tibbetts, L.L. Tsang, C.W. Ching, Insertional mutation of marA vitiates inducible multiple antimicrobial resistance in Salmonella enterica subsp. enterica serovar Choleraesuis, Vet. Microbiol. 109 (2005) 267–274.

doi:10.1016/j.vetmic.2005.05.016.
[124] H. Hächler, S.P. Cohen, S.B. Levy, marA, a regulated locus which controls expression of chromosomal multiple antibiotic resistance in Escherichia coli., J. Bacteriol. 173 (1991) 5532–5538.
[125] H. Lou, M. Chen, S.S. Black, S.R. Bushell, M. Ceccarelli, T. Mach, K. Beis, A.S. Low, V.A. Bamford, I.R. Booth, H. Bayley, J.H. Naismith, Altered antibiotic transport in OmpC mutants isolated from a series of clinical strains of multi-drug resistant E. coli, PLoS One. 6 (2011). doi:10.1371/journal.pone.0025825.
[126] E. Dé, A. Baslé, M. Jaquinod, N. Saint, M. Malléa, G. Molle, J.M. Pagès, A new mechanism of antibiotic resistance in Enterobacteriaceae induced by a structural modification of the major porin, Mol. Microbiol. 41 (2001) 189–198. doi:10.1046/j.1365-2958.2001.02501.x.
[127] M. VERON, R. CHATELAIN, Taxonomic Study of the Genus Campylobacter Sebald and Veron and Designation of the Neotype Strain for the Type Species, Campylobacter fetus (Smith and Taylor) Sebald and Veron, Int. J. Syst. Bacteriol. 23 (1973) 122–134. doi:10.1099/00207713-23-2-122.
[128] J.L. Penner, The genus *Campylobacter*: A decade of progress, Clin. Microbiol. Rev. 1 (1988) 157–172. doi:10.1128/CMR.1.2.157.Updated.
[129] P. Hugenholtz, D.W. Waite, I. Vanwonterghem, C. Rinke, D.H. Parks, Y. Zhang, K. Takai, S.M. Sievert, J. Simon, B.J. Campbell, T.E. Hanson, T. Woyke, M.G. Klotz, Comparative Genomic Analysis of the Class Epsilonproteobacteria and Proposed Reclassification to Epsilonbacteraeota (phyl. nov.), Front. Microbiol. 8 (2017). doi:10.3389/fmicb.2017.00682.
[130] W.C. Hazeleger, J.A. Wouters, F.M. Rombouts, T. Abee, Physiological activity of \emph{Campylobacter jejuni} far below the minimal growth temperature, Appl. Environ. Microbiol. 64 (1998) 3917–3922.
[131] S. Pathogens, HHS Public Access, 1848 (2016) 3047–3054. doi:10.1016/j.bbamem.2015.02.010.Cationic.
[132] C.O. Gill, L.M. Harris, Survival and growth of Campylobacter fetus subsp. jejuni on meat and in cooked foods, Appl. Environ. Microbiol. 44 (1982) 259–263.
[133] M. Stahl, J. Butcher, A. Stintzi, Nutrient Acquisition and Metabolism by Campylobacter jejuni, Front. Cell. Infect. Microbiol. 2 (2012) 1–10. doi:10.3389/fcimb.2012.00005.
[134] D. Hofreuter, V. Novik, J.E. Galán, Metabolic Diversity in Campylobacter jejuni Enhances Specific Tissue Colonization, Cell Host Microbe. 4 (2008) 425–433. doi:10.1016/j.chom.2008.10.002.
[135] J. Parkhill, B.W. Wren, K. Mungall, J.M. Ketley, C. Churcher, D. Basham, T.

Chillingworth, R.M. Davies, T. Feltwell, S. Holroyd, K. Jagels, a V Karlyshev, S. Moule, M.J. Pallen, C.W. Penn, M. a Quail, M. a Rajandream, K.M. Rutherford, a H. van Vliet, S. Whitehead, B.G. Barrell, The genome sequence of the food-borne pathogen Campylobacter jejuni reveals hypervariable sequences., Nature. 403 (2000) 665–668. doi:10.1038/35001088.

[136] J. Velayudhan, M. a Jones, P. a Barrow, D.J. Kelly, L -Serine Catabolism via an Oxygen-Labile L -Serine Dehydratase Is Essential for Colonization of the Avian Gut by Campylobacter jejuni L -Serine Catabolism via an Oxygen-Labile L -Serine Dehydratase Is Essential for Colonization of the Avian Gut by Campyl, Infect. Immun. 72 (2004) 260–268. doi:10.1128/IAI.72.1.260.

[137] S.A. Leach, P. Harvey, R. Wali, Changes with growth rate in the membrane lipid composition of and amino acid utilization by continuous cultures of Campylobacter jejuni., J. Appl. Microbiol. 82 (1997) 631–640.

[138] E. Guccione, M. Del Rocio Leon-Kempis, B.M. Pearson, E. Hitchin, F. Mulholland, P.M. Van Diemen, M.P. Stevens, D.J. Kelly, Amino acid-dependent growth of Campylobacter jejuni: Key roles for aspartase (AspA) under microaerobic and oxygen-limited conditions and identification of AspB (Cj0762), essential for growth on glutamate, Mol. Microbiol. 69 (2008) 77–93. doi:10.1111/j.1365-2958.2008.06263.x.

[139] M. Stahl, L.M. Friis, H. Nothaft, X. Liu, J. Li, C.M. Szymanski, A. Stintzi, L-fucose utilization provides Campylobacter jejuni with a competitive advantage., Proc. Natl. Acad. Sci. U. S. A. 108 (2011) 7194–7199. doi:10.1073/pnas.1014125108.

[140] B.R. Merrell, R.I. Walker, J.C. Coolbaugh, Campylobacter fetus ss. Jejuni, a newly recognized enteric pathogen: morphology and intestinal colonization., Scan. Electron Microsc. 4 (1981) 125–131.

[141] S. Altekruse, N. Stern, P. Fields, D. Swerdlow, Campylobacter jejuni--an emerging foodborne pathogen., Emerg. Infect. Dis. 5 (1999) 28–35. doi:10.3201/eid0501.990104.

[142] K.T. Young, L.M. Davis, V.J. DiRita, Campylobacter jejuni: molecular biology and pathogenesis, Nat. Rev. Microbiol. 5 (2007) 665–679. doi:10.1038/nrmicro1718.

[143] R.F. De Boer, A. Ott, P. Güren, E. Van Zanten, A. Van Belkum, A.M.D. Kooistra-Smid, Detection of Campylobacter species and Arcobacter butzleri in stool samples by use of real-time multiplex PCR, J. Clin. Microbiol. 51 (2013) 253–259. doi:10.1128/JCM.01716-12.

[144] N.O. Kaakoush, N. Casta??o-Rodr??guez, H.M. Mitchell, S.M. Man, Global epidemiology of campylobacter infection, Clin. Microbiol. Rev. 28 (2015) 687–720. doi:10.1128/CMR.00006-15.

[145] L.K.R. Larson, A.R. Spickler, Zoonotic Campylobacteriosis Campylobacteriosis, Cent. Food Secur. Public Heath. (2013) 1–7.
[146] J. Haiko, B. Westerlund-Wikström, The Role of the Bacterial Flagellum in Adhesion and Virulence, Biology (Basel). 2 (2013) 1242–1267. doi:10.3390/biology2041242.
[147] J.E. Christensen, S.A. Pacheco, M.E. Konkel, Identification of a Campylobacter jejuni-secreted protein required for maximal invasion of host cells, Mol. Microbiol. 73 (2009) 650–662. doi:10.1111/j.1365-2958.2009.06797.x.
[148] V. Bronnec, H. Turoňová, A. Bouju, S. Cruveiller, R. Rodrigues, K. Demnerova, O. Tresse, N. Haddad, M. Zagorec, Adhesion, biofilm formation, and genomic features of Campylobacter jejuni Bf, an atypical strain able to grow under aerobic conditions, Front. Microbiol. 7 (2016). doi:10.3389/fmicb.2016.01002.
[149] L.D. Kalischuk, A.G. Buret, A role for Campylobacter jejuni-induced enteritis in inflammatory bowel disease?, AJP Gastrointest. Liver Physiol. 298 (2010) G1–G9. doi:10.1152/ajpgi.00193.2009.
[150] A.P. Heikema, Z. Islam, D. Horst-Kreft, R. Huizinga, B.C. Jacobs, J.A. Wagenaar, F. Poly, P. Guerry, A. van Belkum, C.T. Parker, H.P. Endtz, Campylobacter jejuni capsular genotypes are related to Guillain-Barrè syndrome, Clin. Microbiol. Infect. 21 (2015) 852.e1-852.e9. doi:10.1016/j.cmi.2015.05.031.
[151] B.M. Allos, Association between Campylobacter Infection and Guillain-Barré Syndrome, J. Infect. Dis. 176 (1997) S125–S128. doi:10.1086/513783.
[152] I. Nachamkin, B.M. Allos, T. Ho, Campylobacter species and Guillain-Barré syndrome., Clin. Microbiol. Rev. 11 (1998) 555–67.
[153] N. Yuki, Guillain-Barré syndrome and anti-ganglioside antibodies: a clinician-scientist's journey., Proc. Jpn. Acad. Ser. B. Phys. Biol. Sci. 88 (2012) 299–326. doi:10.2183/pjab.88.299.
[154] N. Yuki, Ganglioside mimicry and peripheral nerve disease, Muscle and Nerve. 35 (2007) 691–711. doi:10.1002/mus.20762.
[155] N. Yuki, N. Shahrizaila, Guillain-Barré syndrome animal model: The first proof of molecular mimicry in human autoimmune disorder, J. Biomed. Biotechnol. 2011 (2011). doi:10.1155/2011/829129.
[156] K. Kaida, T. Ariga, R.K. Yu, Antiganglioside antibodies and their pathophysiological effects on Guillain-Barr?? syndrome and related disorders - A review, Glycobiology. 19 (2009) 676–692. doi:10.1093/glycob/cwp027.
[157] F.M. Aarestrup, J. Engberg, Antimicrobial resistance of thermophilic Campylobacter, Vet. Res. 32 (2001) 311–321. doi:10.1051/vetres:2001127.
[158] European Union, Ban on antibiotics as growth promoters in animal feed

enters into effect, Regulation. (2006) 1.
[159] J. Zhou, M. Zhang, W. Yang, Y. Fang, G. Wang, F. Hou, A seventeen-year observation of the antimicrobial susceptibility of clinical Campylobacter jejuni and the molecular mechanisms of erythromycin-resistant isolates in Beijing, China, Int. J. Infect. Dis. 42 (2016) 28–33. doi:10.1016/j.ijid.2015.11.005.
[160] G.M. Ruiz-Palacios, The health burden of Campylobacter infection and the impact of antimicrobial resistance: playing chicken., Clin. Infect. Dis. 44 (2007) 701–3. doi:10.1086/509936.
[161] T. Luangtongkum, B. Jeon, J. Han, P. Plummer, C.M. Logue, Q. Zhang, Antibiotic resistance in *Campylobacter*: emergence, transmission and persistence, Future Microbiol. 4 (2010) 189–200. doi:10.2217/17460913.4.2.189.Antibiotic.
[162] Ö. ASLANTAŞ, Broilerlerden İzole Edilen Termofilik Campylabacter'lerin Genotipik, Antimikrobiyal Direnç ve Virulens Profilleri, Kafkas Univ. Vet. Fak. Derg. 23 (2017) 547–554. doi:10.9775/kvfd.2016.17261.
[163] W. Summers, M.D. Resistance, Microbial Drug Resistance, Bact. Resist. to Antimicrob. Second Ed. 61 (2007) 1–9. doi:doi:10.1201/9781420008753.ch1.
[164] J. Engberg, F.M. Aarestrup, D.E. Taylor, P. Gerner-Smidt, I. Nachamkin, Quinolone and macrolide resistance in Campylobacter jejuni and C. coli: Resistance mechanisms and trends in human isolates, Emerg. Infect. Dis. 7 (2001) 24–34. doi:10.3201/eid0701.700024.
[165] J. Lin, L. Overbye Michel, Q. Zhang, CmeABC functions as a multidrug efflux system in Campylobacter jejuni, Antimicrob. Agents Chemother. 46 (2002) 2124–2131. doi:10.1128/AAC.46.7.2124-2131.2002.
[166] B. Ge, P. McDermott, Role of efflux pumps and topoisomerase mutations in fluoroquinolone resistance in Campylobacter jejuni and Campylobacter coli, Antimicrob. Agents Chemother. 49 (2005) 3347–3354. doi:10.1128/AAC.49.8.3347.
[167] M. Lehtopolku, P. Kotilainen, M. Haanperä-Heikkinen, U.-M. Nakari, M.-L. Hänninen, P. Huovinen, A. Siitonen, E. Eerola, J. Jalava, A.J. Hakanen, Ribosomal mutations as the main cause of macrolide resistance in Campylobacter jejuni and Campylobacter coli., Antimicrob. Agents Chemother. 55 (2011) 5939–41. doi:10.1128/AAC.00314-11.
[168] N.M. Iovine, Resistance mechanisms in Campylobacter jejuni., Virulence. 4 (2013) 230–240. doi:10.4161/viru.23753.
[169] S.M. Logan, T.J. Trust, Outer Membrane Characteristics of Campylobacter jejuni, Infect. Immun. 38 (1982) 898–906.

[170] Q. Zhang, J.C. Meitzler, S. Huang, T. Morishita, Sequence Polymorphism , Predicted Secondary Structures , and Surface- Exposed Conformational Epitopes of Campylobacter Major Outer Membrane Protein, Infect. Immunol. 68 (2000) 5679–5689. doi:10.1128/IAI.68.10.5679-5689.2000.
[171] J.M. Bolla, E. Loret, M. Zalewski, J.M. Pages, Conformational analysis of the Campylobacter jejuni porin, J. Bacteriol. 177 (1995) 4266–4271.
[172] G. Labesse, E. Garnotel, S. Bonnel, C. Dumas, J.M. Pages, J.M. Bolla, MOMP, a Divergent Porin from Campylobacter: Cloning and Primary Structural Characterization, Biochem. Biophys. Res. Commun. 280 (2001) 380–387. doi:10.1006/bbrc.2000.4129.
[173] J.M. Bolla, E. Loret, M. Zalewski, J.M. Pages, Conformational-Analysis of the Campylobacter-Jejuni Porin, J. Bacteriol. 177 (1995) 4266–4271.
[174] K. Amako, S.N. Wai, A. Umeda, M. Shigematsu, A. Takade, Electron microscopy of the major outer membrane protein of Campylobacter jejuni, Microbiol Immunol. 40 (1996) 749–754.
[175] C. Jansen, V.G. P, In vitro assembly of outer membrane protein PhoE of E . coli ., (1996).
[176] E. Dé, M. Jullien, G. Labesse, J.M. Pagès, G. Molle, J.M. Bolla, MOMP (major outer membrane protein) of Campylobacter jejuni; a versatile pore-forming protein, FEBS Lett. 469 (2000) 93–97. doi:10.1016/S0014-5793(00)01244-8.
[177] I. Moser, W. Schroeder, J. Salnikow, Campylobacter jejuni major outer membrane protein and a 59-kDa protein are involved in binding to fibronectin and INT 407 cell membranes, FEMS Microbiol. Lett. 157 (1997) 233–238. doi:10.1016/S0378-1097(97)00480-1.
[178] V. Bronnec, H. Turoňová, A. Bouju, S. Cruveiller, R. Rodrigues, K. Demnerova, O. Tresse, N. Haddad, M. Zagorec, Adhesion, biofilm formation, and genomic features of Campylobacter jejuni Bf, an atypical strain able to grow under aerobic conditions, Front. Microbiol. 7 (2016) 1–14. doi:10.3389/fmicb.2016.01002.
[179] J. Mahdavi, N. Pirinccioglu, N.J. Oldfield, E. Carlsohn, J. Stoof, A. Aslam, T. Self, S.A. Cawthraw, L. Petrovska, N. Colborne, C. Sihlbom, T. Boren, K.G. Wooldridge, D.A.A. Ala'Aldeen, A novel O-linked glycan modulates Campylobacter jejuni major outer membrane protein-mediated adhesion to human histo-blood group antigens and chicken colonization, Open Biol. 4 (2014) 130202–130202. doi:10.1098/rsob.130202.
[180] D. a Scott, Vaccines against Campylobacter jejuni., J. Infect. Dis. 176 Suppl (1997) S183–S188. doi:Doi 10.1086/513791.
[181] O. Sahin, N. Luo, S. Huang, Q. Zhang, Effect of Campylobacter-specific

maternal antibodies on Campylobacter jejuni colonization in young chickens, Appl. Environ. Microbiol. 69 (2003) 5372–5379. doi:10.1128/AEM.69.9.5372-5379.2003.
[182] D.R. Sizemore, B. Warner, J. Lawrence, A. Jones, K.P. Killeen, Live, attenuated Salmonella typhimurium vectoring Campylobacter antigens, Vaccine. 24 (2006) 3793–3803. doi:10.1016/j.vaccine.2005.07.026.
[183] X.Z. Fuzhou Xu, Development and Evaluation of CmeC Subunit Vaccine against Campylobacter jejuni, J. Vaccines Vaccin. 1 (2010) 1–8. doi:10.4172/2157-7560.1000112.
[184] P. Łaniewski, M. Kuczkowski, K. Chrzastek, A. Woźniak, A. Wyszyńska, A. Wieliczko, E.K. Jagusztyn-Krynicka, Evaluation of the immunogenicity of Campylobacter jejuni CjaA protein delivered by Salmonella enterica sv. Typhimurium strain with regulated delayed attenuation in chickens, World J. Microbiol. Biotechnol. 30 (2014) 281–292. doi:10.1007/s11274-013-1447-5.
[185] A. Islam, R. Raghupathy, M.J. Albert, Recombinant PorA, the major outer membrane protein of Campylobacter jejuni, provides heterologous protection in an adult mouse intestinal colonization model, Clin. Vaccine Immunol. 17 (2010) 1666–1671. doi:10.1128/CVI.00255-10.
[186] G. Winter, Xia2: An expert system for macromolecular crystallography data reduction, J. Appl. Crystallogr. 43 (2010) 186–190. doi:10.1107/S0021889809045701.
[187] A.J. McCoy, R.W. Grosse-Kunstleve, P.D. Adams, M.D. Winn, L.C. Storoni, R.J. Read, Phaser crystallographic software, J. Appl. Crystallogr. 40 (2007) 658–674. doi:10.1107/S0021889807021206.
[188] P. Emsley, K. Cowtan, Coot: Model-building tools for molecular graphics, Acta Crystallogr. Sect. D Biol. Crystallogr. 60 (2004) 2126–2132. doi:10.1107/S0907444904019158.
[189] G.N. Murshudov, A.A. Vagin, E.J. Dodson, Refinement of macromolecular structures by the maximum-likelihood method, Acta Crystallogr. Sect. D Biol. Crystallogr. 53 (1997) 240–255. doi:10.1107/S0907444996012255.
[190] H. Zheng, M.D. Chordia, D.R. Cooper, M. Chruszcz, P. Müller, G.M. Sheldrick, W. Minor, Validation of metal-binding sites in macromolecular structures with the CheckMyMetal web server., Nat. Protoc. 9 (2014) 156–170. doi:10.1038/nprot.2013.172.
[191] M. Montal, P. Mueller, Formation of bimolecular membranes from lipid monolayers and a study of their electrical properties., Proc. Natl. Acad. Sci. U. S. A. 69 (1972) 3561–3566. doi:10.1073/pnas.69.12.3561.
[192] T.N. Petersen, S. Brunak, G. von Heijne, H. Nielsen, SignalP 4.0:

discriminating signal peptides from transmembrane regions, Nat. Methods. 8 (2011) 785–786. doi:10.1038/nmeth.1701.
[193] S. McNicholas, E. Potterton, K.S. Wilson, M.E.M. Noble, Presenting your structures: The CCP4mg molecular-graphics software, Acta Crystallogr. Sect. D Biol. Crystallogr. 67 (2011) 386–394. doi:10.1107/S0907444911007281.
[194] J. Zhuang, A. Engel, J.M. Pagés, J.M. Bolla, The Campylobacter jejuni porin trimers pack into different lattice types when reconstituted in the presence of lipid., Eur. J. Biochem. 244 (1997) 575–579. doi:DOI 10.1111/j.1432-1033.1997.t01-1-00575.x.
[195] B. Van Den Berg, Structural basis for outer membrane sugar uptake in pseudomonads, J. Biol. Chem. 287 (2012) 41044–41052. doi:10.1074/jbc.M112.408518.
[196] L. Sun, F. Bertelshofer, G. Greiner, R.A. Böckmann, Characteristics of Sucrose Transport through the Sucrose-Specific Porin ScrY Studied by Molecular Dynamics Simulations, Front. Bioeng. Biotechnol. 4 (2016) 1–10. doi:10.3389/fbioe.2016.00009.
[197] J. Michels, A. Geyer, V. Mocanu, W. Welte, A.L. Burlingame, M. Przybylski, Structure and functional characterization of the periplasmic N-terminal polypeptide domain of the sugar-specific ion channel protein (ScrY porin)., Protein Sci. 11 (2002) 1565–74. doi:10.1110/ps.2760102.
[198] K.R. Mahendran, M. Kreir, H. Weingart, N. Fertig, M. Winterhalter, Permeation of antibiotics through Escherichia coli OmpF and OmpC porins: screening for influx on a single-molecule level., J. Biomol. Screen. Off. J. Soc. Biomol. Screen. 15 (2010) 302–307. doi:10.1177/1087057109357791.
[199] P. Raj Singh, M. Ceccarelli, M. Lovelle, M. Winterhalter, K.R. Mahendran, Antibiotic permeation across the OmpF channel: Modulation of the affinity site in the presence of magnesium, J. Phys. Chem. B. 116 (2012) 4433–4438. doi:10.1021/jp2123136.
[200] T. Schirmer, T. Keller, Y. Wang, J. Rosenbusch, Structural basis for sugar translocation through maltoporin channels at 3.1 A resolution, Science (80-.). 267 (1995) 512–514. doi:10.1126/science.7824948.
[201] A. Charbit, Maltodextrin transport through LamB, Front. Biosci. 8 (2003) s265. doi:10.2741/1046.
[202] P.E. Klebba, M. Hofnung, A. Charbit, A model of maltodextrin transport through the sugar-specific porin, LamB, based on deletion analysis, EMBO J. 13 (1994) 4670–4675.
[203] J.M. Bolla, E. De, A. Dorez, J.M. Pages, Purification, characterization and sequence analysis of Omp50, a new porin isolated from Campylobacter jejuni, Biochem. J. 352 (2000) 637–643. doi:Doi 10.1042/0264-

6021:3520637.
[204] L. Dedieu, J.M. Pagès, J.M. Bolla, Use of the omp50 Gene for Identification of Campylobacter Species by PCR, J. Clin. Microbiol. 42 (2004) 2301–2305. doi:10.1128/JCM.42.5.2301-2305.2004.
[205] L. Dedieu, J.M. Pagès, J.M. Bolla, The omp50 gene is transcriptionally controlled by a temperature-dependent mechanism conserved among thermophilic Campylobacter species, Res. Microbiol. 159 (2008) 270–278. doi:10.1016/j.resmic.2008.03.002.
[206] Q. Xia, W.T. Muraoka, Z. Shen, O. Sahin, H. Wang, Z. Wu, P. Liu, Q. Zhang, Adaptive mechanisms of Campylobacter jejuni to erythromycin treatment, BMC Microbiol. 13 (2013) 133. doi:10.1186/1471-2180-13-133.
[207] N. Corcionivoschi, L.A.J. Alvarez, T.H. Sharp, M. Strengert, A. Alemka, J. Mantell, P. Verkade, U.G. Knaus, B. Bourke, Mucosal Reactive Oxygen Species Decrease Virulence by Disrupting Campylobacter jejuni Phosphotyrosine Signaling, Cell Host Microbe. 12 (2012) 47–59. doi:10.1016/j.chom.2012.05.018.
[208] C. Grangeasse, R. Terreux, S. Nessler, Bacterial tyrosine-kinases: Structure-function analysis and therapeutic potential, Biochim. Biophys. Acta. 1804 (2010) 628–634. doi:10.1016/j.bbapap.2009.08.018.
[209] H. Liu, J.H. Naismith, An efficient one-step site-directed deletion, insertion, single and multiple-site plasmid mutagenesis protocol, BMC Biotechnol. 8 (2008) 91. doi:10.1186/1472-6750-8-91.
[210] M. Caffrey, C. Porter, Crystallizing membrane proteins for structure determination using lipidic mesophases., J. Vis. Exp. 3 (2010) 2–6. doi:10.3791/1712.
[211] L.A. Kelley, S. Mezulis, C.M. Yates, M.N. Wass, M.J.E. Sternberg, The Phyre2 web portal for protein modeling, prediction and analysis, Nat. Protoc. 10 (2015) 845–858. doi:10.1038/nprot.2015.053.
[212] E. Eren, J. Parkin, A. Adelanwa, B. Cheneke, L. Movileanu, S. Khalid, B. Van Den Berg, Toward understanding the outer membrane uptake of small molecules by Pseudomonas aeruginosa, J. Biol. Chem. 288 (2013) 12042–12053. doi:10.1074/jbc.M113.463570.
[213] M. Zahn, S.P. Bhamidimarri, A. Baslé, M. Winterhalter, B. Van Den Berg, Structural Insights into Outer Membrane Permeability of Acinetobacter baumannii, Structure. 24 (2016) 221–231. doi:10.1016/j.str.2015.12.009.
[214] J. Liu, E. Eren, J. Vijayaraghavan, B.R. Cheneke, M. Indic, B. Van Den Berg, L. Movileanu, OccK channels from pseudomonas aeruginosa exhibit diverse single-channel electrical signatures but conserved anion selectivity, Biochemistry. 51 (2012) 2319–2330. doi:10.1021/bi300066w.

[215] D.C. Lee, J. Zheng, Y.-M. She, Z. Jia, Structure of Escherichia coli tyrosine kinase Etk reveals a novel activation mechanism., EMBO J. 27 (2008) 1758–66. doi:10.1038/emboj.2008.97.
[216] C. Grangeasse, S. Nessler, I. Mijakovic, Bacterial tyrosine kinases: evolution, biological function and structural insights., Philos. Trans. R. Soc. Lond. B. Biol. Sci. 367 (2012) 2640–55. doi:10.1098/rstb.2011.0424.
[217] H. Yaginuma, S. Kawai, K. V Tabata, K. Tomiyama, A. Kakizuka, T. Komatsuzaki, H. Noji, H. Imamura, Diversity in ATP concentrations in a single bacterial cell population revealed by quantitative single-cell imaging, Sci Rep. 4 (2014) 6522. doi:10.1038/srep06522.
[218] Q. Ding, K.S. Tan, The Danger Signal Extracellular ATP Is an Inducer of Fusobacterium nucleatum Biofilm Dispersal, Front. Cell. Infect. Microbiol. 6 (2016) 1–8. doi:10.3389/fcimb.2016.00155.
[219] S.L. Fraser, M. Arnett, Enterobacter Infections, eMedicine. (2010) 1–8.
[220] M.L. Mezzatesta, F. Gona, S. Stefani, Enterobacter cloacae complex: clinical impact and emerging antibiotic resistance., Future Microbiol. 7 (2012) 887–902. doi:10.2217/fmb.12.61.
[221] M. Delgado-Valverde, J. Sojo-Dorado, A. Pascual, J. Rodriguez-Bano, Clinical management of infections caused by multidrug-resistant Enterobacteriaceae, Ther. Adv. Infect. Dis. 1 (2013) 49–69. doi:10.1177/2049936113476284.
[222] V. Loiwal, A. Kumar, P. Gupta, S. Gomber, V.G. Ramachandran, Enterobacter aerogenes outbreak in a neonatal intensive care unit, Pediatr. Int. 41 (1999) 157–161. doi:10.1046/j.1442-200X.1999.4121033.x.
[223] C. Bosi, A. Davin-Regli, C. Bornet, M. Mallea, J.M. Pages, C. Bollet, Most Enterobacter aerogenes strains in France belong to a prevalent clone, J. Clin. Microbiol. 37 (1999) 2165–2169.
[224] H. Marchandin, S. Godreuil, H. Darbas, H. Jean-Pierre, E. Jumas-Bilak, C. Chanal, R. Bonnet, Extended-Spectrum β-Lactamase TEM-24 in an Aeromonas Clinical Strain: Acquisition from the Prevalent Enterobacter aerogenes Clone in France [1], Antimicrob. Agents Chemother. 47 (2003) 3994–3995. doi:10.1128/AAC.47.12.3994-3995.2003.
[225] C. Arpin, C. Coze, A.M. Rogues, J.P. Gachie, C. Bebear, C. Quentin, Epidemiological study of an outbreak due to multidrug-resistant Enterobacter aerogenes in a medical intensive care unit, J. Clin. Microbiol. 34 (1996) 2163–2169.
[226] J.W. Chow, M.J. Fine, D.M. Shlaes, J.P. Quinn, D.C. Hooper, M.P. Johnson, R. Ramphal, M.M. Wagener, D.K. Miyashiro, V.L. Yu, Enterobacter bacteremia: Clinical features and emergence of antibiotic resistance during therapy, Ann.

Intern. Med. 115 (1991) 585–590. doi:10.7326/0003-4819-115-8-585.
[227] S.H. Choi, E.L. Jung, J.P. Su, S.H. Choi, S.O. Lee, J.Y. Jeong, M.N. Kim, H.W. Jun, S.K. Yang, Emergence of antibiotic resistance during therapy for infections caused by Enterobacteriaceae producing AmpC β-lactamase: Implications for antibiotic use, Antimicrob. Agents Chemother. 52 (2008) 995–1000. doi:10.1128/AAC.01083-07.
[228] S.M. Diene, V. Merhej, M. Henry, A. El Filali, V. Roux, C. Robert, S. Azza, F. Gavory, V. Barbe, B. La Scola, D. Raoult, J.M. Rolain, The rhizome of the multidrug-resistant enterobacter aerogenes genome reveals how new "Killer Bugs" are created because of a sympatric lifestyle, Mol. Biol. Evol. 30 (2013) 369–383. doi:10.1093/molbev/mss236.
[229] Y. De Gheldre, N. Maes, F. Rost, R. De Ryck, P. Clevenbergh, J.L. Vincent, M.J. Struelens, Molecular epidemiology of an outbreak of multidrug-resistant Enterobacter aerogenes infections and in vivo emergence of imipenem resistance, J. Clin. Microbiol. 35 (1997) 152–160.
[230] A. Davin-Regli, J.-M. Bolla, C.E. James, J.-P. Lavigne, Jacqueline Chevalier, E. Garnotel, A. Molitor, J.-M. Pagès, Membrane Permeability and Regulation of Drug "Influx and Efflux" in Enterobacterial Pathogens, Curr Drug Targets. 9 (2008) 750–759. doi:10.2174/138945008785747824.
[231] E. Valade, A. Davin-Regli, J.M. Bolla, J.M. Pag, Bacterial Membrane, a Key for Controlling Drug Influx and Efflux, in: Antibiot. Targets, Mech. Resist., 2013: pp. 217–240. doi:10.1002/9783527659685.ch9.
[232] C. Bornet, N. Saint, L. Fetnaci, M. Dupont, A. Davin-Régli, C. Bollet, J.M. Pagès, Omp35, a new Enterobacter aerogenes porin involved in selective susceptibility to cephalosporins, Antimicrob. Agents Chemother. 48 (2004) 2153–2158. doi:10.1128/AAC.48.6.2153-2158.2004.
[233] C.E. James, K.R. Mahendran, A. Molitor, J.M. Bolla, A.N. Bessonov, M. Winterhalter, J.M. Pagès, How β-lactam antibiotics enter bacteria: A dialogue with the porins, PLoS One. 4 (2009). doi:10.1371/journal.pone.0005453.
[234] M. Mallea, J. Chevalier, C. Bornet, A. Eyraud, A. Davin-Regli, C. Bollet, J.M. Pagès, Porin alteration and active efflux: Two in vivo drug resistance strategies used by Enterobacter aerogenes, Microbiology. 144 (1998) 3003–3009. doi:10.1099/00221287-144-11-3003.
[235] J.P. Lavigne, A. Sotto, M.H. Nicolas-Chanoine, N. Bouziges, J.M. Pagès, A. Davin-Regli, An adaptive response of Enterobacter aerogenes to imipenem: Regulation of porin balance in clinical isolates, Int. J. Antimicrob. Agents. 41 (2013) 130–136. doi:10.1016/j.ijantimicag.2012.10.010.
[236] R.N. Charrel, J.M. Pagès, P. De Micco, M. Mallea, Prevalence of outer membrane porin alteration in beta-lactam-antibiotic-resistant Enterobacter

aerogenes., Antimicrob. Agents Chemother. 40 (1996) 2854–8.
[237] T.G.G. Battye, L. Kontogiannis, O. Johnson, H.R. Powell, A.G.W. Leslie, iMOSFLM: A new graphical interface for diffraction-image processing with MOSFLM, Acta Crystallogr. Sect. D Biol. Crystallogr. 67 (2011) 271–281. doi:10.1107/S0907444910048675.
[238] I.W. Davis, L.W. Murray, J.S. Richardson, D.C. Richardson, MolProbity: Structure validation and all-atom contact analysis for nucleic acids and their complexes, Nucleic Acids Res. 32 (2004). doi:10.1093/nar/gkh398.
[239] H. Nikaido, K. Nikaido, S. Harayama, Identification and characterization of porins in Pseudomonas aeruginosa, J. Biol. Chem. 266 (1991) 770–779.
[240] J.M. Pages, C.E. James, M. Winterhalter, The porin and the permeating antibiotic: a selective diffusion barrier in Gram-negative bacteria, Nat Rev Microbiol. 6 (2008) 893–903. doi:10.1038/nrmicro1994.
[241] A. Prilipov, P.S. Phale, P. Van Gelder, J.P. Rosenbusch, R. Koebnik, Coupling site-directed mutagenesis with high-level expression: Large scale production of mutant porins from E. coli, FEMS Microbiol. Lett. 163 (1998) 65–72. doi:10.1016/S0378-1097(98)00151-7.
[242] E.M. Nestorovich, C. Danelon, M. Winterhalter, S.M. Bezrukov, Designed to penetrate: Time-resolved interaction of single antibiotic molecules with bacterial pores, Proc. Natl. Acad. Sci. 99 (2002) 9789–9794. doi:10.1073/pnas.152206799.
[243] H. Bajaj, M.A. Scorciapino, L. Moynié, M.G.P. Page, J.H. Naismith, M. Ceccarelli, M. Winterhalter, Molecular Basis of Filtering Carbapenems by Porins from β-Lactam-resistant Clinical Strains of Escherichia coli., J. Biol. Chem. (2015). doi:10.1074/jbc.M115.690156.
[244] M.F. Richter, B.S. Drown, A.P. Riley, A. Garcia, T. Shirai, R.L. Svec, P.J. Hergenrother, Predictive compound accumulation rules yield a broad-spectrum antibiotic, Nature. 545 (2017) 299–304. doi:10.1038/nature22308.

7. Appendices

A. Buffer and media composition

A.1 MOMP

2YT media	16 g bacto tryptone, 10 g bacto yeast extract, 5 g NaCl (adjust pH to 7).
Columbia blood agar	Peptone 2 g, corn starch 1 g, NaCl 5g, agar 7.3g, 5% (v/v) blood sheep
Lysis buffer	10mM Tris-EDTA pH 7.4
Extraction buffer 1	20 mM Tris-HCl pH 7.4, 0.1 % (w/v) sodium lauryl Sarcosinate
Extraction buffer 2	20 mM Sodium sulphate pH 7.5, 1% (v/v) OPOE
Anion exchange buffers	
Buffer A	30 mM Sodium sulphate, 10 mM NaCl, 0.6 % (v/v) OPOE
Buffer B	30 mM Sodium sulphate, 1 M NaCl, 0.6 % (v/v) OPOE
SEC buffer	10 mM Tris-HCl pH 8, 150 mM NaCl, 0.45 % (v/v) C_8E_4

A.2 Omp50

Auto –Induction medium (1L)	ZY (10 g N-Z-amine, 5 g yeast extract) media supplemented with 1mM $MgSO_4$, 0.5% glycerol, 0.05% glucose, 0.2% lactose, 25 mM $(NH_4)_2SO_4$, 50 mM KH_2PO_4, 50mM Na_2HPO_4
LB (1L)	10 g tryptone, 5 g yeast extract, 10 g NaCl
TB (1L)	12 g tryptone, 24 g yeast extract, 4 mL glycerol
TPB (1L)	20 g tryptose, 2 g dextrose, 5 g NaCl, 2.5 g Na_2PO_4
Lysis buffer	50 mM Sodium phosphate pH 7.4, 250 mM NaCl, 10 % glycerol
Extraction buffer	50 mM sodium phosphate pH 8, 250 mM NaCl, 5 mM β-mercaptoethanol, 7% OPOE
Wash buffer	50 mM sodium phosphate pH 8, 250 mM NaCl, 5 mM β-mercaptoethanol, 50 mM imidazole, 1% OPOE
Elution buffer	50 mM sodium phosphate pH 8, 250 mM NaCl, 5 mM β-mercaptoethanol, 250 mM imidazole, 1% OPOE
Dialysis buffer	10 mM Tris-HCl pH 8, 250 mM NaCl, 2 mM β-mercaptoethanol, 10% glycerol, 1% OPOE

SEC buffer	10 mM Tris-HCl pH 8, 150 mM NaCl, 0.45 % (v/v) C_8E_4
IB buffer	20 mM Hepes pH7, 300 mM NaCl
Refolding buffer	50 mM sodium phosphate, 250 NaCl, 2 mM β-mercaptoethanol (supplemented with chosen detergents)
Proteolytic enzymes buffers	
A-Chymotrypsin	1 mM HCl, 2 mM $CaCl_2$
Trypsine	1 mM HCl, 2 mM $CaCl_2$
Papain	H_2O
Subtilisin A	10 mM NaOAc
Western blot buffers	
Anode buffer 1	300 mM Trizma base, 20% methanol
Anode buffer 2	25 mM Trizma base, 20% methanol
Cathode buffer	5.2 g amino capronic acid, 20% methanol, 0.01% SDS
A3. Omp35/36	
LB (1L)	10 g tryptone, 5 g yeast extract, 10g NaCl
Lysis buffer	50 mM Sodium phosphate pH 7.4, 250 mM NaCl, 10 % glycerol
Extraction buffer	50 mM sodium phosphate pH 8, 250 mM NaCl, 5 mM β-mercaptoethanol, 7% OPOE

Wash buffer	50 mM sodium phosphate pH 8, 250 mM NaCl, 5 mM β-mercaptoethanol, 50 mM imidazole, 1% OPOE
Elution buffer	50 mM sodium phosphate pH 8, 250 mM NaCl, 5 mM β-mercaptoethanol, 250 mM imidazole, 1% OPOE
Dialysis buffer	10 mM Tris-HCl pH 8, 250 mM NaCl, 2 mM β-mercaptoethanol, 10% glycerol, 1% OPOE
SEC buffer	10 mM Tris-HCl pH 8, 150 mM NaCl, 0.45 % (v/v) C_8E_4

B. Crystallization screenings

PEGsI&II, MemGold I&II crystallization screenings were purchased from Qiagen and Molecular Dimension, respectively. Composition can be found her:

https://www.qiagen.com/products/protein/crystallization/compositiontables/

http://www.sfr-biosciences.fr/medias/documents/copy_of_document-l3/mad-es-doc-021-130716pegs-ii-suite

https://www.moleculardimensions.com/applications/upload/MD1-39%20MemGold.pdf

https://www.moleculardimensions.com/products/4234-MemGold2/

C. PDB codes

Protein name	PDB code
OmpC	2j1n
LamB	1MAL
OccD1	4FOZ
CymA	4D5B
OmpG	2F1C
FhuA	2GRX
SusCD	2FQ6
OmpT	1I78
OMPLA	1QD6
BamA	4K3B
BamB	4XGA
MOMP	5LDT(native), 5LDV(rec)
Omp35	5O78 (to be published)
Omp36	5O9C (to be published)

D. Publication

s